POLITECNICO DI MILANO
Department of Electronics, Information and Bioengineering
Master of Science in Biomedical Engineering

A Model of Acoustic Waves Propagation in the Tracheo-bronchial Tree in Healthy and Pathological Conditions

Advisor:

Prof. Andrea ALIVERTI

Co-advisor:

Francesca PENNATI

Master Thesis of:
Lorenzo ALIBONI
Student ID: 852486

Academic Year 2016-2017

To my parents Simonetta and Maurizio,
I will never be able to express enough gratitude for everything you did for me.
Thanks for the opportunities you offered me, for your support and your advice.
Thanks for always being there for me.
Without you I will not be who I am. I am proud of being your son.

Love You

ACKNOWLEDGMENTS

I express sincere appreciation and thankfulness to my advisor Professor Andrea Aliverti for his supervision and patience throughout this project. Also, I would like to thank my co-advisor Francesca Pennati for her support and guidance.

I am grateful to professor Thomas Royston head of the Bioengineering Department and of the Acoustics and Vibration Laboratory at the University of Illinois at Chicago and to Brian Henri for their help and support.

Last, but not least, I would like to thank my family, my mother Simonetta, my father Maurizio and my sister Camilla for their love, support and encouragement. A final thought to my grandparents and, in particular, to my grandfather Egidio: hope I will be a man and an engineer like him one day.

LA

TABLE OF CONTENTS

CHAPTER		PAGE
1	**INTRODUCTION**	1
1.1	Background & Motivation	1
1.2	Anatomy of the Human Respiratory System	3
1.2.1	The Lower Respiratory Tract	5
1.2.2	Gross Anatomy of Lungs	8
1.2.3	Respiratory Muscles and Bones	10
1.3	Pathologies of the Airways Tree	12
1.3.1	Asthma	12
1.3.2	Fibrosis	14
1.3.3	Pulmonary Infiltrates	15
1.4	Abnormal Breath Sounds and Pathologies	16
1.4.1	Crackles	18
1.4.2	Wheezes	19
1.4.3	Stridor	20
1.4.4	Bronchial Breath Sounds	21
1.4.5	Pleural Rub	21
1.4.6	Rhonchi	21
1.4.7	Squawks	22
1.5	Objectives and Structure of the Thesis	23
2	**THEORY**	25
2.1	Acoustic Impedance	25
2.2	Impedance of a Sound Wave Propagating in Cylinder	26
2.3	Mathematical and Acoustical Description of the Lower Respiratory Tract	31
2.3.1	The Horsfield Model	31
3	**ANALYTICAL MODELS**	40
3.1	Generation of the Geometries	40
3.1.1	Data for Validation and Preliminary Acoustical Analysis	41

TABLE OF CONTENTS

CHAPTER			PAGE
	3.1.2	Data for the Analysis of Asthma Pathology	44
	3.2	Acoustical Analysis	48
	3.2.1	Simulation of the Asthma Pathology	51
	3.2.2	Simulation of the Airways Fibrosis Condition	52
	3.2.3	Simulation of Pulmonary Infiltrate Condition	52
4	**NUMERICAL MODELS**		53
	4.1	Generation of the Meshes	54
	4.2	Acoustical Simulations	55
5	**RESULTS**		57
	5.1	Validation of the Analytical Model	57
	5.2	Comparison Between the Beginning of Inspiratory and Expiratory Phases	65
	5.3	Simulation of Pathological Conditions	71
	5.3.1	Simulation of the Asthma Pathology	71
	5.3.2	Simulation of the Fibrosis Condition	77
	5.3.3	Simulation of the Pulmonary Infiltrate Condition	83
	5.4	Application of the Model to Control and Asthmatic Groups	89
	5.4.1	Validation of the Asthmatic Data	91
	5.4.2	Results for the Control Group	93
	5.4.3	Results for the Asthmatic Group	97
	5.4.4	Comparison between the Control and the Asthmatic Group	101
6	**DISCUSSION**		107
	6.1	General Consideration on the Acoustic Behavior of the System	108
	6.2	Validation of the Model	111
	6.3	Comparison Between the Beginning of Inspiratory and Expiratory Phases	111
	6.4	Simulation of Pathological Conditions	112
	6.4.1	Simulation of the Asthma Pathology	113
	6.4.2	Simulation of the Airways Fibrosis Condition	114
	6.4.3	Simulation of the Pulmonary Infiltrate Condition	115

TABLE OF CONTENTS

CHAPTER		PAGE
6.5	Application of the Model to Control and Asthmatic Group.....	116
6.5.1	Validation of the Asthmatic Data.....	117
6.5.2	Analysis of the Results for the Control Group.....	118
6.5.3	Analysis of the Results for the Asthmatic Group	119
6.5.4	Comparison between the Control and the Asthmatic Group	123
6.6	Limitations of the Model.....	123
6.7	Conclusions	126
6.8	Future Directions.....	127
APPENDIX		129
CITED LITERATURE.....		130
VITA.....		134

LIST OF TABLES

TABLE		PAGE
1	GEOMETRICAL FEATURES OF HUMAN LOWER RESPIRATORY TRACT ...	8
2	LUNGS LOBES AND SEGMENTS	11
3	CLASSIFICATION AND FEATURES OF CRACKLES	19
4	MORPHOLOGICAL PARAMETERS OF HUMAN AIRWAY MODEL; n IS THE HORSFIELD ORDER, l AND d ARE THE LENGTH AND DIAMETER, h IS THE WALL THICKNESS AND C THE FRACTION OF CARTILAGE.....	33
5	MECHANICAL PROPERTIES OF THE SOFT TISSUE.....	50
6	MECHANICAL PROPERTIES OF AIR	50
7	FEATURES OF THE FINAL MERGED MESHES IN THE TWO RESPIRATORY PHASES CONSIDERED	54
8	SOFT TISSUE MECHANICAL PROPERTIES FOR THE NUMERICAL SIMULATIONS	56
9	AIR MECHANICAL PROPERTIES FOR THE NUMERICAL SIMULATIONS…	56
10	ANALYSIS OF THE ERROR FOR THE BEGINNING OF INSPIRATORY PHASE – MEDIAN AND MAXIMUM VALUE FOR THE FOUR FREQUENCIES OF INTEREST	63
11	ANALYSIS OF THE ERROR FOR THE BEGINNING OF EXPIRATORY PHASE – MEDIAN AND MAXIMUM VALUE FOR THE FOUR FREQUENCIES OF INTEREST	64
12	COMPARISON BETWEEN THE AVERAGE VALUES OF THICKNESS OF THE DATA FROM LITERATURE AND THE MEASUREMENTS OBTAINED DURING THE PROCEDURE OF VALIDATION	92

LIST OF FIGURES

FIGURE		PAGE
1	Schematic representation of the respiratory system (image adapted from http://organanatomy.com)	4
2	Schematics of the abnormal breath sounds and associated pathologies	17
3	Exemplification of a Sound Wave Propaganting in a Cylinder	26
4	The acoustic model of a single bifurcating airway segment	34
5	Visual layout of the process of identification and generation of the morpho-geometrical features of the airway tree (a representative expiratory case is reported)	42
6	Geometry (left) and diameter distribution (right) at the beginning of the inspiratory phase	43
7	Geometry (left) and diameter distribution (right) at the beginning of the expiratory phase	43
8	Internal diameters in the control subjects at low respiratory volume (black circles) and high respiratory volume (white circles) from generation 0 to 5. The mean values are represented with a continuous line for the low respiratory volume and with a dashed line for the high respiratory volumes.	45
9	Internal diameters in the asthmatic subjects at low respiratory volume (black circles) and high respiratory volume (white circles) from generation 0 to 5. The mean values are represented with a continuous line for the low respiratory volume and with a dashed line for the high respiratory volumes. **, $p<0.01$	45
10	Exemplificative picture representing the Full Width at Half Maximum method applied during the validation procedure of the literature data of thickness.	47
11	Generated meshes in ANSYS®. The mesh for the beginning of the inspiratory phase is reported on the left, whereas the mesh for the beginning of the expiratory phase is reported on the right.	54
12	Terminal impedance (Z_T) curve fitting. Valid for both the inspiratory and expiratory phase.	55
13	Magnitude of acoustic pressure in logarithmic scale [dB]. Comparison between the analytical (left) and numerical (right) results at the beginning of the inspiratory phase. From the top to the bottom the results at 200 Hz, 400 Hz, 600 Hz and 800 Hz are reported.	58

LIST OF FIGURES

FIGURE		PAGE
14	Real part of acoustic pressure [Pa]. Comparison between the analytical (left) and numerical (right) results at the beginning of the inspiratory phase. From the top to the bottom the results at 200 Hz, 400 Hz, 600 Hz and 800 Hz are reported.	59
15	Magnitude of acoustic pressure in logarithmic scale [dB]. Comparison between the analytical (left) and numerical (right) results at the beginning of the expiratory phase. From the top to the bottom the results at 200 Hz, 400 Hz, 600 Hz and 800 Hz are reported	60
16	Real part of acoustic pressure [Pa]. Comparison between the analytical (left) and numerical (right) results at the beginning of the expiratory phase. From the top to the bottom the results at 200 Hz, 400 Hz, 600 Hz and 800 Hz are reported.	61
17	Identification of the interpolating points in COMSOL Multiphysics®.	62
18	Error representation (top) and error distribution (bottom) for the beginning of the inspiratory phase. From the right to the left the four frequencies of interest in the following order: 200 Hz, 400 Hz, 600 Hz and 800Hz.	63
19	Error representation (top) and error distribution (bottom) for the beginning of the expiratory phase. From the right to the left the four frequencies of interest in the following order: 200 Hz, 400 Hz, 600 Hz and 800Hz.	64
20	Magnitude of the acoustic pressure in logarithmic scale at 200 Hz. Comparison between the beginning of the inspiratory phase (left) and the beginning of expiratory phase (right)	66
21	Trend of the magnitude of the acoustic pressure in logarithmic scale at low frequency in the trachea (left), left main Bronchus (middle) and right main bronchus (right) for the inspiratory (blue) and expiratory (orange) phases.	66
22	Magnitude of the acoustic pressure in logarithmic scale at high frequency. Comparison between the beginning of the inspiratory phase (left) and the beginning of expiratory phase (right).	67
23	Trend of the magnitude of the acoustic pressure in logarithmic scale at high frequency in the trachea (left), left main Bronchus (middle) and right main bronchus (right) for the inspiratory (blue) and expiratory (orange) phases.	67

LIST OF FIGURES

FIGURE		PAGE
24	Real part of the acoustic pressure in logarithmic scale at low frequency. Comparison between the beginning of the inspiratory phase (left) and the beginning of expiratory phase (right).	68
25	Trend of the real part of the acoustic pressure in logarithmic scale at 200 Hz in the trachea (left), left main Bronchus (middle) and right main bronchus (right) for the inspiratory (blue) and expiratory (orange) phases.	68
26	Real part of the acoustic pressure in logarithmic scale at high frequency. Comparison between the beginning of the inspiratory phase (left) and the beginning of expiratory phase (right).	69
27	Trend of the real part of the acoustic pressure in logarithmic scale at high frequency in the trachea (left), left main Bronchus (middle) and right main bronchus (right) for the inspiratory (blue) and expiratory (orange) phases.	69
28	Magnitude of the wall radial velocity in logarithmic scale at low frequency. Comparison between the beginning of the inspiratory phase (left) and the beginning of expiratory phase (right).	70
29	Magnitude of the wall radial velocity in logarithmic scale at high frequency. Comparison between the beginning of the inspiratory phase (left) and the beginning of expiratory phase (right).	70
30	Magnitude of the acoustic pressure in logarithmic scale at low frequency. Comparison between healthy (left) and asthma (right).	72
31	Trend of the magnitude of the acoustic pressure in logarithmic scale at low frequency in the trachea (left), left main Bronchus (middle) and right main bronchus (right) for the healthy case (green) and asthma case (red).	72
32	Magnitude of the acoustic pressure in logarithmic scale at high frequency. Comparison between healthy (left) and asthma (right).	73
33	Trend of the magnitude of the acoustic pressure in logarithmic scale at high frequency in the trachea (left), left main Bronchus (middle) and right main bronchus (right) for the healthy case (green)	73
34	Real part of the acoustic pressure in logarithmic scale at low frequency. Comparison between healthy (left) and asthma (right).	74

LIST OF FIGURES

FIGURE		PAGE
35	Trend of the real part of the acoustic pressure in logarithmic scale at low frequency in the trachea (left), left main Bronchus (middle) and right main bronchus (right) for the healthy case (green)	74
36	Real part of the acoustic pressure in logarithmic scale at high frequency. Comparison between healthy (left) and asthma (right)	75
37	Trend of the real part of the acoustic pressure in logarithmic scale at high frequency in the trachea (left), left main Bronchus (middle) and right main bronchus (right) for the healthy case (green)	75
38	Magnitude of the wall radial velocity in logarithmic scale at low frequency. Comparison between healthy (left) and asthma (right)	76
39	Magnitude of the wall radial velocity in logarithmic scale at high frequency. Comparison between healthy (left) and asthma (right)	76
40	Magnitude of the acoustic pressure in logarithmic scale at low frequency. Comparison between healthy (left) and fibrosis (right)	78
41	Trend of the magnitude of the acoustic pressure in logarithmic scale at low frequency in the trachea (left), left main Bronchus (middle) and right main bronchus (right) for the healthy case (green)	78
42	Magnitude of the acoustic pressure in logarithmic scale at high frequency. Comparison between healthy (left) and fibrosis (right)	79
43	Trend of the magnitude of the acoustic pressure in logarithmic scale at high frequency in the trachea (left), left main Bronchus (middle) and right main bronchus (right) for the healthy case (green)	79
44	Real part of the acoustic pressure in logarithmic scale at low frequency. Comparison between healthy (left) and fibrosis (right)	80
45	Trend of the magnitude of the acoustic pressure in logarithmic scale at low frequency in the trachea (left), left main Bronchus (middle) and right main bronchus (right) for the healthy case (green)	80
46	Real part of the acoustic pressure in logarithmic scale at high frequency. Comparison between healthy (left) and fibrosis (right)	81

LIST OF FIGURES

FIGURE		PAGE
47	Trend of the magnitude of the acoustic pressure in logarithmic scale at high frequency in the trachea (left), left main Bronchus (middle) and right main bronchus (right) for the healthy case (green) and fibrosis case (red).	81
48	Magnitude of the wall radial velocity in logarithmic scale at low frequency. Comparison between healthy (left) and fibrosis (right)	82
49	Magnitude of the wall radial velocity in logarithmic scale at high frequency. Comparison between healthy (left) and fibrosis (right)	82
50	Position of the inferior lobar bronchus analyzed in the case of the LLL Pulmonary infiltrate	83
51	Magnitude of the acoustic pressure in logarithmic scale at low frequency. Comparison between healthy (left) and LLL pulmonary infiltrate (right).	84
52	Trend of the magnitude of the acoustic pressure in logarithmic scale at low frequency in the inferior lobar bronchus for the healthy case (green) and pulmonary infiltration (red).	84
53	Magnitude of the acoustic pressure in logarithmic scale at high frequency. Comparison between healthy (left) and LLL pulmonary infiltrate (right).	85
54	Trend of the magnitude of the acoustic pressure in logarithmic scale at high frequency in the inferior lobar bronchus for the healthy case (green) and pulmonary infiltration (red).	85
55	Real Part of the acoustic pressure in logarithmic scale at low frequency. Comparison between healthy (left) and LLL pulmonary infiltrate (right).	86
56	Trend of the real part of the acoustic pressure in logarithmic scale at low frequency in the inferior lobar bronchus for the healthy case (green) and pulmonary infiltration (red).	86
57	Real part of the acoustic pressure in logarithmic scale at high frequency. Comparison between healthy (left) and LLL pulmonary infiltrate (right).	87
58	Trend of the real part of the acoustic pressure in logarithmic scale at high frequency in the inferior lobar bronchus for the healthy case (green) and pulmonary infiltration (red).	87
59	Magnitude of the wall radial velocity in logarithmic scale at low frequency. Comparison between healthy (left) and LLL pulmonary infiltrate (right).	88

LIST OF FIGURES

FIGURE		PAGE
60	Magnitude of the wall radial velocity in logarithmic scale at high frequency. Comparison between healthy (left) and LLL pulmonary infiltrate (right).	88
61	Input (black symbols) and terminal (white symbols) acoustic impedance from generation 0 to 4 at high respiratory volume in the control subjects. Low (circles) and high (diamonds) frequencies are reported. The symbols indicate the median values, the lower and the upper bars correspond to the 25th percentile and the 75th percentile, respectively. **, $p<0.01$; ***, $p<0.001$ between low and high frequency.	94
62	Input (black symbols) and terminal (white symbols) acoustic impedance from generation 0 to 4 at low respiratory volume in the control subjects. Low (circles) and high (diamonds) frequencies are reported The symbols indicate the median values, the lower and the upper bars correspond to the 25th percentile and the 75th percentile, respectively. ***, $p<0.001$ between low and high frequency.	94
63	Acoustic pressure distribution from generation 0 to 4 at high respiratory volume in control subjects. Low frequency (black circles) and high frequencies (white circles) are reported. For each generation the values are shown along 9 equally spaced points. The symbols indicate the median value, the lower and the upper bars correspond to the 25th percentile and the 75th percentile, respectively.	96
64	Acoustic pressure distribution from generation 0 to 4 at low respiratory volumes in control subjects. Low frequency (black circles) and high frequencies (white circles) are reported. For each generation the values are shown along 9 equally spaced points. The symbols indicate the median value, the lower and the upper bars correspond to the 25th percentile and the 75th percentile, respectively.	96
65	Input (black symbols) and terminal (white symbols) acoustic impedance from generation 0 to 4 at high respiratory volume in the asthmatic subjects. Low (circles) and high (diamonds) frequencies are reported. The symbols indicate the median values, the lower and the upper bars correspond to the 25th percentile and the 75th percentile, respectively. *, $p<0.05$; ***$p<0.001$; between low and high frequency for each generation, ...	98

LIST OF FIGURES

FIGURE		PAGE
66	Input (black symbols) and terminal (white symbols) acoustic impedance from generation 0 to 4 at low respiratory volume in the asthmatic subjects. Low (circles) and high (diamonds) frequencies are reported The symbols indicate the median values, the lower and the upper bars correspond to the 25th percentile and the 75th percentile, respectively. *, p<0.05; ***p<0.001; between low and high frequency for each generation,.	98
67	Acoustic pressure distribution from generation 0 to 4 at high respiratory volumes in asthmatic subjects. Low frequency (black circles) and high frequencies (white circles) are reported. For each generation the values are shown at 9 equally-spaced points. The symbols indicate the median value, the lower bar and the upper bars correspond to the 25th percentile and the 75th percentile, respectively. ***, p<0.001 between low and high frequency.	100
68	Acoustic pressure distribution from generation 0 to 4 at low respiratory volumes in asthmatic subjects. Low frequency (black circles) and high frequencies (white circles) are reported. For each generation the values are shown along 9 equally spaced points. The symbols indicate the median values, the lower and the upper bars correspond to the 25th percentile and the 75th percentile, respectively.	100
69	Internal diameter as a function of the airway generation order for control (in blue) and asthma (in red) groups. High respiratory volume case is reported on the left, whereas the low respiratory volume case is reported on the right. The mean values are reported with a blue line for the control group and with a red line for the asthmatic group. *, p<0.05; **, p<0.01 between healthy and asthma groups.....	102
70	Acoustic impedance as a function of the airway generation order for control (in blue) and asthma (in red) groups at low frequency. High respiratory volume case is reported on the left, whereas the low respiratory volume case is reported on the right. Filled symbols indicate the median input impedance, whereas empty symbols represent the median terminal impedance, the lower and the upper bars correspond to the 25th percentile and the 75th percentile, respectively. *, p<0.05; **, p<0.01 between healthy and asthma group	103
71	Acoustic impedance as a function of the airway generation order for control (in blue) and asthma (in red) groups at high frequency. High respiratory volume case is reported on the left, whereas the low respiratory volume case is reported on the right. Filled symbols indicate the median input impedance, whereas empty symbols represent the median terminal impedance, the lower and the upper bars correspond to the 25th percentile and the 75th percentile, respectively. *, p<0.05; **, p<0.01 between healthy and asthma group	103

LIST OF FIGURES

FIGURE		PAGE
72	Acoustic pressure distribution as a function of the airway generation order for control (in blue) and asthma (in red) groups at low frequency. High respiratory volume case is reported on the left, whereas the low respiratory volume case is reported on the right. The symbols indicate the median value, the lower and the upper bars correspond to the 25th percentile and the 75th percentile, respectively. For each generation the values are shown along 9 equally spaced points. ***, $p<0.001$ between health and asthma	105
73	Acoustic pressure distribution as a function of the airway generation order for control (in blue) and asthma (in red) groups at high frequency. High respiratory volume case is reported on the left, whereas the low respiratory volume case is reported on the right. The symbols indicate the median value, the lower and the upper bars correspond to the 25th percentile and the 75th percentile, respectively. For each generation the values are shown along 9 equally spaced points. *, $p<0.05$; **, $p<0.01$ between health and asthma	105
74	Transmission Line Analogy. Resulting circuit for each element.....	109

LIST OF ABBREVIATIONS

AHP	Audible Human Project
ATS	American Thoracic Society
CDC	Center for Disease Control and Prevention
COPD	Chronic Obstructive Pulmonary Disease
CT	Computed Tomography
ECM	Extra Cellular Matrix
FRC	Functional Residual Capacity
GUI	Graphic User Interface
HF	High Frequency
HRCT	High Resolution Computerized Tomography
IDW	Initial Deflection Width
i.e.	id est
LF	Low Frequency
LLL	Left Lower Lobe
LMB	Left Main Bronchus
LUL	Left Upper Lobe
MRE	Magnetic Resonance Elastography
PI	Pulmonary Infiltration
RLL	Right Lower Lobe
RMB	Right Main Bronchus
RML	Right Middle Lobe
RUL	Right Upper Lobe
RV	Residual Volume

LIST OF ABBREVIATIONS

SI	International System of Units
SLDV	Scanning Laser Doppler Vibrometry
TCL	Tool Command Language
TLC	Total Lung Capacity
2CD	Two Cycle Duration

SUMMARY

Auscultation has been used qualitatively by clinicians for hundreds of years to diagnose and monitor the progression of pulmonary pathologies. Auscultation technique is based on the clinical evidence that the morphological and functional alterations of the respiratory system determined by diseases and injuries result in measurable changes in lung sounds generation and propagation. Centuries of clinical practice have led to an extensive cataloging of respiratory sounds and their alterations resulting from pathological conditions. However, the information collected over these years suffers from a lack of quantitative information as well as of a proper understanding and description of the phenomena involved. The quantification of the effect of pathology-induced structural and mechanical modifications on the sound transmission in the respiratory system has received arguably even less attention. A better understanding of sound propagation and of its alterations by pathological conditions or injuries would be extremely valuable not only in terms of clinical interpretation and significance, but also from a research oriented point of view.

This project was developed in collaboration with the University of Illinois at Chicago with the long-term objective of creating a computational model able to precisely mimic the creation, propagation and noninvasive measurement of naturally-occurring sounds associated with the respiratory system physiology as well as the alterations induced by the pathologies.

Fitting the general scope mentioned above, this preliminary work was divided into two parts.

In the first part of this thesis, in the context of the Acoustics and Vibration Laboratory of the University of Illinois at Chicago, an analytical code developed in MATLAB® was validated thanks to Finite Element Analysis and shown to be able to provide accurate and quantitative information about the sound propagation in the lower respiratory tract over a specific frequency range (200-800 Hz). The model assumes to input a known pressure at the inlet of the trachea:

what is evaluated is the response of the system to the inlet pressure in term of propagation of the acoustic waves over different frequencies. The procedure of validation of the model was performed in physiological conditions for a single subject with the bronchial tree generated starting from CT data at the beginning of both the inspiratory and expiratory phases of the respiratory cycle.

The model was successively modified to roughly simulate the morphometrical and mechanical alterations induced by three specific pathological condition such as asthma, a generalized fibrosis and a severe mono-lateral pulmonary infiltrate. For the asthma case a homogeneous bronchoconstriction of the small airways was hypothesized; for the fibrosis case the elastic modulus of the airway walls was increased by a factor five; for the pulmonary infiltrate in the lower left lobe the terminal impedance of the affected lobe was increased by a factor 10^5.

These approaches, although extremely simplified, allowed a first analysis of the effect of these pathologies on sound propagation throughout the tracheobronchial tree. It was demonstrated that a modeling approach of the pathologies consisting of alterations affecting one parameter only (either geometrical or mechanical) induced remarkable modifications of the acoustic response of the system for the fibrosis and the pulmonary infiltrate cases. The stiffening of the airway walls, characteristic of the fibrotic condition, caused the acoustic pressure to propagate further into the tracheobronchial tree with respect to the physiological case, whereas the simulation of the pulmonary infiltrate condition deeply modified the acoustic pressure distribution in the affected lobe (the lower left lobe was arbitrarily chosen), causing the pressure to increase in the airway branches located in that specific part of the lung. The simulation of the asthma pathology through a simplified approach did not provide satisfactory results as the acoustic pressure distribution remained substantially unchanged.

In the second part of the project, developed in the Laboratory of Biomedical Technologies of the Politecnico di Milano, the model was tested on real pathological data from asthmatic

subjects and compared with data gathered from a control group. Low and high respiratory volumes were considered as well as the behavior at low and high frequencies. This rigorous approach to the simulation of the complexity (and heterogeneity) of a pathological condition such as asthma allowed a more precise estimation of the asthma effects on the acoustic properties of the tracheobronchial tree. This is to be considered the first attempt towards a future clinical application, with the aim to provide an insight into possible diagnostic markers. As a most evident result, it was observed that the asthmatic group was characterized by higher values of acoustic impedance and lower values of acoustic pressure with respect to the control group. The pathological induced alterations in terms of acoustic parameters were proved to be extremely statistically significant at low respiratory volume and low frequency, suggesting those two setting as the best standard to evaluate the presence of the pathology through the proposed model.

Thanks to the success of the validation procedure, the model described in this project was proven to effectively and accurately describe the acoustic response of the human tracheobronchial tree to a known input acoustic pressure over a defined frequency range. In addition to that, the computational time of the analytical code in MATLAB was extremely fast (around 7.16 seconds, visualization included) for a multifrequency analysis, if compared to the finite element simulations where, more than one hour was required, to obtain result for frequencies ranged from 200 Hz to 800 Hz. The preliminary and simplified simulations of some pathological conditions demonstrated that the model was sensitive to the pathology-induced alterations in the case of the fibrosis and pulmonary infiltration and able to provide specific markers for those conditions. For the asthma case it was proved that, given the complexity of the pathology, a mono-parametric simplification of the model might not be suitable. Comparing the preliminary and ineffective simulations to the results obtained from the application of the model to real pathological data, it was evident that relying on a more rigorous approach allowed

not only to collect more information, but in the case of asthma influences the possibility of the model to be even sensitive to the pathology.

The road towards a possible clinical application is long and the model will need further investigations especially in terms of coupling with the lung parenchyma and with the chest wall as well as in terms of accuracy of the geometries generated for the simulations. It is also important to remark that the proper modeling of the acoustics of the respiratory system is still an open field of research. Nonetheless, in a long-time perspective the model proposed in this work might eventually support clinicians in their everyday practice of diagnosis providing a useful and immediate comparison with the auscultation technique.

SOMMARIO

La auscultazione è stata usata per centinaia di anni dai medici per diagnosticare e monitorare la progressione delle patologie polmonari in maniera qualitativa. Questa tecnica si basa sulla evidenza clinica che le alterazioni morfologiche e funzionali del sistema respiratorio indotte da malattie e lesioni risulti in cambiamenti misurabili nella generazione e propagazione di suoni. Secoli di applicazioni clinica hanno condotto ad una esaustiva individuazione e catalogazione dei suoni respiratori e delle loro alterazioni a seguito dell'insorgere di patologie. Nonostante ciò, le informazioni raccolte in questi anni mancano del rigore di una quantificazione oggettiva così come di una adeguata comprensione dei fenomeni coinvolti. La descrizione in termini quantitativi degli effetti sulla propagazione del suono delle alterazioni indotte a livello strutturale e meccanico ha ricevuto, discutibilmente, ancora meno attenzione. Una migliore comprensione di questi fenomeni sarebbe di grande valore non soltanto in termini di interpretazione e significatività clinica, ma anche da un punto di vista della ricerca.

Questo progetto è frutto di una collaborazione con la University of Illinois at Chicago e si pone come obbiettivo a lungo termine quello di creare un modello computazionale capace di imitare in maniera precisa la creazione, la propagazione e la misurazione non invasiva dei suoni fisiologicamente associati al sistema respiratorio e delle alterazioni legate alle patologie.

In linea con l'obbiettivo generale appena specificato, questo progetto è stato diviso in due parti. Nella prima parte di questo lavoro, nel contesto del Acoustics and Vibration Laboratory della University of Illinois at Chicago, è stato validato, tramite analisi agli elementi finiti, un codice analitico in MATLAB® ed è stato dimostrato come tale codice sia in grado di fornire informazioni accurate e quantitative circa la propagazione di suoni in tratto respiratorio inferiore in uno specifico range di frequenze (200-800 Hz). Il modello assume di dare in ingresso una pressione nota a livello della trachea: ciò che viene valutata è la risposta del

sistema in termini di propagazione delle onde acustiche alle diverse frequenze. La procedura di validazione del modello è stata effettuata in condizioni fisiologiche per un singolo soggetto. La geometria dell'albero tracheale è stata generata a partire da dati ottenuti tramite CT nelle fasi iniziali di inspirazione ed espirazione del ciclo respiratorio.

Il modello è stato successivamente modificato per simulare, seppur in maniera approssimativa, le alterazioni indotte da tre specifiche patologie quali l'asma, una condizione di fibrosi generalizzata e un grave infiltrato polmonare monolaterale. Nel caso dell'asma è stata ipotizzata una broncocostrizione omogenea a livello delle piccole vie respiratorie; nel caso della fibrosi è stato incrementato il modulo elastico delle pareti delle vie respiratorie di un fattore 5; nel caso dell'infiltrato polmonare si è aumentata l'impedenza terminale del lobo interessato (il lobo inferiore sinistro) di un fattore 10^5.

Questi approcci, seppur estremamente semplificati, hanno permesso una prima analisi degli effetti di tali patologie sulla propagazione del suono all'interno dell'albero tracheobronchiale. Nei casi di fibrosi e di infiltrato polmonare, è stato dimostrato che un approccio modellistico delle patologie con alterazioni di un solo parametro (geometrico o meccanico) induce notevoli alterazioni nella risposta acustica del sistema. L'incremento di rigidezza delle pareti delle vie respiratorie, caratteristico della condizione fibrotica, ha causato una maggiore penetrazione all'interno dell'albero tracheale della pressione acustica. La simulazione dell'infiltrato polmonare ha rivelato che tale condizione modifica in maniera marcata la distribuzione della pressione acustica determinando un incremento dei valori a livello delle vie respiratore localizzate nella parte di polmone interessata. La simulazione dell'asma attraverso l'approccio semplificato descritto in precedenza non ha fornito risultati soddisfacenti dal momento che la distribuzione della pressione acustica è rimasta sostanzialmente inalterata.

Nella seconda parte del progetto, sviluppata nel Laboratorio di Tecnologie Biomediche del Politecnico di Milano, il modello è stato testato su dati reali acquisiti di soggetti sani e asmatici.

Le geometrie sono state ricavate ad alti e bassi volumi polmonari e l'analisi effettuata sia ad alte che basse frequenze. Questo approccio più rigoroso alla simulazione della complessità (ed eterogeneità) di una condizione patologica quale l'asma ha permesso una stima più precisa degli effetti di tale patologia sulle proprietà acustiche dell'albero tracheobronchiale e deve essere considerato un primo passo verso una futura applicazione clinica con lo scopo di fornire possibili indicatori diagnostici.

Come risultato più evidente, è stato osservato che il gruppo di soggetti asmatici era caratterizzato da valori maggiori di impedenza acustica e valori minori di pressione acustica se confrontati con il gruppo di controllo. Le alterazioni indotte dalla patologia sono risultate particolarmente rilevanti da un punto di vista statistico a bassi volumi respiratori e basse frequenze, suggerendo queste due condizioni come il migliore standard per valutare la presenza della patologia attraverso il modello proposto.

Grazie al successo della procedura di validazione, si è dimostrato che il modello proposto in questo progetto è in grado di descrivere efficacemente e accuratamente la risposta acustica dell'albero tracheobronchiale umano ad una pressione acustica in un definito range di frequenze. Inoltre, il tempo di calcolo per il codice analitico in MATLAB si è dimostrato estremamente ridotto (circa 7.16 secondi, visualizzazione inclusa) per un'analisi multifrequenza, se confrontato con le simulazioni agli elementi finiti che richiedono più di un'ora, per ottenere risultati per frequenze incluse tra 200 Hz e 800 Hz.

Le simulazioni preliminari e semplificate di alcune condizioni patologiche hanno dimostrato che il modello è sensibile alle alterazioni determinate dalle patologie nel caso di fibrosi e infiltrazione polmonare ed è anche in grado di fornire alcuni specifici indicatori per tali condizioni. Nel caso dell'asma, è stato verificato che, data la complessità della patologia, una semplificazione eccessiva potrebbe non essere adeguata. Comparando le simulazioni preliminari e, di fatto, inefficaci con i risultati ottenuti dall'applicazione del modello a dati

reali, è risultato evidente come, l'utilizzo di un approccio più rigoroso ha permesso non solo di raccogliere maggiori informazioni, ma anche di influenzare la sensibilità stessa del modello alla patologia.

La strada verso una possibile applicazione clinica è lunga e il modello necessita di ulteriori indagini, sia in termini di estensione del modello al parenchima polmonare e alle pareti della cassa toracica, sia in termini di accuratezza delle geometrie generate per le simulazioni. Ciò non di meno, in una prospettiva a lungo termine questo modello potrebbe supportare i medici nella loro pratica quotidiana di diagnosi, fornendo un immediato termine di paragone con la tecnica di auscultazione.

CHAPTER 1

INTRODUCTION

1.1 Background & Motivation

The basic principle of auscultation is the knowledge that pulmonary pathologies generally lead to morphological and functional alterations in the lungs and airways morphology which eventually result in measurable changes in breath sound generation and propagation. Auscultation performed with stethoscopes has been used for hundreds of years and still today represents the most common and immediate way for diagnosis purposes based on the changes of breath sounds. However, this technique presents some limitations related to the fact that it is highly skill dependent and subject to inter and intra observer variability. Furthermore, it can only provide qualitative information and exclusively at a single location. Over the last few decades an increasing interest in a quantitative characterization of the sound generation and propagation in the respiratory system has led to a constant effort towards the generation of proper mechano-acoustical models to represent these phenomena. The first challenge to be faced was the natural geometrical complexity of the branching system that characterizes the human tracheobronchial tree. Both Strahler et al. and Horsefield et al. [1] proposed a model able to properly quantify the complexity and asymmetry of the branching pattern of the bronchial tree, with the latter being able to represent a higher order branching system. Wodicka et al. [2] elaborated a model of sound propagation from inside the respiratory tract to the thorax surface caused by wall motion in large airways. To model the wall structure and dynamics, the analogy with an electrical distributed parameters model (transmission line) was used and the system was simplified to account for the first five generations of the bronchial tree. Jackson et al. [3], [4] studied the frequency dependency of the acoustic impedance of the subglottal

respiratory tract, Habib et al. [5] managed to identify the constituent relations to relate the alterations of the acoustic impedance to the airway geometry and the airway wall mechanical properties. In Royston et al. [6] sound propagation from trachea to thorax surface in healthy and pneumothorax conditions was simulated. Dai et al. [7], [8] studied both numerically and experimentally the sound transmission in the lungs.

In this work an analytical model of the sound propagation based on the considerations of Royston et al. [6] will be to applied to airway trees generated by anatomical images collected at different phases of the respiratory cycle. The model assumes to input a known pressure at the inlet of the trachea: what is evaluated is the response of the system to the inlet pressure in term of propagation of the acoustic waves over different frequencies. In the first instance, the analytical model, developed in MATLAB (r2016a, The MathWorks Inc., Natick, MA, 2016) by Brian Henry [9] in the context of the "Audible Human Project" (AHP), will be validated via numerical simulations in COMSOL Multiphysics® (COMSOL Multiphysics® v. 5.2a, www.comsol.com, Stockholm, Sweden) in the physiological conditions for a single subject with the bronchial tree generated at the beginning of both the inspiratory and expiratory phases of the respiratory cycle. This procedure will also allow a preliminary comparison, in terms of acoustic pressure distribution, between the two different respiratory phases taken into consideration.

Successively, the morphometry of the same two trees and the mechanical properties of the airways will be modified to simulate some pathology-induced alterations of the architecture of the airways and the sound propagation will be analyzed under those circumstances. The effect of the alteration of one or more parameters simulating the pathology of asthma and the conditions of a generalized fibrosis and pulmonary infiltrate will be presented.

Finally, the model will be applied to data recovered from five asthmatic patients to determine the sensitivity to real pathological data and to identify one or more specific parameters to be

used as markers of the pathological condition with respect to a reference control group composed of five healthy subjects. This approach will provide a further step towards a possible clinical application of the model.

The long-term goal of this project is the creation of a computational model able to precisely mimic the creation, propagation and non-invasive measurement of naturally-occurring sounds associated airway physiology as well as the alterations induced by airways pathology. Such a comprehensive computational model would have a significant impact on medical education and research. From a research-oriented point of view, the enhanced understanding of waves propagation within the airways will allow to couple this computational approach to new emerging imaging techniques and, specifically, to magnetic resonance elastography (MRE).

1.2 Anatomy of the Human Respiratory System

The respiratory system supplies the body with the oxygen necessary for its physiological activity and expels the byproducts of this activity in form of carbon dioxide. In the term respiration four distinct and fundamental processes are involved [10]:

- Pulmonary ventilation, consisting in the addition to or removal from lungs of the volume of gas;
- External respiration, a process taking place in lungs by which blood is recharged with oxygen and discharged with carbon dioxide;
- Transport in which oxygen is moved from lungs to tissues and carbon dioxide from tissue to lungs;
- Internal respiration which consists in the gas exchange between systemic blood vessels and tissues at a peripheral level.

Figure 1 shows the gross anatomy of the respiratory system.

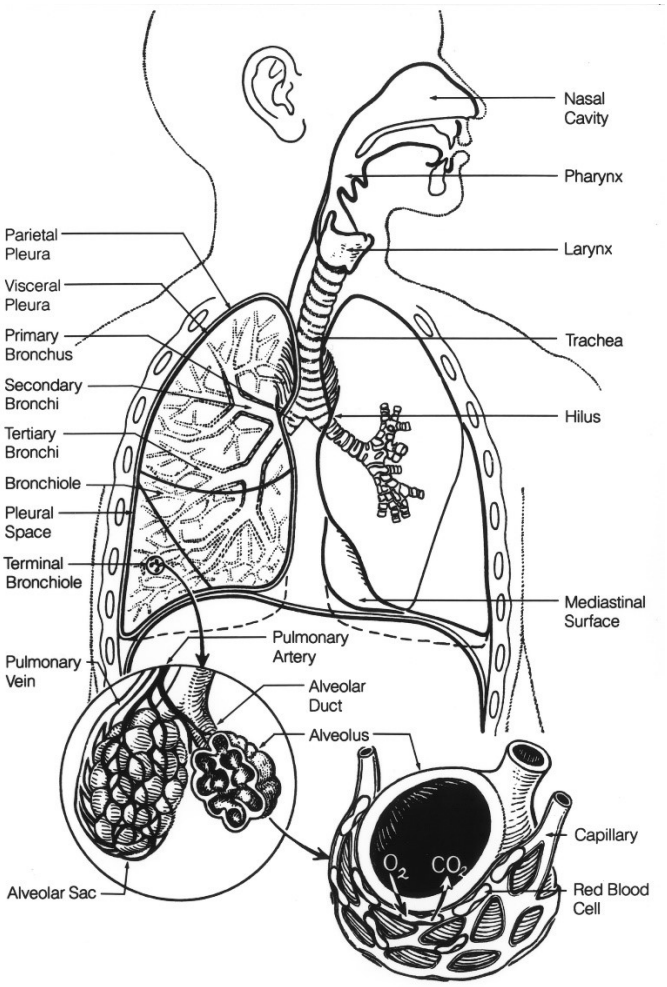

Figure 1: Schematic representation of the respiratory system (image adapted from http://organanatomy.com)

The respiratory system is generally divided into two main parts: the upper and the lower tract. The upper respiratory system includes the nose with its nasal cavity, the paranasal sinuses, the pharynx and the larynx. This portion of the ventilatory tract has the main aim of filtering out foreign materials from the inhaled air, warming it to body temperature and finally humidifying it [11]. These steps are fundamental for the proper functioning of the whole system and to prevent any possible damage to the lower respiratory tract. The lower respiratory tract includes the trachea, the lungs, the bronchi and the alveoli. Because of its importance in sound propagation the lower respiratory tract will be the object of further detailed descriptions (see

Section 1.2.1). In addition to those components, the muscles and bones of the thorax will be briefly described in Section 1.2.3.

1.2.1 The Lower Respiratory Tract

As mentioned above, the lower respiratory tract is made up of trachea, the lungs, the bronchi and the alveoli. The trachea is a conduit with length approximately ranging between 12–14 cm, descending from the larynx, through the neck, into mediastinum which is space in the thoracic chest surrounded by the lungs (sides), the spine column (rear) and the sternum (front). The trachea wall is supported and reinforced by sixteen to twenty U-shaped rings of hyaline cartilage joined by fibro-elastic connective tissue as well as by bands of smooth muscles. The anterolateral wall with the cartilaginous rings and the posterior fibromuscular membrane compose the two main regions of the tracheal wall. Despite its structure, the tracheal conduit remains flexible allowing the tracheal size and shape to vary in accordance with neck and head motions. The walls are lined internally by mucosa [12]. The dimensions and configuration of the trachea are also modified by the respiration, especially when ample thoracic displacements occur. The tracheal anatomy is also subjected to a great inter-subject variability. In adult males, the tracheal external diameter is around 1.3-2.5 cm and 1.3-2.7 cm in the coronal and sagittal plane respectively [13] [14] whereas in adult females the same diameters are approximately 1.0-2.1 cm and 1.0-2.3 cm [12][14][15] .

At the level of the fourth thoracic vertebra, the trachea branches into a pair of primary bronchi, one bronchus to each lung. The main stem bronchi are asymmetrical structures: in particular, the left bronchus has a diameter of 10–14 mm and a length of approximately 50 mm whereas the right bronchus is generally larger, but shorter (diameter ranging between 12–16 mm, and length approximately equal to 25 mm) [11]. In general, the branching angle of the left bronchus is sharper (25°- 30° circa with respect to the midline) than the right one

(approximately 45° from the midline) [13]. The generation of branches of different diameter and unequal length is defined as irregular dichotomy. Because of this asymmetry, at the level of the division region it is possible to recognize a transition zone. Each stem bronchus enters the respective lung. After entering the respective lung, the main bronchus generates the lobar bronchi (superior, middle and inferior). From the lobar bronchi the tertiary bronchi (called also segmental bronchi) arise, followed by the sub-segmental bronchi and by the terminal bronchi [16]. As far as the structure is concerned, the bronchus wall is made up of five layers: a mucosa, a muscular, a submucosa, a fibrocartilaginous layer and a peri-bronchial stratum. This wall structure is a function of the size of the bronchi. For large bronchi the structure of the wall resembles the one of the tracheal wall with the peculiarity that the cartilaginous rings completely surround the wall [17]. On the contrary, for bronchi of medium size the walls have more irregular (sometimes helical) cartilaginous rings and, situated between the muscle and the fibrocartilaginous layer, a venous plexus can be recognized.

The bronchioles arise from the terminal bronchi. There are three to four generations of bronchioles which eventually lead to the terminal bronchioles [11]. Each terminal bronchiole divides to form either another terminal bronchiole or a respiratory bronchiole which are the narrowest and smallest airway aimed at the transport of air to and from the alveolar ducts. Because of the presence of some alveolar structures, gas exchange (in minimal part) already takes place in the respiratory bronchioles. The number of alveoli lining the bronchioles walls tends to increase moving closer to the alveolar ducts [10]. These ducts are completely covered by alveoli as their wall can be seen to be constituted of exclusively by entry tips of alveoli.

At least five or more ramifications of alveolar ducts have been described. Those ducts terminate into the alveolar sac which is the closed end and final (distal) airway. As regard the structure, the bronchiolar wall can be subdivided into three layers: one layer of mucosa, one of muscle fibers (the thickest) and a thin outer layer made of connective tissue which is connected to the

lung parenchyma and tends to disappear in small bronchioles. This entire structure is lined by an epithelium that stops at the entrance of the alveoli [11]. The alveoli are the basic structures of the lung deputed to gas exchange. The dimensions and shape of the alveoli are subject to a certain variability, but they can be approximated as spherical objects sized between 150–300 μm. The alveolar space is separated from the pulmonary capillary by an extremely thin (thickness 0.2 μm) barrier. Gas exchange between oxygen (O_2) and carbon dioxide (CO_2) occurs by simple diffusion, in a process which lasts approximately 0.25 s and is extremely efficient thanks to huge number of alveoli (estimated around 300 millions) which creates an exchange surface approximately equal to 80 m^2 [11].

To conclude, the airways divide by asymmetric dichotomous branching which implies that, although the division of a segment into two daughter branches is common, it still exists a certain variability in both the size and the number of the branches [16]. As a general statement, it can be inferred that the higher the generation number, the narrower and the shorter are the respiratory conduits. It is also verified that the number of conduits increases accordingly to the generation level. TABLE 1 reports some noteworthy features of the human lower respiratory tract.

Approximately 23 generations of branches are identifiable starting from the trachea down to the alveoli. These generations are generally categorized in three zones [12]:

1. Conductive Zone: beginning with the trachea corresponding to generations 0-16;
2. Transitory Zone identifiable with the respiratory bronchioles (generations 17-19);
3. Respiratory Zone: composed by alveolar ducts and sacs (generations 20-23).

TABLE 1: GEOMETRICAL FEATURES OF HUMAN LOWER RESPIRATORY TRACT

	Human
Anatomy	Right Lung: 3 lobes Left Lung: 2 lobes
Diameter of the trachea [mm]	13-27
Diameter of the main bronchus [mm]	10-16
Diameter of the bronchiole [mm]	< 1
Diameter of the terminal bronchiole [mm]	0.6
Diameter of the respiratory bronchiole [mm]	0.5
Diameter of the alveoli [mm]	0.2-0.4

1.2.2 Gross Anatomy of Lungs

The lungs are cone-like organs primarily deputed to respiration. Humans are characterized by the presence of two lungs: right lung and left lung. The structure of each lung is characterized by the presence of a spherical apex which extends into the root of the neck, a convex upward base in the lower part, 3 borders (inferior, anterior and posterior), and 2 faces (the coastal one, pointing outward and the mediastinal one which is internal and with pericardial depression). The diaphragm lies under the base of each lung.

The right lung has three sub-sections, named lobes (lower, middle, upper). The left lung has only two lobes (lower and upper). The separation among lobes is determined anatomically by fissures. Pulmonary lobes are sectioned into segments, segments into lobules. The right upper lobe has three segments (posterior, anterior, apical); the right middle two (lateral, medial), the right inferior five (superior, anterior basal, lateral basal, posterior basal, medial basal). Two

compartments can be identified in the left upper lobe: superior and inferior (or lingular) which consists of three segments (posterior, anterior and apical) and two segments (inferior and superior), respectively. The left lower lobe includes five segments (superior or apical, lateral and medial basal and anterior and posterior basal). TABLE 2 adapted from [11] summarizes the structure of the human lungs. Although the left lung, contrarily to the right one, is not anatomically characterized by a middle lobe, it does show a corresponding feature. Indeed, it can be observed a protuberance of the upper lobe which goes under the name of lingula. This projection on the left lobe can be considered as an anatomical counterpart to the right middle lobe. Both lungs at their root show a central recession called hilum, where both the airways and blood vessels enter and exit the lung [11]. The septa and sheaths among the pulmonary compartments (lobes, segments, lobules, and acini) and among the alveoli are interconnected thanks to the lung parenchyma. The lung parenchyma is the essential tissue of the lungs, and is generally described as a three dimensional deformable tissue network [11]. The pulmonary parenchyma is enclosed by the visceral pleura to which is also attached. Two pleurae are present in the lungs: the visceral pleura which covers the surface of each lung and dips into the cavity between the lobes and the parietal pleura, which is the outer membrane attached to the thoracic cavity. The parietal pleura also separates the pleural cavity from the mediastinum that is the cavity located between the vertebral column, the sternum and the lungs, containing the heart and its and the related circulatory vessels, the esophagus, the thymus, the esophagus, the first two generations of the airway tree (namely trachea and main bronchi) and the vessels related to the lymphatic circulation. The two pleurae are separated from each other thanks to a thin (20–80 μm) fluid space which allows the two layers to slide without restrains one with respect to the other [11]. The pleural fluid is generated from parietal pleura itself and reabsorbed by the lymphatic system, this process results in a total volume of fluid ranging between 25-30 cm^3 [10], [11]. Several functions are associated to the pleural fluid. First, it creates a moist, slippery

surface which allows the opposing membranes of the pleurae to slide across one another as the lungs move within the thorax. Second, it holds the lungs tight against the thoracic wall therefore avoiding the collapse of the whole structure [10].

1.2.3 Respiratory Muscles and Bones

The thorax is bounded by the bones of the spine and rib cage and their associated muscles. The joint structure of muscles and bones goes under the name of thoracic cage. The side and the top of the thoracic cage are formed by the chest wall (i.e. the ribs and the spine), while on the back side the thoracic vertebrae from T2 to T12 and the vertebral column are located. The musculature of the thorax includes the intercostal muscles and the diaphragm. During inspiration, the contraction of both the muscles is observed. This causes the diaphragm to move down and the ribs cage to rise. In this way, when the air is sucked into the lungs, thoracic cavity is enlarged. The increasing volume of the thoracic cavity causes a drop in the pressure around the lungs and their consequent expansion. During expiration, the relaxation of the muscles causes the reverse process. For this reason, the quiet expiration is assumed to be passive, the inspiration is active (in other words the contraction of the muscles is involved) [18].

TABLE 2: LUNGS LOBES AND SEGMENTS

Lung	Lobe	Segments
Right	Upper	Apical
		Anterior
		Posterior
	Middle	Medial
		Lateral
	Lower	Superior Basal
		Medial Basal
		Anterior Basal
		Lateral Basal
		Posterior Basal
Left	Upper	Apical
		Anterior
		Posterior
	Lower	Superior Basal
		Medial Basal
		Anterior Basal
		Lateral Basal
		Posterior Basal

1.3 Pathologies of the Airways Tree

The pathologies considered in this dissertation are asthma, generalized fibrosis and pulmonary infiltrate. In the following paragraphs a brief description of the modification induced at the level of the respiratory system by those pathologies is provided. In relation to the further developments in this work, the attention is focused on the pathology-induced alterations in terms of mechanical and geometrical properties at a macroscopic level. The cellular modifications at the microscopic level, as well as the pathogenesis of the disease in terms of cellular response will be not be described.

1.3.1 Asthma

The clinical significance of asthma has remarkably increased over the last decades [19]. The latest estimates by the Center for Disease Control and Prevention (CDC) indicate that roughly 1 American over 13 is affected by this pathology, resulting in a total number of approximately 24.5 million of subjects. This impressive number corresponds to 7.4 and 8.6 percent of adults and children population of the United States of America, respectively. For this reason, asthma is nowadays considered one of most diffused and costly disease in the US.

Despite its relevance, the pathogenesis of asthma still is not fully understood [19]. In a very generic and simplified description, asthma can be referred as an inflammatory pathology affecting the small airways (i.e. airways with a diameter smaller than 2 mm). Indeed, *ex vivo* examination of airways of patient who died of asthma has shown an airway lumen severely occluded by mucus plugs made up of glycoproteins generated from epithelial cells and plasma proteins exuded from airway vasculature. The mechanism of generation of the inflammatory process will not be discussed in this dissertation. The three most common and characteristic features of asthma are the following [19]:

1. airways inflammation;

2. mucous hypersecretion;
3. airways hyper-responsiveness.

The result of the combination of these factors is bronchoconstriction and airflow obstruction. An average value of reduction of the airway diameter in asthma can be approximated around the 50/60 % [20]. The duration and severity of the pathology can deeply affect wall thickening and consequently the level of constriction [21].

Although the three conditions mentioned above are theoretically reversible in their initial stages, if the pathology is not stopped in its progression those changes tend to become permanent leading to the process of airway remodeling which is a term used to refer to the alterations in composition, quantity and organization of the constituting elements of the airway wall. Consequently, even if most attention has been focused on the acute inflammatory phase of this disease, it is important to remark asthma is a chronic disease. The general features recognizable in patients with airway remodeling are an increment of tissue under the epithelium of the airway wall, a thickening of the wall itself and hypertrophy of the smooth muscle.

The clinical most significant consequence of asthma is, as already mentioned, the obstruction of the airway lumen. This constriction causes the resistance of the airway to increase and consequently, per Heigen-Poiseuille Law, a reduction of the airway flow to the lungs.

In this situation, in order to restore the flow some compensatory mechanisms take place [19]:

1. increment of the tension generated by the inspiratory muscles;
2. hyperventilation.

Although temporarily effective, over a long period the mechanisms mentioned above cause an increased work of breathing associated to the inspiratory phase, complicated also by dynamic hyperinflation of the lungs (it is important to remember that at high volumes the respiratory muscles can generate less power determining the so-called length-tension inappropriateness).

The reduction of the airway flow can also affect the oxygenation of the lungs. In general, the human body, can compensate for this effect by redirect the blood flow from the constricted areas to the healthy ones. This phenomenon goes under the name of hypoxic vasoconstriction and it can only happen because asthma is a heterogeneous disease process, which can severely affect some areas of the lungs, while leaving other areas relatively normal. Hyperventilation and hypoxic vasoconstriction generally prevent the oxygen level from becoming critically low, nonetheless when the bronchoconstriction is severe those two mechanisms cannot be sufficient to guarantee a correct oxygen distribution, causing symptoms of dyspnea in the patients. Some of the most common symptoms of asthma are here listed below:

- Shortness of Breath;
- Cough;
- Chest Tightness;
- Dyspnea;
- Mucus Production;
- Wheezing.

1.3.2 Fibrosis

In its general meaning, the term fibrosis refers to the growth of fibrous connective tissue as a restorative response to trauma or damage. This tissue deposition can occur as a part of the physiological healing process meant to the reestablish the normal structure and function of the damaged tissue or, when excessive and uncontrolled, can be associated to different pathological processes. In its pathological form, fibrosis is determined by an abnormal accumulation of extracellular matrix (ECM) proteins results in scarring and stiffening of the affected tissue, which end up interfering with the normal functioning of the tissue.

Airways fibrosis is associated with a variety of pathologies among which asthma, chronic obstructive pulmonary disease and cystic fibrosis can be mentioned [22]. From what stated above it is clear that airways fibrosis needs to be analyzed considering the complexity of the clinical picture of the mentioned pathologies. However, it is also verified that by itself fibrosis of the airways causes a remarkable stiffening of the airways wall which results in the modification of the physiology of the whole respiratory system [23].

1.3.3 Pulmonary Infiltrates

The term "pulmonary infiltrate" was born in the radiological clinical practice to generically describe any sort of blockage in the air space of the lungs that is recognizable on a radiology scan. The causes the blockages can generally include any substance foreign to the lung that progressively accumulates and eventually occludes an air space. They can also be ascribed to naturally-occurring substances in the lung that accumulate in a quantity greater than the physiological condition. Pulmonary infiltrates lead to increased soft tissue density of the lung, that is easily observable on a scan and to a reduction of the respiratory capacity of the subject. Although the causes of the infiltrations can be both infectious and non-infectious, pulmonary infiltrates are most commonly associated with the condition of pneumonia [24]. Other possible causes can be acknowledged such as acute respiratory distress syndrome, atelectasis, tuberculosis and the prolongated exposure to radiotherapy as a consequence of breast or lung cancer [23], [25]. Recently also sickle cell disease has been demonstrated to be a likely cause of this pathological condition [26]. The pulmonary infiltrates are generally localized in one lobe, even though they can also affect more lobes at the same time. The lobe(s) involved can be either be either localized on the same lung (unilateral infiltrate) or on different lungs (bilateral infiltrate). The position and the dimension of the infiltrate can vary significantly according to the severity of the pathology. In general, the alveoli and the terminal branches are

the locations that are more likely to be affected. However, in case of severe pathologies the increase resistance of the last generations, can affect also medium sized airways and eventually prevent the air from sufficiently propagating in an entire lobe.

1.4 Abnormal Breath Sounds and Pathologies

In accordance to their acoustic properties, respiratory sounds are categorized into normal and abnormal (or adventitious). Normal respiratory sounds are the ones generated in healthy airways and lungs by physiological unforced breathing. Normal respiratory sounds are generally subdivided in tracheobronchial and vesicular, the former are heard at the level of the trachea, the latter over the thorax [27]. The deficiency of the normal breath sounds or the manifestation of adventitious (i.e. superimposed to normal sounds) breath sounds can be symptom of a pulmonary disease. For this reason, the ability to discriminate between normal respiratory sounds and adventitious ones is fundamental for an accurate medical diagnosis. The analysis of the respiratory sounds allows to obtain invaluable information regarding the physiopathology of lungs and airways [28]. As shown in Figure 2, thanks to clinical practice it is nowadays possible to associate the presence of a given breath sound to one or more pathologies. The integration of these information with the analysis of the overall medical case, results in an effective way to diagnose pathologies.

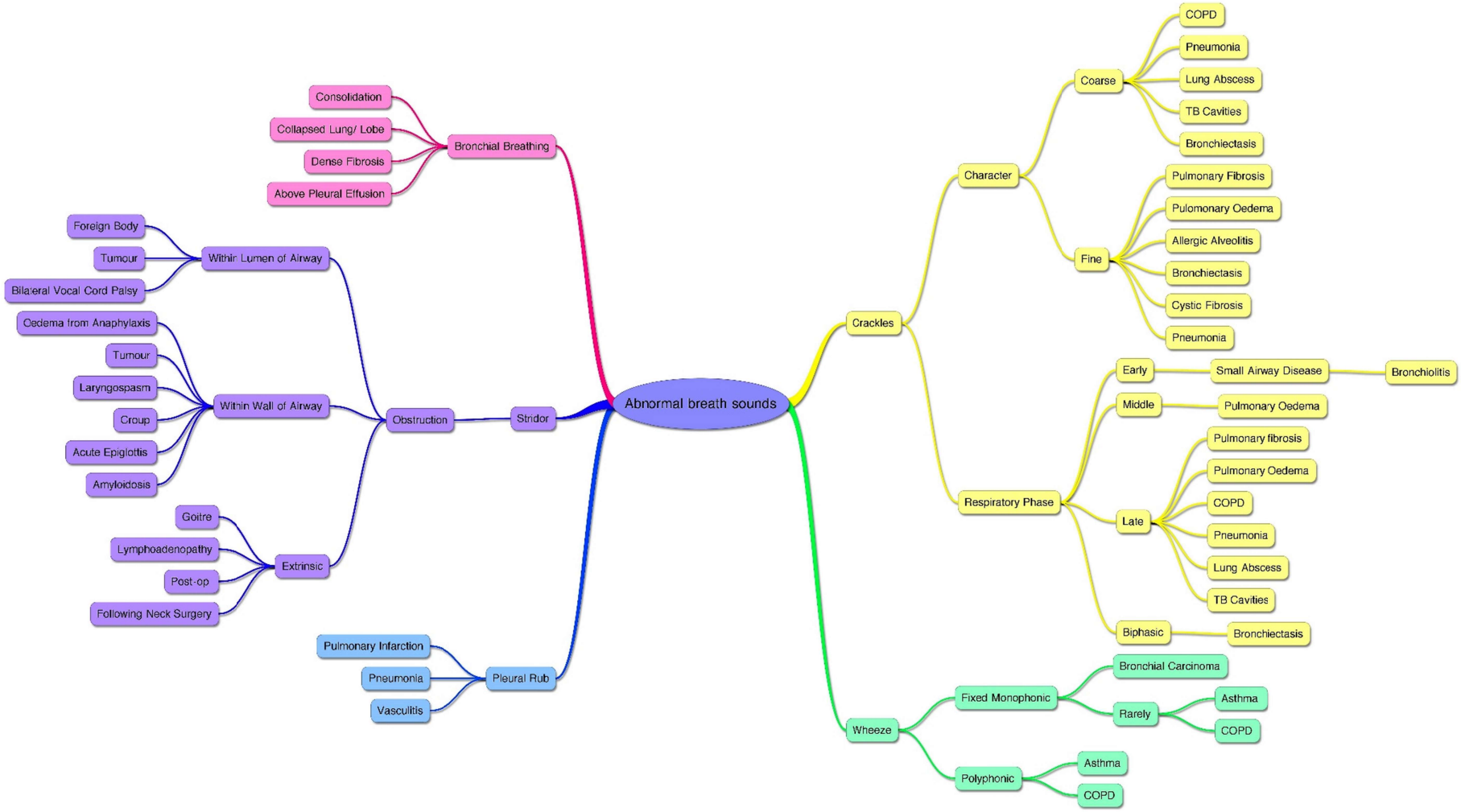

Figure 2: Schematics of the abnormal breath sounds and associated pathologies

1.4.1 Crackles

Crackles (also known as crepitations) correspond to short, discontinuous and non-stationary sounds [28]. They are generated when airways that were abnormally closed (due to accumulation of secretions or to airway collapse) open in the inspiration phase. The sudden opening of an obstructed airway causes an immediate re-equilibration of the pressures on both sides determining peculiar vibrations in the airway walls. They can be heard also during expiration, though this is far less common to happen [29]. Fredberg et Al. [30] suggested that the cross-section of the airways which are subject to the sudden closing and opening is one of the possible factors affecting the character of crackling sounds. Crackles are generally distinguished in [29]:

- Fine Crackles which are characterized by a shorter duration (around 5 ms) and a higher pitch. Often, they are also repetitive. Typical frequency is around 650 Hz. From the clinical point of view, they usually start in the basal part of the lung. They are altered by body position change, but not by coughing and they are not transmitted to mouth.

- Coarse Crackles which are characterized by a longer duration (15 ms) and a lower pitch. Typical frequency is around 350 Hz. From the clinical point of view there is no a specific location where the sound starts, however it can be altered by coughing (but not body position changes) and it can be transmitted to mouth.

- Biphasic Crackles which are a combination of coarse and fine crackles.

Although some reference values of the characteristic frequency have been mentioned, it is important to observe that, in general, the frequency range of crackles is extremely broad and

ranges between 300 Hz and 1000 Hz. It is also verified that fine crackles have a higher frequency content with respect to coarse crackles, extending up to 2000 Hz [29]–[31].

From a clinical perspective, the classification of the American Thoracic Society (ATS) is adopted: fine and coarse crackles are categorized considering two time domain parameters 2CD (two Cycle Duration) and IDW (Initial Deflection Width) [29]. 2CD is the duration of a crackle from the beginning of the initial deflection to the end of two cycle whereas IDW is the length of time of the first deflection in a crackle waveform. Those parameters as well as other more qualitative information are reported in TABLE 3.

TABLE 3: CLASSIFICATION AND FEATURES OF CRACKLES

	Intensity	**Pitch**	**2CD duration**	**IDW duration**
Coarse crackles	Loud	Low	About 10 ms	About 1.5 ms
Fine crackles	Less loud	Higher	<5 ms	About 0.7 ms

Crackles are associated to a variety of pathologies like bronchiectasis, chronic obstructive pulmonary disease (COPD), edema and fibrosis [28], [29], [32], [33].

1.4.2 Wheezes

Wheezes are adventitious and continuous sounds which are heard at end of the inspiratory phase or in the early expiratory phase. They can be considered the result of the gradual reopening (during inspiration) or closure (during expiration) of a collapsed airway lumen. The reduction of the cross-section of the airway lumen causes the air flow velocity to increase, generating a harmonic vibration of the airway wall. It is suggested that their generation is more likely to happen between generations 2-7 of the tracheobronchial tree [32]. Their duration is between 100 ms and 250 ms and they are generally represented as sinusoidal oscillations. The average

frequency content is located between 100-1000 Hz and with some harmonics that can occasionally go far beyond 1000 Hz [31]. The application of theoretical models of flutter in a flow-limited collapsible conduit shows that the frequency of wheezing could be affected by parameters like the airway wall bending elasticity, thickness and the tension in the longitudinal direction [34].

Wheezes are divided in high pitched wheezes and low-pitched wheezes. In clinical practice, it is common the association of high and low pitch wheezes with diseases of the small and large airways, respectively. However, there are few experimental evidences to confirm this association. A second distinction can be made between monophonic and polyphonic wheezes: the former has a single pitch and tone localized in a specific area, the latter show multiple pitches and tonal qualities distribute over a certain area of the lung.

Wheezes can be generally detected in subjects affected by obstructive diseases, in particular asthma and COPD [32]–[35].

1.4.3 Stridor

Stridor are intense continuous monophonic sounds which can be best heard over extra-thoracic airways. Stridor tends to be more recognizable during inspiration due to the collapse of extra-thoracic airways because of the lower internal lumen pressure. The use of the stethoscope helps to identify the areas where the intensity is maximum, although in general stridor can be heard without any specific instrument. Clinical evidences show that the maximum intensity can be recognized at the level of the larynx or at the thoracic inlet. For this reason, stridor is usually considered as an indicator of upper airway obstruction. Signal analysis reveals that stridor have a sinusoidal waveform with fundamental frequency generally higher 500 Hz [28], [32].

1.4.4 Bronchial Breath Sounds

Bronchial breath sounds are blasting sounds and are audible throughout inspiration and expiration. They occur due to the lack of air in the lung tissue between the chest wall and the large airways. This is likely to happen in the consolidated lung of pneumonia or pulmonary fibrosis. They are commonly heard in the anterior part over the manubrium of the sternum and in the posterior part between the vertebrae C7 and T3. Generally, they show as a main feature a higher frequency content with respect to normal ones: this is because in consolidation phenomena causes a reduction of the low-pass filtering role of the alveolar region. In normal auscultation, they are very similar to normal tracheal breathing and therefore particularly difficult to recognize. For this reason, their clinical relevance is relatively low [32].

1.4.5 Pleural Rub

Pleural Rub is described as a creaking, coarse, grating or leathery sound. It is often localized over the lung bases (posteriorly). Pleural rub tends to recur at the same moment in each respiratory cycle, often in both inspiration and expiration: ordinarily, the expiratory component is specular to the inspiratory component. It is caused by friction between inflamed visceral and parietal surfaces of the pleura during breathing [32]. The duration of the signal is in the order of 200 ms and the typical frequency content is in the range 200-2000 Hz. Clinically speaking the sound is very similar to repetitive crackles and it almost impossible to distinguish between the two especially if the rub is limited to the inspiration phase, nonetheless pleural rub can be an indicator of pleural inflammation or pleural tumors [32].

1.4.6 Rhonchi

Rhonchi are defined as musical low-pitched sounds. They are characterized by rapidly damping periodic waveforms. The duration is generally higher than 100 ms and frequency content lower

than 300 Hz. They are generally associated with abnormal airway collapsibility and the creation of breach of fluid films. As they generally clear with coughing, clinical practice suggests that secretions in larger airways play an important role in generating these sounds. For the reasons mentioned above, rhonchi can be considered as indicators of airway lumen constriction associated with the thickening of the mucosa, edema or bronchospasm (e.g. bronchitis and COPD) [32].

1.4.7 Squawks

Squawks are defined as mixed sound since they are characterized by a crackle followed by short musical component (which resembles a wheeze). They are likely to occur in fibrotic pulmonary disorders. Acoustically, their waveform is similar to that of short wheezes, but they are often preceded by a crackle [9]. Squawks mean duration is approximately of 90–320 ms. Forgacs [36] suggested that squawks are produced when an obstructed airway abruptly opens in inspiration, while, for a short amount of time, the airway walls remain coupled one to the other in a mechanism very similar to the one responsible for the production of wheezes [9],[32].

1.5 Objectives and Structure of the Thesis

The objective of this project is to provide a first insight of the sound propagation in the tracheobronchial tree in normal and pathological condition. To achieve this goal an analytical model in MATLAB [9] is validated via numerical simulations in COMSOL Multiphysics® in the physiological conditions. Two respiratory phases are considered: the beginning of the inspiratory phase and the beginning of the expiratory phase. After the validation of the model, the morphometry of the trees and the mechanical properties of the airways are modified to simulate some pathology-induced alterations of the architecture of the airways and the sound propagation is analyzed under those circumstances. In particular, the effect of the alteration of one or more morphometrical parameters representative of the asthma pathology and of the conditions of generalized fibrosis and pulmonary infiltrate are presented. Finally, the model is applied to real pathological data obtained from five asthmatic subjects and compared to the results collected from a control group composed of an equal number of healthy subjects. In this phase, on one hand the sensitivity of the model to real pathological condition is evaluated, on the other hand it is analyzed the possibility to identify, in terms of acoustics parameters, specific markers of the pathology able to significantly differentiate the asthmatic population from the control one.

The introductory (Chapter 1) section briefly describes the anatomy of the respiratory system as well as the main features of the pathological conditions taken into consideration in this work. In Chapter 2, the theoretical model underlying the code used for the analysis is presented. The analytical model section (Chapter 3) presents the process of generation of the geometries and the settings of the analytical simulations: it is also explained how the model was modified to account for pathology-induced alterations and how the real pathological data were obtained. Chapter 4 deals with the numerical simulations used for the validation of the analytical model. The results both in terms of validation of the model and simulations of the

pathological conditions are reported in Chapter 5, together with the results concerning the application of the model to the asthmatic population and the comparison with the healthy one. Finally, the discussion of the results is developed in Chapter 6. The discussion is focused on the validation and the preliminary acoustic simulations as well as on the application of the model to the healthy and asthmatic population and their consequent comparison.

CHAPTER 2

THEORY

2.1 Acoustic Impedance

The general concept of impedance implies the ratio of a driving force to the correspondent velocity respond. The acoustic impedance Z is defined as the acoustic pressure P divided by the acoustic volumetric flow U. In the most general case, the acoustic impedance is a frequency-dependent value.

$$Z = \frac{P}{U} \tag{2.1}$$

For a chosen frequency, it indicates the amount of sound pressure which a given air vibration can generate. The SI unit of measurement for acoustic impedance is $Pa \cdot s/m^3$, also known as acoustic ohm. Another common notation is the one of specific acoustic impedance. In this definition, the normalization of the volume flow with respect to the cross-sectional area is included, thus obtaining:

$$z = \frac{P}{u} \tag{2.2}$$

Where u is the particle velocity.

The specific impedance, as well the volumetric one, is complex value and can expressed as:

$$z = r + jx \tag{2.3}$$

Where r and x denote the specific acoustic resistance and the specific acoustic reactance, respectively.

2.2 Impedance of a Sound Wave Propagating in Cylinder

The general case of a harmonic planar sound wave propagating in a cylinder will be now considered. This is a simplified base model which will be useful in further analysis. The hypothesis of rigid walls is introduced. It is also assumed that at a certain point $x = 0$ along the cylinder the acoustic impedance changes from Z_0 to Z_T as reported in Figure 3.

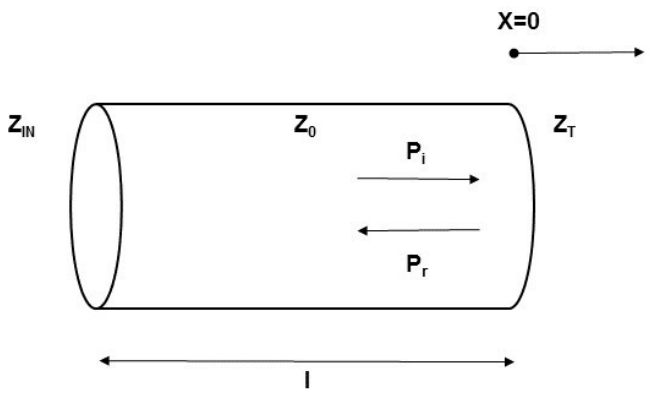

Figure 3: Exemplification of a Sound Wave Propaganting in a Cylinder

Considering a wave travelling in the positive x direction represented by:

$$P_i = Ae^{j(\omega t - kx)} \tag{2.4}$$

That reaches the above-mentioned point, it is known that a reflected wave propagating in the negative x direction will be generated. This wave will be described by the following equation.

$$P_r = Be^{j(\omega t + kx)} \tag{2.5}$$

In $x = 0$ the continuity of pressure and the continuity of the normal velocity must be satisfied. This implies:

$$P_i + P_r = P \tag{2.6}$$

and (given that the incident wave and the reflected wave generate two flows which have opposite directions):

$$U_i - U_r = U \tag{2.7}$$

By dividing (2.6) and (2.7) accordingly to the definition of impedance it holds:

$$Z = \frac{P}{U} = \frac{P_i + P_r}{U_i - U_r} \tag{2.8}$$

Recalling and inverting the definition of acoustic impedance, it is possible to write

$$U_i = \frac{P_i}{Z_0} = Y_0 P_i = Y_0 A e^{j(\omega t - kx)} \tag{2.9}$$

$$U_r = \frac{P_r}{Z_0} = Y_0 P_r = Y_0 B e^{j(\omega t + kx)} \tag{2.10}$$

The substitution of (2.4), (2.5), (2.9), (2.10) in (2.8) and the simplification of the term $e^{-j\omega t}$, lead to:

$$Z = \frac{P}{U} = \frac{Ae^{-jkx} + Be^{jkx}}{Ae^{-jkx} - Be^{jkx}} \tag{2.11}$$

The definition of the reflection coefficient R as the ratio between the pressure of the incident wave and the pressure of the reflected wave as expressed below,

$$R = \frac{P_i}{P_r} = \frac{Ae^{j(\omega t - kx)}}{Be^{j(\omega t + kx)}} \tag{2.12}$$

and the evaluation in $x = 0$, allow to write:

$$Z_T = \frac{A + RA}{\frac{A - RA}{Z_0}} = Z_0 \frac{1 + R}{1 - R} \tag{2.13}$$

Solving (2.13) for R:

$$R = \frac{Z_T - Z_0}{Z_0 + Z_T} \tag{2.14}$$

The generic impedance Z is dependent on the position on the tube and of chosen frequency can consequently be written as:

$$\begin{aligned} Z = \frac{P}{U} = \frac{Ae^{-jkx} + Be^{jkx}}{Ae^{-jkx} - Be^{jkx}} = Z_0 \frac{Ae^{-jkx} + RAe^{jkx}}{Ae^{-jkx} - RAe^{jkx}} = \\ = Z_0 \frac{Ae^{-jkx} + \frac{Z_T - Z_0}{Z_0 + Z_T} Ae^{jkx}}{Ae^{-jkx} - \frac{Z_T - Z_0}{Z_0 + Z_T} Ae^{jkx}} = \\ = Z_0 \frac{(Z_0 + Z_T)Ae^{-jkx} + (Z_T - Z_0)Ae^{jkx}}{(Z_0 + Z_T)Ae^{-jkx} - (Z_T - Z_0)Ae^{jkx}} \end{aligned} \tag{2.15}$$

By substituting in (2.15)

$$e^{-jkx} = cos(-kx) + jsin(-kx) = cos(kx) - sin(kx) \tag{2.16}$$

$$e^{jkx} = cos(kx) + jsin(kx) \tag{2.17}$$

It is possible to obtain

$$Z = \frac{P}{U} = Z_0 \frac{Z_T\, cos(kx) - Z_0 jsin(kx)}{Z_0\, cos(kx) - Z_T jsin(kx)} \tag{2.18}$$

Rearranging (2.18) and computing the impedance at the input of the cylinder (i.e. for $x = -l$)

$$Z_{IN} = Z_0 \frac{Z_T + Z_0 jtan(kl)}{Z_0 + Z_T jtan(kl)} \tag{2.19}$$

Recalling that the following equality holds:

$$jtan(kl) = tanh(jkl) \tag{2.20}$$

Equation (2.20) can be written as:

$$Z_{IN} = Z_0 \frac{Z_T + Z_0 tanh(jkl)}{Z_0 + Z_T tanh(jkl)} \tag{2.21}$$

Finally, by introducing the following relations:

$$\gamma^2 = -k^2 \tag{2.22}$$

$$\gamma = \alpha + j\beta \tag{2.23}$$

$$k = \beta - j\alpha \tag{2.24}$$

The input impedance in (2.21) can be expressed as:

$$Z_{IN} = Z_0 \frac{Z_T + Z_0 tanh(\gamma l)}{Z_0 + Z_T tanh(\gamma l)} \tag{2.25}$$

Or, equivalently,

$$Z_{IN} = \frac{Z_T + Z_0 tanh(\gamma l)}{1 + \frac{Z_T}{Z_0} tanh(\gamma l)} \tag{2.26}$$

For the discussion that will be done in this chapter it is useful to compute the acoustic pressure inside the cylinder, in particular it is possible to take advantage of the analogy with the transmission line in order to compute the ratio between the pressure at the input and the pressure at the output of the tube as done in Jackson et Al [3].

This leads to the following result:

$$\frac{P_T}{P_{IN}} = \frac{1}{cosh(\gamma l) + \frac{Z_0}{Z_T} sinh(\gamma l)} = Z_T \frac{1}{Z_T cosh(\gamma l) + Z_0 sinh(\gamma l)} \tag{2.27}$$

For the analysis that will be performed later in this discussion, it is worth expressing equation (2.27) as:

$$Z_T \frac{P_{in}}{P_T} = Z_T cosh(\gamma l) + sinh(\gamma l)\, Z_0 \tag{2.28}$$

2.3 Mathematical and Acoustical Description of the Lower Respiratory Tract

To deal with the model of sound transmission in the region below the glottis, is necessary to consider two fundamental parts:

1. the description, in terms of mathematical formulation, of the acoustical properties of the single airway segment;
2. the complexity of the airway tree which, for a human subject, approximately involves 10^7 terminal branches.

As far as the first part is concerned, the considerations in 2.2 can be easily extended to accomplish this objective. The second task is a more challenging one as it implies the introduction of a mathematical and geometrical model. The model proposed in this dissertation is based on the Horsfield model.

2.3.1 The Horsfield Model

The Horsfield model is a geometrical representation of the bronchial tree able to properly take into account its natural asymmetric dichotomy and is based on the assumption of self-consistency [8]. It was proposed by Horsfield and Al. in the 1982 and, although some approximations are reasonably introduced, it can be considered a comprehensive morphometric model of the airways [4]. For a human subject, 35 segments of different sizes and characteristics are identified. Number n=35 is assigned to the trachea (the largest) and n=1 is assigned to terminal bronchiole which is supposed to branch directly into two alveoli (no respiratory bronchioles are here considered). For each segment the model specifies the length, the diameter, wall thickness and area fraction of cartilage. The so-called recursion index (Δ^n) allows to account for the asymmetry of the system at each airway bifurcation: a nth ordered airway generates two segments of order n-1 and n-1-Δ^n, respectively. The recursion index (Δ^n)

is considered as a structural parameter and is not constant all over the bronchial tree. Although Horsfield et Al. proposed a table containing some reference values for the parameters mentioned above, in this dissertation the one proposed by Habib et Al. [5] will be considered as it allows to account for both the non-rigidity of the airway wall and the presence of the terminal respiratory tissues. The Habib table readapted from [5] is reported in TABLE 4.

As a final, but relevant remark on these data, it is important to notice that they are based on casts of the lung airways, consisting of tube-shaped segments that bifurcate progressively into smaller components which all can be regarded as mono-dimensional as far as the acoustical point of view is concerned. This consideration further legitimates the use of equations in 2.2 to describe the acoustic impedances and the acoustic pressures, provided that the non-rigidity of the walls is already taken into account in the definition of the structural properties themselves as previously specified. The self-consistency of the model is given by the fact that for a chosen airway order n, the daughter segments are of same two orders, independently on the position in the lung.

TABLE 4: MORPHOLOGICAL PARAMETERS OF HUMAN AIRWAY MODEL; n IS THE HORSFIELD ORDER, l AND d ARE THE LENGTH AND DIAMETER, h IS THE WALL THICKNESS AND C THE FRACTION OF CARTILAGE.

n	$l^{(n)}$ [cm]	$d^{(n)}$ [cm]	$h^{(n)}$ [cm]	$C^{(n)}$	$\Delta^{(n)}$
1	0.0480	0.0800	0.00520	0.0000	0
2	0.0480	0.0800	0.00520	0.0000	0
3	0.0480	0.0800	0.00520	0.0000	0
4	0.0480	0.0800	0.00520	0.0000	0
5	0.0480	0.0800	0.00520	0.0000	0
6	0.0590	0.0800	0.00520	0.0000	0
7	0.0750	0.0430	0.00290	0.0000	0
8	0.1050	0.0480	0.00320	0.0000	0
9	0.1310	0.0530	0.00360	0.0000	0
10	0.1100	0.0630	0.00420	0.0000	0
11	0.2500	0.0760	0.00500	0.0000	1
12	0.3100	0.0950	0.00600	0.0000	2
13	0.3600	0.1100	0.00670	0.0000	2
14	0.4200	0.1400	0.00490	0.0000	3
15	0.4800	0.1600	0.00850	0.0000	3
16	0.5170	0.1800	0.00910	0.0000	3
17	0.6300	0.2000	0.00960	0.0224	3
18	0.6400	0.2180	0.01000	0.0262	3
19	0.7700	0.2400	0.01050	0.0309	3
20	0.8100	0.2500	0.01070	0.0329	3
21	0.8200	0.2700	0.01110	0.0370	3
22	0.9200	0.2800	0.01120	0.0390	3
23	0.8000	0.2900	0.01140	0.0410	3
24	0.9900	0.3100	0.01180	0.0450	3
25	0.9500	0.3500	0.01260	0.0526	3
26	0.8600	0.3500	0.01260	0.0526	3
27	1.0800	0.4300	0.01490	0.0671	3
28	0.9700	0.5400	0.02050	0.0851	3
29	1.1300	0.5900	0.02440	0.0926	3
30	1.1300	0.5900	0.02440	0.2000	3
31	1.0500	0.7300	0.04090	0.2500	3
32	1.1000	0.8000	0.05280	0.3300	3
33	2.2000	1.4000	0.13480	0.5000	3
34	5.0000	1.2000	0.17350	0.5000	2
35	10.0000	1.6000	0.37240	0.6700	1

From an acoustical point of view, it is significant the possibility to compute the acoustic impedance at the input of the trachea as well as the acoustic pressure distribution in the airways. Indeed, both these parameters will be dependent on the airway geometry and the changes it can possibly experience. Thanks to the self-consistency of the model the computation of the acoustic impedance can be performed in a "relatively" simple way. The first step is the computation of this impedance at the level of the terminal bronchiole (n=1) and then reiterate the procedure for n=2, 3, …, 35 (where n=35 is the trachea). Taking as a reference Figure 4:

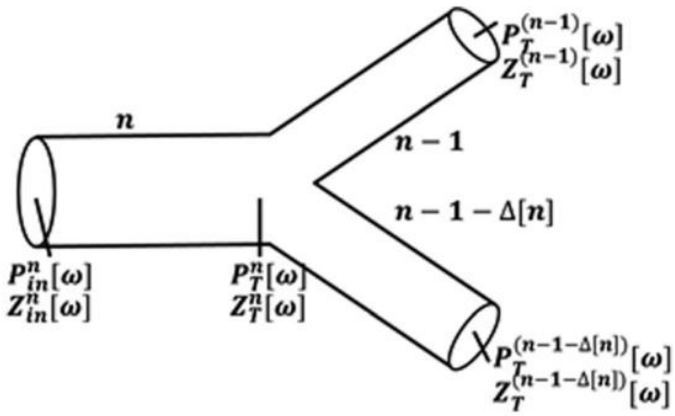

Figure 4: The acoustic model of a single bifurcating airway segment

By a simple extension of the formula (2.18), the input (i.e. considered at the end adjacent to the trachea) acoustic impedance Z_{in} can be defined as:

$$Z_{in}^{(n)}[\omega] = \frac{Z_T^{(n)}[\omega]cosh(\gamma_0^{(n)}[\omega]l^{(n)}) + Z_0^{(n)}[\omega]sinh(\gamma_0^{(n)}[\omega]l^{(n)})}{cosh(\gamma_0^{(n)}[\omega]l^{(n)}) + \left(Z_T^{(n)}[\omega]/Z_0^{(n)}[\omega]\right)sinh(\gamma_0^{(n)}[\omega]l^{(n)})} \tag{2.29}$$

Or, by the definition of $\tanh(x) = \frac{\sinh(x)}{\cosh(x)}$, as:

$$Z_{in}^{(n)}[\omega] = \frac{Z_T^{(n)}[\omega] + Z_0^{(n)}[\omega]tanh(\gamma_0^{(n)}[\omega]l^{(n)})}{1 + \left(Z_T^{(n)}[\omega]/Z_0^{(n)}[\omega]\right)tanh(\gamma_0^{(n)}[\omega]l^{(n)})} \tag{2.30}$$

Where $Z_0^n[\omega]$ is the characteristic impedance and $\gamma_0^n[\omega]$ is characteristic propagation coefficient of the nth airway segment [4]. The values of these two parameters can be computed thanks to the following equations [5], [37], [38]:

$$Z_0^{(n)}[\omega] = \sqrt{Z^{(n)}[\omega]/Y^{(n)}[\omega]} \tag{2.31}$$

$$\gamma_0^{(n)}[\omega] = \sqrt{Z^{(n)}[\omega]Y^{(n)}[\omega]} \tag{2.32}$$

$$Z^{(n)}[\omega] = \frac{j\omega\rho_g}{A^{(n)}\left(1 - F_v^{(n)}[\omega]\right)} \tag{2.33}$$

$$Y^{(n)}[\omega] = \frac{j\omega A^{(n)}}{\rho_g c_g^2}\left(1 + 0.402F_t^{(n)}[\omega]\right) + \frac{1}{Z_w^{(n)}[\omega]l^{(n)}} \tag{2.34}$$

$$F_v^{(n)}[\omega] = \frac{2}{a^{(n)}\sqrt{(-j\omega\rho_g/\eta_g)}}\frac{J_1\left[a^{(n)}\sqrt{(-j\omega\rho_g/\eta_g)}\right]}{J_0\left[a^{(n)}\sqrt{(-j\omega\rho_g/\eta_g)}\right]} \tag{2.35}$$

$$F_t^{(n)}[\omega] = \frac{2}{a^{(n)}\sqrt{(-j\omega C_g/\kappa_g)}}\frac{J_1\left[a^{(n)}\sqrt{(-j\omega C_g/\kappa_g)}\right]}{J_0\left[a^{(n)}\sqrt{(-j\omega C_g/\kappa_g)}\right]} \tag{2.36}$$

$$Z_w^{(n)}[\omega]^{-1} = \frac{c^{(n)}}{Z_{w,c}^{(n)}[\omega]} + \frac{1 - c^{(n)}}{Z_{w,s}^{(n)}[\omega]} \tag{2.37}$$

In the equations described above $Z^{(n)}[\omega]$ and $Y^{(n)}[\omega]$ represent respectively the series impedance and shunt admittance of the nth airway segment. The subscript "g" denotes the properties related to the gas (i.e. air) component:

- ρ_g is the density;
- c_g is the wave speed in the given gas;
- η_g is the viscosity;
- C_g is the specific heat at constant pressure;
- κ_g is the coefficient of heat conduction;
- A(n) and a(n) are respectively the cross section and the radius of the n order segment.

- J_1 is the Bessel function of order 1;
- J_0 is the Bessel function of order 0;
- $F_t^{(n)}[\omega]$ is a term related to the storage of kinetic energy and its dissipation at the walls due to viscous losses;
- $F_v^{(n)}[\omega]$ is a term associated to the thermal dissipation occurring at the walls due to the failure of adiabaticity condition;

The term $Z_w^{(n)}[\omega]$ denotes the effective volumetric impedance of the wall of the nth-order airway segment. Since the wall can be constituted of two different materials, namely cartilage and soft tissue, their relation in terms of fractional content are exemplified by $c^{(n)}$ and $1 - c^{(n)}$, respectively. As it can be observed from TABLE 4 the presence of cartilage rings is characterized by a decreasing proportion moving downward from the trachea to the terminal segments. In particular, for a human subject the cartilage content is maximum at the trachea $c^{(35)} = 0.67$, gets gradually reduced up to the seventieth order $c^{(n)} = 0.0224$ and is completely absent form airways order $n = 1, \dots, 16$ where, consequently, exclusively soft tissue is considered [6].

The use of a series compliance (C_w), inertance (I_w) and resistance (R_w), and exemplification of each wall section allow the computation of the impedance of the cartilage component $Z_{w,c}^{(n)}[\omega]$ and the soft tissue component $Z_{w,s}^{(n)}[\omega]$. The following relations hold:

$$Z_{w,c\ or\ s}^{(n)}[\omega] = R_w^{(n)} + j\left(\omega I_w^{(n)} - \frac{1}{\omega C_w^{(n)}}\right) \tag{2.38}$$

where

$$R_{w,c\ or\ s}^{(n)} = \frac{4h^{(n)}\eta_{c\ or\ s}}{\pi (d^{(n)})^3 l^{(n)}} \tag{2.39}$$

$$I_{w,c\ or\ s}^{(n)} = \frac{h^{(n)}\rho_{c\ or\ s}}{\pi d^{(n)} l^{(n)}} \tag{2.40}$$

and

$$C_{w,c\ or\ s}^{(n)} = \frac{\pi\left(d^{(n)}\right)^3 l^{(n)}}{4h^{(n)}E_{c\ or\ s}} \tag{2.41}$$

In the equations presented above $\eta_{c\ or\ s}$ denotes the viscosity, $\rho_{c\ or\ s}$ the density $E_{c\ or\ s}$ the elastic Young's modulusof the cartilage or soft tissue respectively.

Nominal material property values are reported in [6]:

- $\eta_c = 18000\ \mathrm{Pa \cdot s}$
- $\eta_s = 160\ \mathrm{Pa \cdot s}$
- $\rho_c = 1140\ \mathrm{Kg/m^3}$
- $\rho_s = 1060\ \mathrm{Kg/m^3}$
- $E_c = 4.40 \times 10^6\ \mathrm{Pa}$
- $E_s = 3.92 \times 10^4\ \mathrm{Pa}$

Finally, the term Z_T express the acoustic impedance at the terminal end of each segment and is provided by:

$$Z_T^{(n)}[\omega] = \begin{cases} \dfrac{N_T}{j\omega c_g + 1/[R_t + j(\omega I_t - 1/[\omega C_t])]}, & n = 1 \\ \dfrac{1}{1/Z_T^{(n-1)}[\omega] + 1/Z_T^{(n-1-\Delta[n])}[\omega]}, & n = 2, \dots, 35 \end{cases} \tag{2.42}$$

Where N_T is the total number of extremity (n=1) bronchiole branches in parallel to the culmination of the lung parenchyma into the soft tissue.

For the model here analyzed, this total number can be computed thanks to the recursive formulation reported below, considering $N_T^{(1)} = 1$ and $N_T = N_T^{(35)}$:

$$N_T^{(n)} = N_T^{(n-1)} + N_T^{(n-1-\Delta[n])} \tag{2.43}$$

The term C_g represents the alveolar gas compliance under compression as expressed by the Dubois six elements terminal airway model [39]. R_t, I_t, C_t denotes properties of the terminal tissue, more specifically resistance, inertia and compliance.

The computation of the acoustic pressure as a function of an input acoustic pressure is extremely complex. This is because (unlike the acoustic impedance case) the hypothesis of self-consistency does not hold for the acoustic pressure since it is not the same among airways of the same order *n* as it is dependent on the length of the path to the trachea. In other words, it is possible to have segments with the same *n*, but which are not connected to the trachea by an equal number of segments. Although the levels of acoustic pressure levels are not alike among segments with the same order, it can be demonstrated that given a certain order *n* the ratio $P_{rat}^{(n)}[\omega]$ between the acoustic pressure at the far end $P_T^{(n)}[\omega]$ and that at the near end (adjacent to the trachea) $P_{in}^{(n)}[\omega]$ is equal for every airway segment of that order and can be obtained by [6]:

$$P_{rat}^{(n)}[\omega] = \frac{P_T^{(n)}[\omega]}{P_{in}^{(n)}[\omega]} = Z_T^{(n)}[\omega]\left\{\frac{cosh\left(\gamma_0^{(n)}[\omega]l^{(n)}\right)}{Z_{in}^{(n)}[\omega]} - \frac{sinh\left(\gamma_0^{(n)}[\omega]l^{(n)}\right)}{Z_0^{(n)}[\omega]}\right\} \tag{2.44}$$

Equation (2.41) above can be alternatively expressed as [8]:

$$P_{rat}^{(n)}[\omega] = \frac{Z_T^{(n)}[\omega]Z_0^{(n)}[\omega]}{Z_{in}^{(n)}[\omega]\left(Z_T^{(n)}[\omega]sinh\left(\gamma_0^{(n)}[\omega]l^{(n)}\right) + Z_0^{(n)}[\omega]\,cosh\left(\gamma_0^{(n)}[\omega]l^{(n)}\right)\right)} \tag{2.45}$$

Either one formulation or the other is extremely useful because it states the dependence of this $P_{rat}^{(n)}[\omega]$ on the impedances $Z_{in}^{(n)}[\omega]$, $Z_T^{(n)}[\omega]$, and $Z_0^{(n)}[\omega]$ which, as explained before, are easier to compute. Furthermore, if the input pressure at the top of the trachea is known and the ratio can be computed, the acoustic pressure at the lower extremity of the trachea can be derived. The pressure at the distal part of the trachea corresponds to the input the pressure at the proximal end of the two main stem bronchi, by knowing the impendence at this new order the corresponding ratio can be computed and finally the pressure at the end of both the main bronchi can be obtained. This procedure can be iteratively performed for the pressure at base or top of any airway order. It can be demonstrated that, by properly rearranging equation (2.45) and substituting the definition of input impedance as expressed in equation (2.30) the very same result of Jackson et Al. reported in equation (2.27) can be found (see Appendix for details). Finally, the pressure in function of the coordinate *x* along a certain segment can be computed applying the following formula [40]:

$$P^{(n)}[x,\omega] = \frac{Z_0^{(n)}[\omega]}{\sinh\left(\gamma_0^{(n)}[\omega]l\right)}\left(\frac{P_{in}^{(n)}[\omega]}{Z_{in}^{(n)}[\omega]}\cosh\left(\gamma_0^{(n)}[\omega](x-l)\right) - \frac{P_T^{(n)}[\omega]}{Z_T^{(n)}[\omega]}\cosh\left(\gamma_0^{(n)}[\omega]x\right)\right) \tag{2.46}$$

Where x varies between 0 (end of the segment closest to the trachea) and l (end of the segment distant from the trachea).

As far as the validity of this model is concerned, it reported that this approach is to be considered valid for frequency lower than 5000 Hz [6]. For higher frequencies, pressure variations can occur across the cross-section of the larger airways: this phenomenon cannot be properly predicted by the current description and therefore a more complex three-dimensional acoustic model should be introduced.

CHAPTER 3

ANALYTICAL MODELS

The first computational step performed in this work was the simulation via analytical model in MATLAB of the acoustic pressure propagation and wall radial velocity in a human tracheobronchial tree for a frequency range of 200-800 Hz. The choice of a multifrequency analysis is justified by the frequency dependency of the mechanical and acoustic properties of the tissues. The range of frequency tested was decided after the consideration that most of the frequency content of physiological and pathological breath sounds is located below 800 Hz. The lower limit was arbitrary chosen at 200 Hz, nonetheless the model could be easily extended to lower frequencies.

3.1 Generation of the Geometries

Two sets of data have been generated. The first set is comprised of two trees obtained from a healthy subject at different respiratory phases (beginning of inspiration and beginning of expiration). Those data have been used, on one hand to validate the model and to assess the precision and the reliability of the model, on the other hand to simulate analytically the effect of some pathologies on the model itself. The second set of data is composed of ten subjects: five control (healthy) subjects and five subjects affected by asthma. Those data allowed firstly to evaluate the sensitivity to real (not simulated) pathological conditions and secondarily a comparison between the physiological and pathological conditions with the aim of identifying, form the acoustical point of view, some distinctive patterns or features of the pathology.

3.1.1 Data for Validation and Preliminary Acoustical Analysis

The human data used for the validation of the model and the preliminary analytical acoustical analysis were obtained from de-identified Computed Tomography (CT) images provided by Dr. Ching-Long (IIHR – Hydro-science and Engineering and the Department of Mechanical and Industrial Engineering, University of Iowa) and generated via the procedure described in [41]. For the given tracheobronchial tree, two different phases of the respiratory cycle were considered: the beginning of expiratory phase and the beginning of inspiratory phase. To generate the geometry and to collect the information related to morphology, the length and the diameter of the constituent segments a Graphic User Interface (GUI) in MATLAB was used. The extrapolation of geometrical and morphological features was performed on the voxelized CT images of the given airways; the whole process was aimed at the generation of a one-dimensional airways tree to be input and analyzed in MATLAB. For each segment, the central proximal and distal points were identified and the tree built as the centerline of the 3D segment. For each segment the GUI allowed the computation of the diameter (calculated as the mean of the diameter in for the distal and proximal point of the segment) and the length (derived as the distance between the proximal and distal points).

A visual example of the procedure for the extraction of the information mentioned above is shown in Figure 5 for the expiratory tracheobronchial tree (the same task was accomplished also for the inspiratory one).

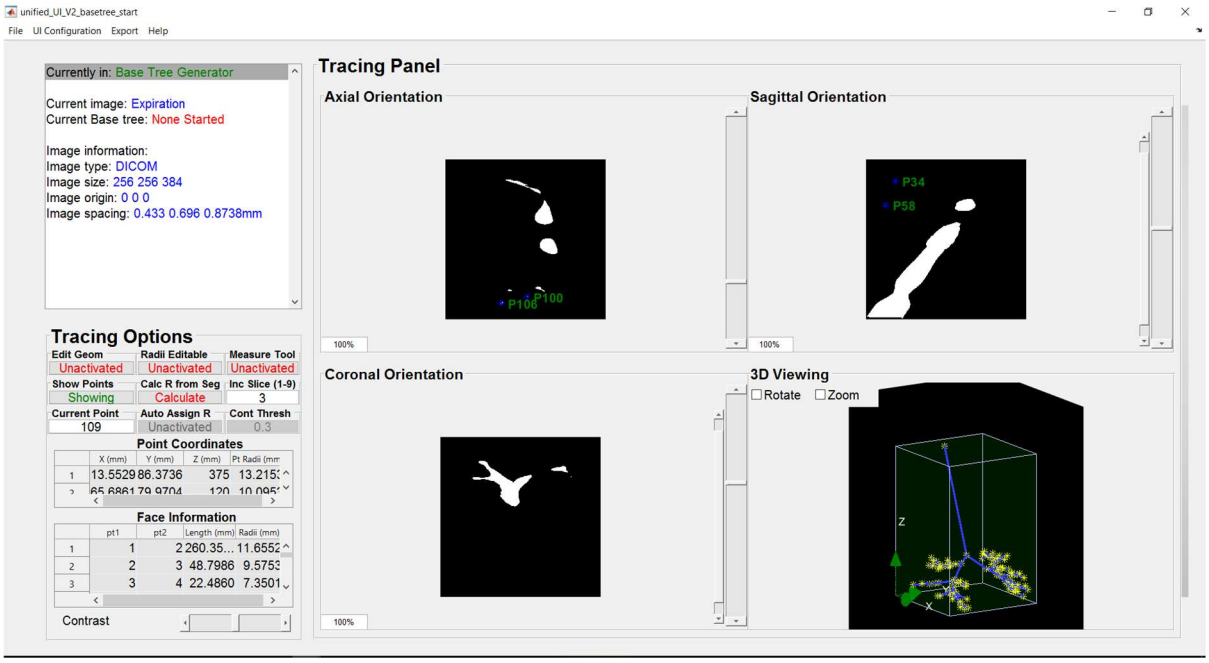

Figure 5: Visual layout of the process of identification and generation of the morpho-geometrical features of the airway tree (a representative expiratory case is reported)

The thickness was manually assigned by evaluating the diameter and fitting it to the closest order of the Habib table (see TABLE 4). To simplify the successive numerical analysis, the lowest value of thickness accepted for the terminal segments was assumed to be 500 micrometers: if the thickness of any segment was lower than that value, it was approximated to be as exactly equal to it. The two generated tracheobronchial trees for the beginning of the of inspiratory and the beginning of the expiratory phase are shown in Figure 6 and Figure 7, respectively.

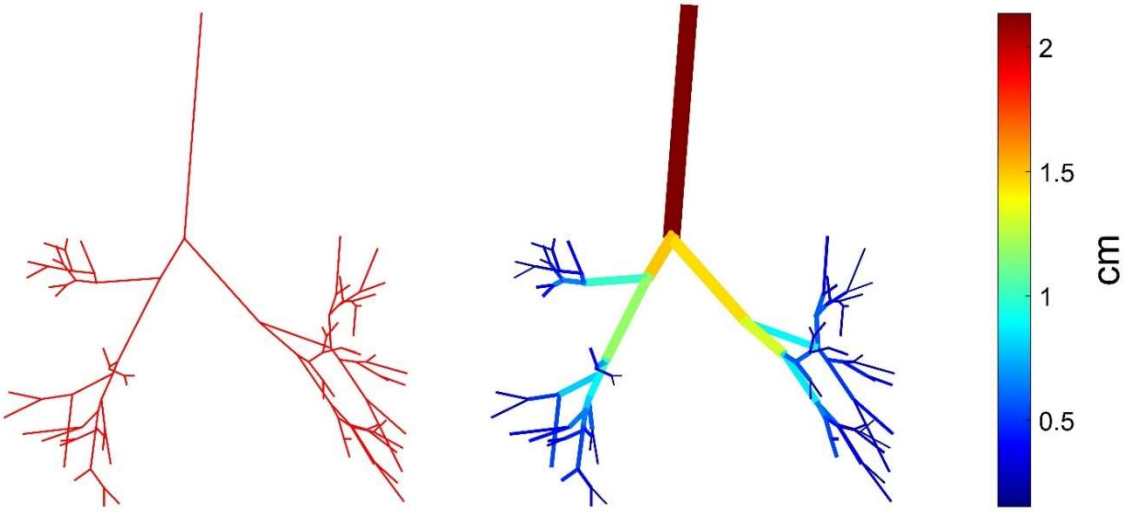

Figure 6: Geometry (left) and diameter distribution (right) at the beginning of the inspiratory phase

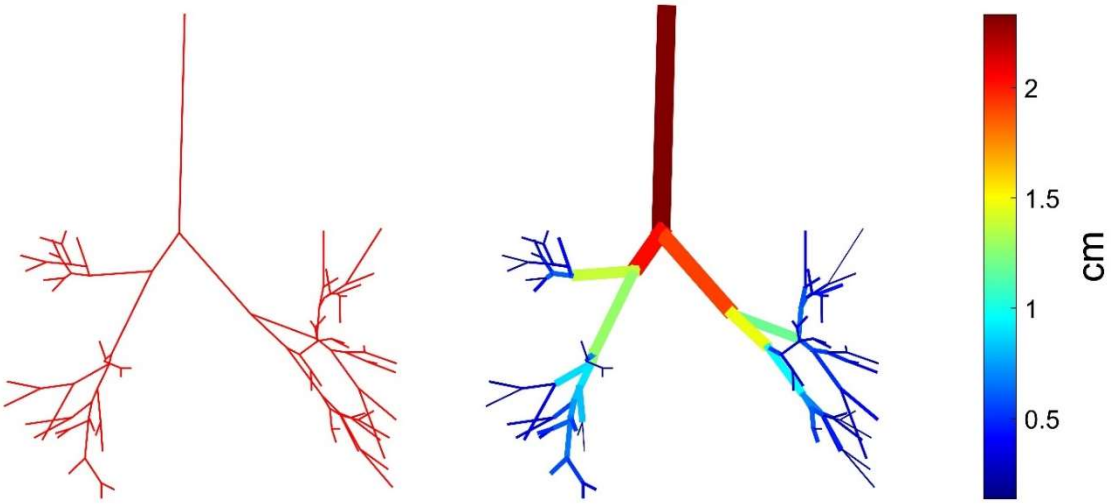

Figure 7: Geometry (left) and diameter distribution (right) at the beginning of the expiratory phase

3.1.2 Data for the Analysis of Asthma Pathology

Data for the analysis of the effects of asthma pathology were obtained from de-identified computerized tomography (CT) images. The population of the study involved five normal (control) patients and five asthmatic patients. The data were provided by Dr. Jason C. Woods (Director of the Center for Pulmonary Imaging Research, Cincinnati Children's Hospital and professor at Departments of Pediatrics and Radiology of the University of Cincinnati) and analyzed at high respiratory volume (TLC) and low respiratory volume (RV/FRC). The extraction of the skeleton of the tree as well as the diameter and the length of the segments are performed, for each subject and each respiratory volume, following the procedure described in the previous paragraph. The values of the internal diameters for the generated geometries are reported at both low and high volumes for the control (Fig. 8) and the asthmatic population (Fig. 9)

The graphs report, when significant, the statistics of the internal diameter differences between the low and the high-volume. The data are proven to be normal through a Normality Test (Shapiro-Wilk) and therefore compared with a t-test. Statistical significance was reported as:

- *, if P-value ≤ 0.05
- **, if P-value ≤ 0.01
- ***, if P-value ≤ 0.001

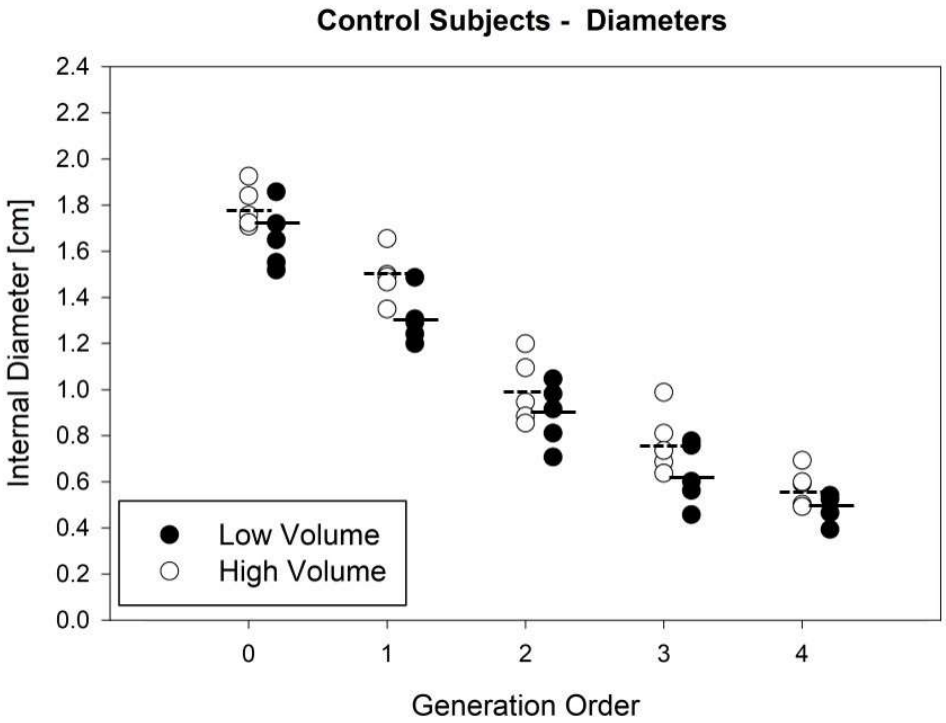

Figure 8: Internal diameters in the control subjects at low respiratory volume (black circles) and high respiratory volume (white circles) from generation 0 to 5. The mean values are represented with a continuous line for the low respiratory volume and with a dashed line for the high respiratory volumes.

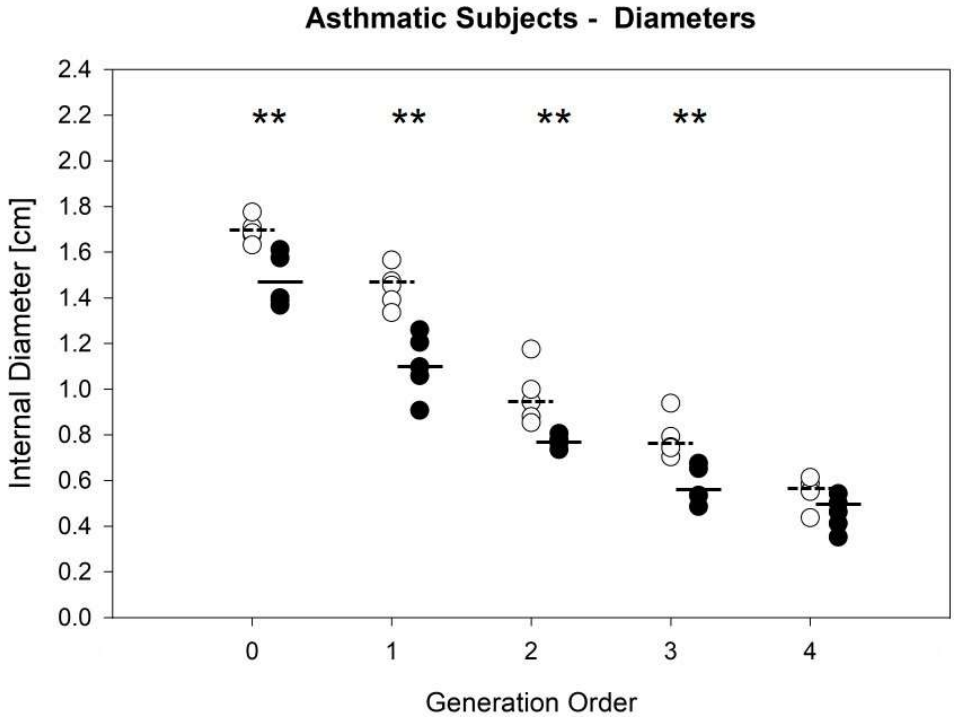

Figure 9: Internal diameters in the asthmatic subjects at low respiratory volume (black circles) and high respiratory volume (white circles) from generation 0 to 5. The mean values are represented with a continuous line for the low respiratory volume and with a dashed line for the high respiratory volumes. **, $p<0.01$

In controls, at each generation we observe that the internal diameter are higher in mean at high volume (Figure 8), even if no significant differences are found between the low and the high respiratory volume.

On the contrary, the asthmatic subjects (Figure 9) show significant diameter differences between the low and the high respiratory volume, at generation 1 ($p=0.004$), 2 ($p=0.002$), 3 ($p=0.008$) and 4 ($p=0.005$)

The assignment of the thickness for the healthy subjects was performed by matching the diameter with the closest order of the Habib Table and assigning the correspondent value of thickness.

The assignment of the thickness for the asthmatic subjects was accomplished using literature data from Montesantos and Al. [42], to account for the heterogeneity in thickness variation along different generations. A procedure of validation of the data from [42] was carried out for some significant generations (up to order 7/8), by comparing data from literature with measurements performed on the CT of the asthmatic subjects. Measurement on CT was performed using the software ImageJ [43]. For those generations in which a measurement on the axial plane was convenient, this was performed by plotting the grayscale profile along a line across the cross section of the segment and evaluating the thickness with the Full Width at Half Maximum (FWHM) technique [44]. When possible, at least three measurements were performed. Two exemplificative pictures of this operation are reported in Figure 10.

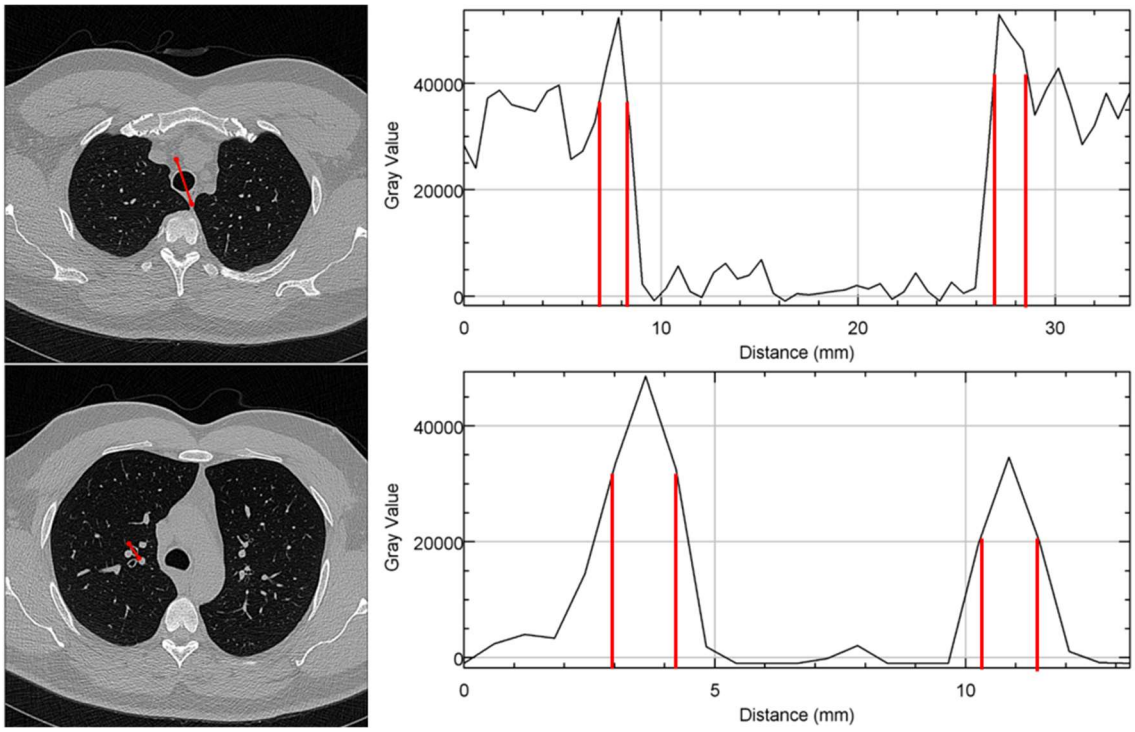

Figure 10: Exemplificative picture representing the Full Width at Half Maximum method applied during the validation procedure of the literature data of thickness.

For those generations in which the information on axial plane could not provide valuable or reliable information, the measurements were performed manually either on the sagittal or coronal plane.

3.2 Acoustical Analysis

The acoustic analysis was performed in MATLAB (r2016a, The MathWorks Inc., Natick, MA, 2016). The code models 1D quasi-planar wave propagation in a branching system. This approach reasonably approximates most of the dynamic behavior up to several hundreds of Hz [8]. At extremely high frequencies the assumptions underlying the model, namely the one dimensionality and quasi planarity of the propagation, begin to lose validity in the larger airways. This is because, in general, the hypothesis of planarity and the approximation of the system by a 1-D wave equation are proven to be valid only if the wavelength corresponding to the highest frequency is sufficiently wider than the cross-section of the largest segment of the tubular structure to be modeled [45]. The pressure can be input either at the inlet of the trachea or in a chosen location: for all the acoustical analysis reported in this dissertation, a pressure with an amplitude of 1 Pa input at the level of the trachea was considered. As mentioned above, the frequency of the input pressure wave was varied between 200 and 800 Hz. The algorithm allows the computation of the acoustic impedance and acoustic pressure according to the formulas reported in paragraph 2.3.1. In addition to those information, the radial velocity of the wall of each airway segment was obtained thanks to the following formula:

$$u_{radial} = P/Z_{w,radial}/i \tag{3.1}$$

Where the term $Z_{w,radial}$ is defined as the volumetric impedance Z_w over the lateral area of the cylinder considered. In this way, the results regarding the wall radial were obtained in the conventional SI unit of m/s. As for the Horsfield model, in the analytical code each segment was modeled as cylinder of known radius, length and thickness, but the calculations are not limited to an always-bifurcating network. In addition to that the code developed was modified

and extended to be able to model properly a full conducting airway tree geometry that does not explicitly obey self-consistency. All geometries that will be presented are, indeed, patient specific as they are obtained through CT data. In term of analytical formulation, the extension of the model to a structure which is not explicitly self-similar implies the reformulation of some of the equations mentioned in 2.3.1. In particular, equation (2.47) is modified as follows:

$$Z_T^{(n-1)} = \frac{1}{1/Z_{in}^{daughter1}[\omega] + 1/Z_{in}^{daughter2}[\omega]} \tag{3.2}$$

$Z_{in}^{daughter1}[\omega]$ and $Z_{in}^{daughter2}[\omega]$ are the input impedances of the two daughter segments at each bifurcation.

The fractional content of cartilage and soft tissue for each segment are defined taking as a reference Habib and Al [5]. The fractional content $c(n)$ of cartilage is assigned for each generation whereas the soft tissue fraction is simply computed as unity minus the cartilage fraction. i. e. $1 - c(n)$.

The material properties of the constituent elements included in the model are assigned in a specific function in accordance to (2.39) - (2.41). The mechanical properties of the cartilage were approximated to be the same of the soft tissue. Thus, in terms of acoustic analysis, the airways walls were assumed to be composed of soft tissue only. The soft tissue behavior was approximated with a Voigt model with Young's Modulus Y_s and the viscosity η_s. The complex elastic modulus of the chosen rheological model is reported in equation (3.2):

$$E = Y_s + i\omega\eta_s \tag{3.3}$$

The mechanical parameters characterizing the airways wall soft tissue (density, elastic modulus and viscosity) are reported in TABLE 5.

TABLE 5: MECHANICAL PROPERTIES OF THE SOFT TISSUE

Property	**Symbol**	**Value**
Density of Soft Tissue $[Kg/m^3]$	ρ_s	1060
Elastic Modulus of Soft Tissue $[Pa]$	Y_s	3.92×10^5
Viscosity of Soft Tissue $[Pa \cdot s]$	η_s	101.90

Parameters characterizing the air, namely density (ρ_g), wave speed (c_g), viscosity (η_g); specific heat at constant pressure (C_g) and coefficient of heat conduction (κ_g), were set at body temperature and are reported in TABLE 6.

TABLE 6: MECHANICAL PROPERTIES OF AIR

Property	**Symbol**	**Value**
Density $[Kg/m^3]$	ρ_g	1.14
Wave Speed $[m/s]$	c_g	343
Viscosity $[Pa \cdot s]$	η_g	1.86×10^{-5}
Poisson coefficient [-]	ν_g	0.4995
Specific Heat at Constant Pressure $[J/Kg \cdot °C]$	C_g	1004.2
Coefficient of Heat Conduction $[J/Kg \cdot °C]$	k_g	0.0268

To recursively perform all the calculations, the terminal impedances of the last generations were assigned. This was done because none of the input tree reaches the terminal bronchioles ($n = 1$ of the Horsfield model) and therefore equation (2.42) for the case $n = 1$, although fully defined from an analytical point of view, could not be used. The chosen version of the code assigned a constant value of impedance to all the terminal segments, instead of it being variable. In this process either the order of the terminal branches was given as an input for the given tracheobronchial tree or it was matched with the closest order of the Habib table by evaluating the measure of the diameter. The numerical values of the terminal impedance, were previously obtained for all the orders of the Habib table over a much wider frequency range.

Once the impedance of the terminal segments was known, equation (3.2) allowed to compute the terminal impedance for each upstream generation. The characteristic impedance and the impedance of the airways walls were obtained thanks to the relations (2.31)-(2.37). The acoustic pressure of each segment was calculated by evaluating formula (2.46) in nine different points along the segment itself. These results were eventually interpolated to obtain the final solution. The wall radial velocity was also interpolated over the same points.

3.2.1 Simulation of the Asthma Pathology

The pathology of asthma was at first simulated taking as a reference Ionescu et Al [46].

It was decided to evaluate the morphologic changes induced by the pathology in terms of radii and thickness of the constituent segments. The inflammation and thickening (due to the infiltration of mucus) of the airways was modeled by increasing the thickness (h) of each segment of 1.5 times. The increased thickness was related to the alteration of the radii through the following equation:

$$R_{asthma} = R_{healthy} - 0.5 \times h \tag{3.4}$$

As asthma is known to affect mainly small airways, the morphometrical alterations were imposed only for those segments with a diameter equal or lower than 2 mm which is a reference value usually applied to identify small size airways.

3.2.2 Simulation of the Airways Fibrosis Condition

The stiffening of the airways wall determined by the abnormal connective tissue growth characterizing the pathological fibrosis was modeled by increasing the elastic modulus of the airways wall. It was decided to multiply the physiological value by a factor 5.

3.2.3 Simulation of Pulmonary Infiltrate Condition

A unilateral pulmonary infiltrate was simulated. The occlusion was supposed to be localized on the lower lobe of the left lung. The consequent increased resistance of the tree was modelled by multiplying the impedance of the left lower lobe (LLL) terminal branches by a factor 10^5.

CHAPTER 4

NUMERICAL MODELS

Numerical simulations were performed in COMSOL Multiphysics® using the dedicated Acoustic - Solid Interaction Frequency Domain Modulus.

The hollow tube network was developed in ANSYS via a series of TCL (tool command) script files, which had the instructions to automatically generate the cylinder geometry segment by segment. Spheres were inserted at the bifurcation junctions to make the connectivity smoother. Two separate sets of scripts were written from MATLAB to depict the inner and outer radius of the hollow tube network, which were merged and volume meshed to provide the hollow tube FE model. The final FE model had two volumes, denoted by the inner (air volume) and outer radius (airway wall thickness) for the hollow tube model to replicate as closely as possible the conducting tree geometry.

Once the FE models were obtained, the numerical simulation were performed with the same parameters of the analytical ones. The validation of the model involved both the inspiratory and expiratory phase in physiological conditions.

4.1 Generation of the Meshes

The meshes for the Finite Element Analysis (FEA) were generated in ANSYS ICEM CFD (ANSYS® Academic Research, Release 16.2). The geometries were exported from MATLAB generating 4 TCL (Tool Command Language) files: two for the inner part and two for the outer points. Each couple of files was meshed separately and then merged together. Some relevant features of the final merged meshes for the human model are reported in TABLE 7.

TABLE 7: FEATURES OF THE FINAL MERGED MESHES IN THE TWO RESPIRATORY PHASES CONSIDERED

Parameter	Inspiration	Expiration
Mesh Type	Tetrahedral/Mixed	Tetrahedral/Mixed
Number of Elements	1723666	1924363
Max Element Size	111.81x176.51x217.20	110.09x178.26x219.57
Min Element Size	24.37x0.63x2.87	23.15x1.15x1.89

Figure 11 shows the two generated meshes in ANSYS®.

Those meshes have been then imported in COMSOL Multiphysics® to perform the finite element analysis.

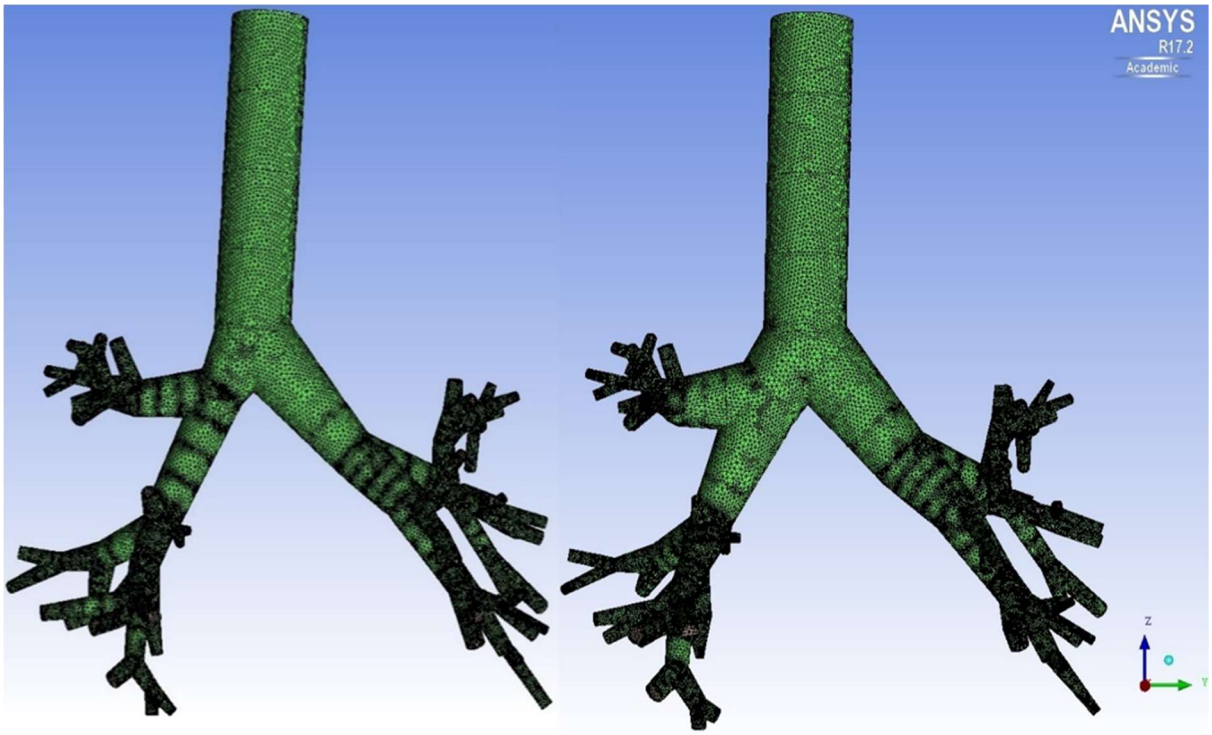

Figure 11: Generated meshes in ANSYS®. The mesh for the beginning of the inspiratory phase is reported on the left, whereas the mesh for the beginning of the expiratory phase is reported on the right.

4.2 Acoustical Simulations

The mesh was imported in COMSOL Multiphysics® as a data file. The computation of the geometry was automatically accomplished by the software. The analysis was performed in the frequency domain using the Acoustic - Solid Interaction Frequency Domain Modulus. The range of frequencies considered was 200-800 Hz, in accordance to the analytical model. In accordance with the analytical model a pressure of amplitude equals to 1 Pa was input at the level of the trachea. Three boundaries were defined: two for the inlet and the outlets and one for the annulus of the trachea. For both air and thickness two domains were introduced. The airways wall was assumed to be composed by soft tissue only. The acoustic properties of the model were set in the acoustic modulus. The acoustic impedance of the terminal branches was assumed to be constant over a chosen frequency. The frequency dependent values were obtained by curve fitting the trend of those terminal impedances in MATLAB for both the real and imaginary part. The complex-valued impedance was then multiplied by the average cross-sectional area of the terminal branches themselves. The results of the fitting were the same for both the expiratory and inspiratory phase and are reported in Figure 12.

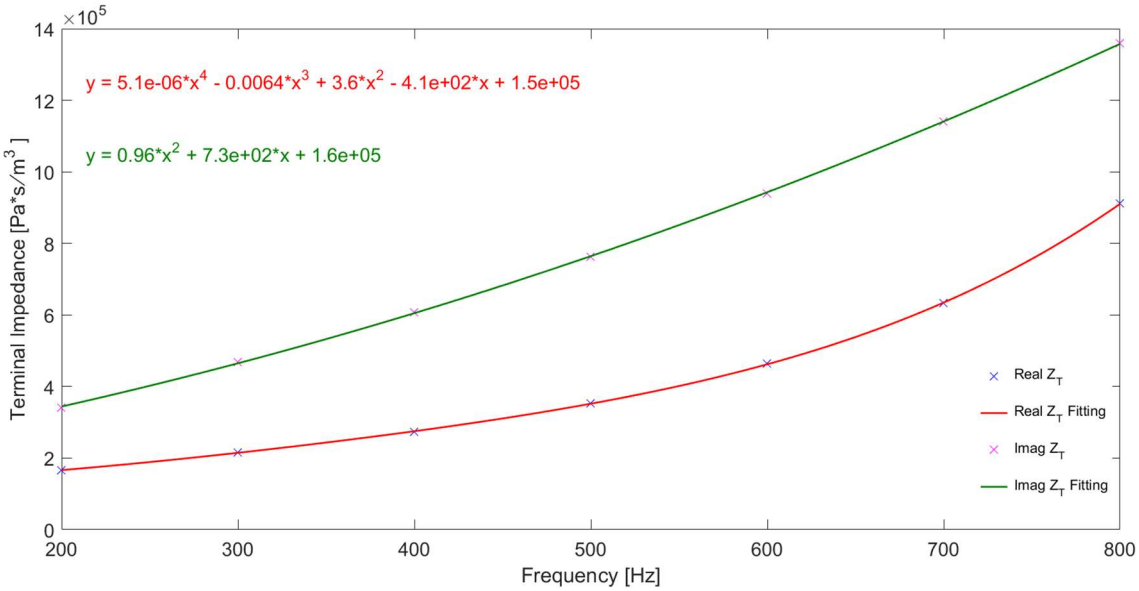

Figure 12: Terminal impedance (Z_T) curve fitting. Valid for both the inspiratory and expiratory phase.

It can be observed that the real part of the terminal impedance was fit with a 4th order polynomial whereas the imaginary part was well approximated by a quadratic form.

The mechanical properties of the constituent materials were defined in accordance to the analytical model. Both the properties of the biological tissue and the air were introduced and are reported in TABLE 8 and TABLE 9, respectively.

TABLE 8: SOFT TISSUE MECHANICAL PROPERTIES FOR THE NUMERICAL SIMULATIONS

Property	**Symbol**	**Value**
Density of Soft Tissue $[Kg/m^3]$	ρ_s	1060
Elastic Modulus of Soft Tissue $[Pa]$	Y_s	3.92×10^5

TABLE 9: AIR MECHANICAL PROPERTIES FOR THE NUMERICAL SIMULATIONS

Property	**Symbol**	**Value**
Density of Air $[Kg/m^3]$	ρ_a	1.14
Speed of Sound $[m/s]$	c_a	343
Poisson Ratio	ν_a	0.4995

In the solid-mechanics module, the hold bar boundary at the level of the annulus of the trachea was defined as a fixed constrain (no displacement).

CHAPTER 5

RESULTS

The results are structured as follows. First, the validity of the analytical model is demonstrated by comparing the results of the analytical MATLAB simulations with the numerical COMSOL Multiphysics® simulations for the healthy case of both the inspiratory and expiratory phase. The results will be shown only for the following frequencies: 200 Hz, 400Hz, 600Hz and 800 Hz.

Second, the results of the simulations at low and high lung volume in the healthy case and the results of the simulation of the pathological conditions are reported.

Third, the results of the application of the model to real data are presented.

5.1 Validation of the Analytical Model

The results for the inspiratory and expiratory phases from both analytical and numerical model are reported for the four frequencies of interest.

Figure 13 shows the magnitude of the acoustic pressure normalized in logarithmic scale at the four frequencies of interest at the beginning of the inspiratory phase.

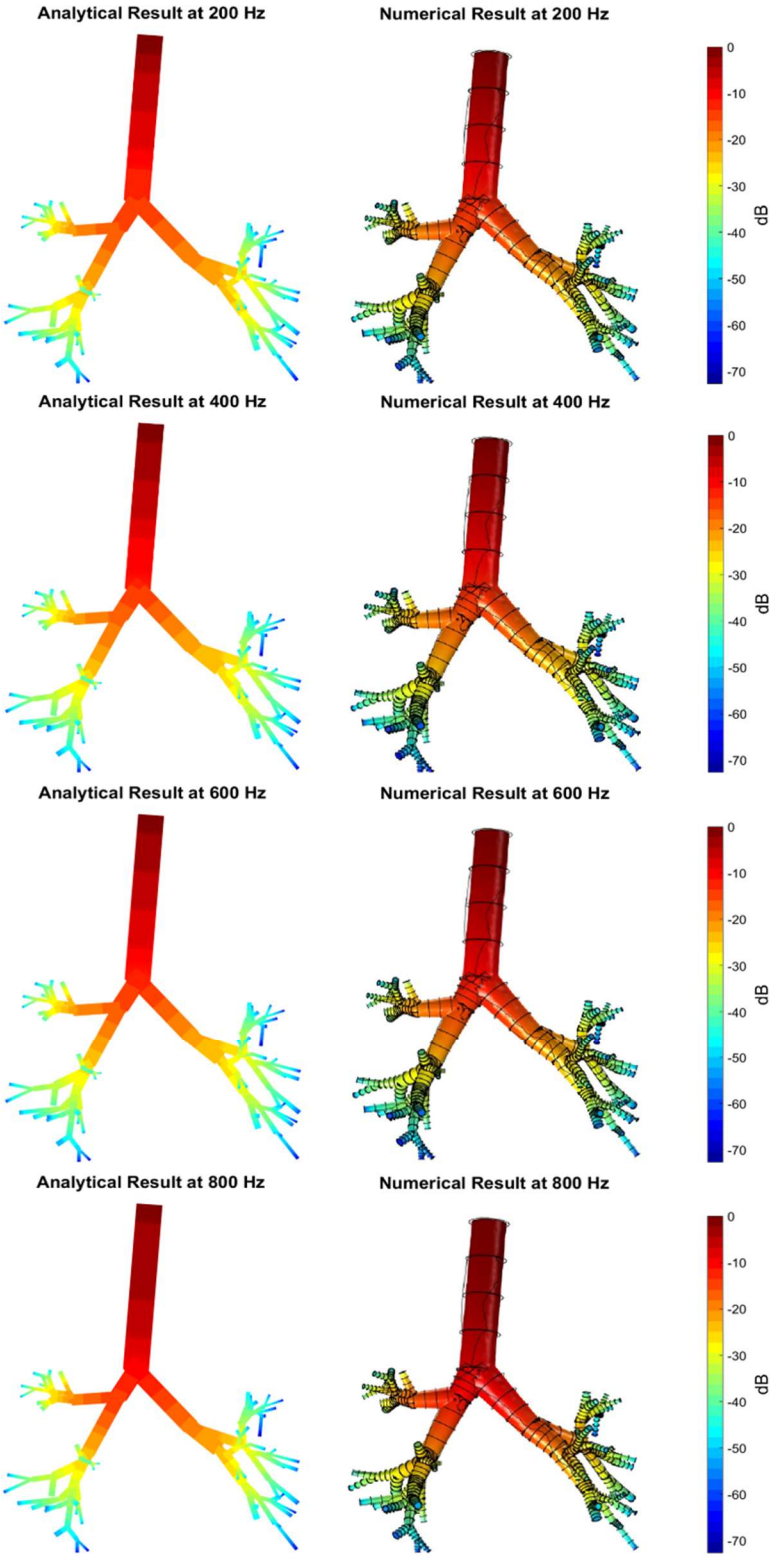

Figure 13: Magnitude of acoustic pressure in logarithmic scale [dB]. Comparison between the analytical (left) and numerical (right) results at the beginning of the inspiratory phase. From the top to the bottom the results at 200 Hz, 400 Hz, 600 Hz and 800 Hz are reported.

Figure 14 shows distribution of real part of the acoustic pressure in Pascal at the frequencies of interest at the beginning of the inspiratory phase.

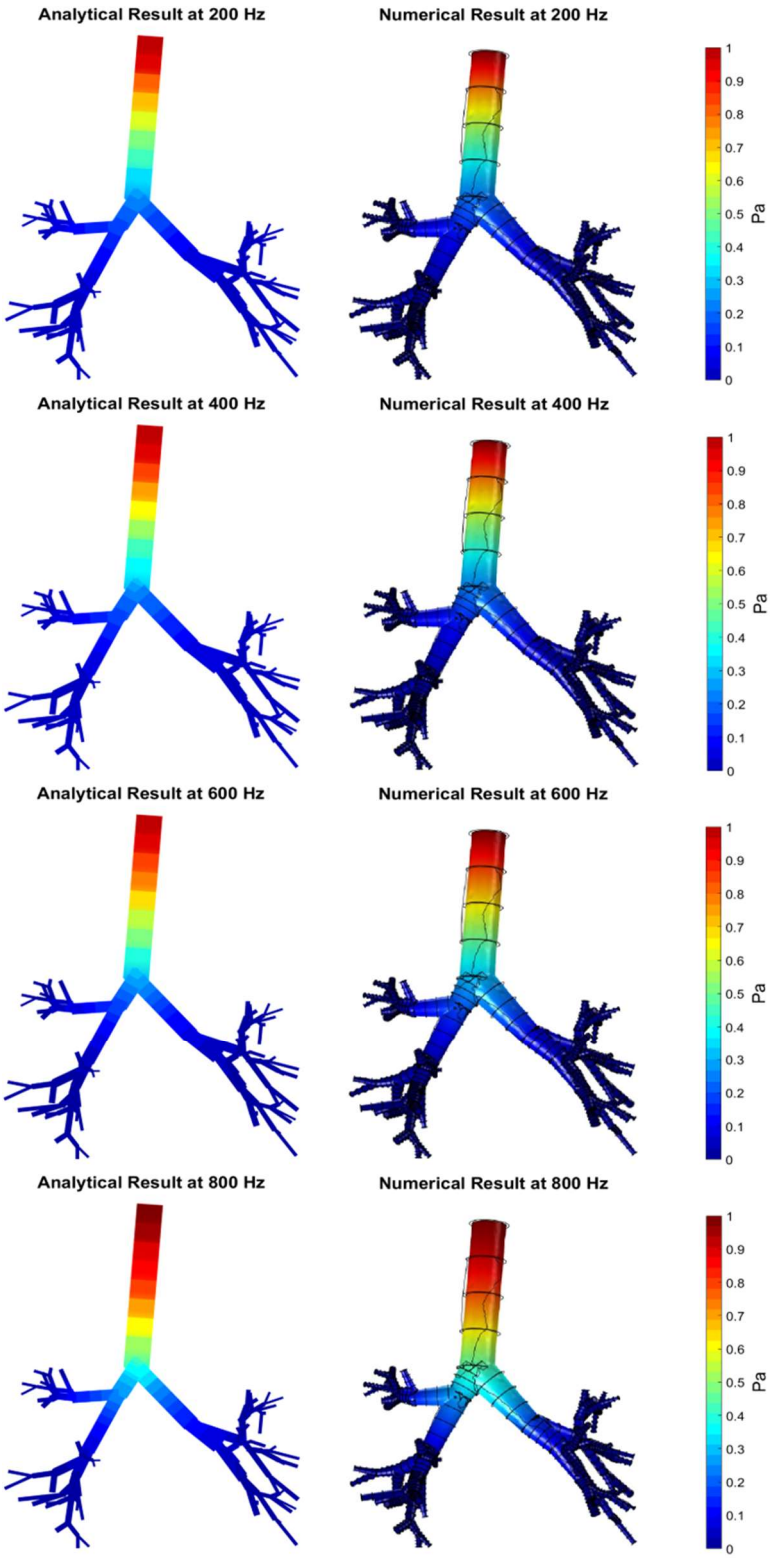

Figure 14: Real part of acoustic pressure [Pa]. Comparison between the analytical (left) and numerical (right) results at the beginning of the inspiratory phase. From the top to the bottom the results at 200 Hz, 400 Hz, 600 Hz and 800 Hz are reported.

Figure 15 reports the magnitude of the acoustic pressure at the beginning of the expiratory phase at the frequencies of interest.

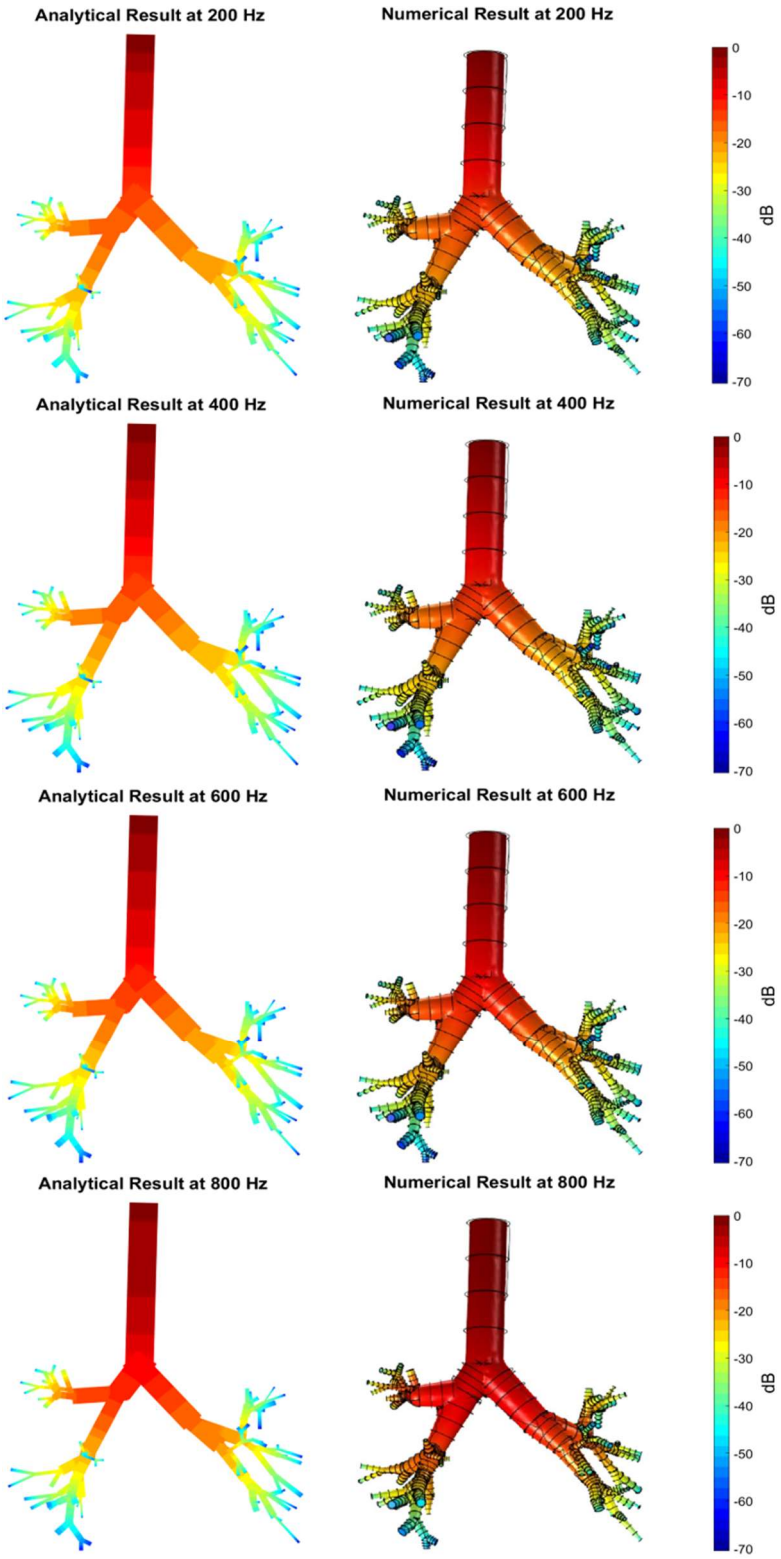

Figure 15: Magnitude of acoustic pressure in logarithmic scale [dB]. Comparison between the analytical (left) and numerical (right) results at the beginning of the expiratory phase. From the top to the bottom the results at 200 Hz, 400 Hz, 600 Hz and 800 Hz are reported

Figure 16 shows the distribution of the real part of the acoustic pressure in Pascal at 200 Hz (first row), 400 Hz (second row), 600 Hz (third row), 800 Hz (fourth row) at the beginning of the expiratory phase.

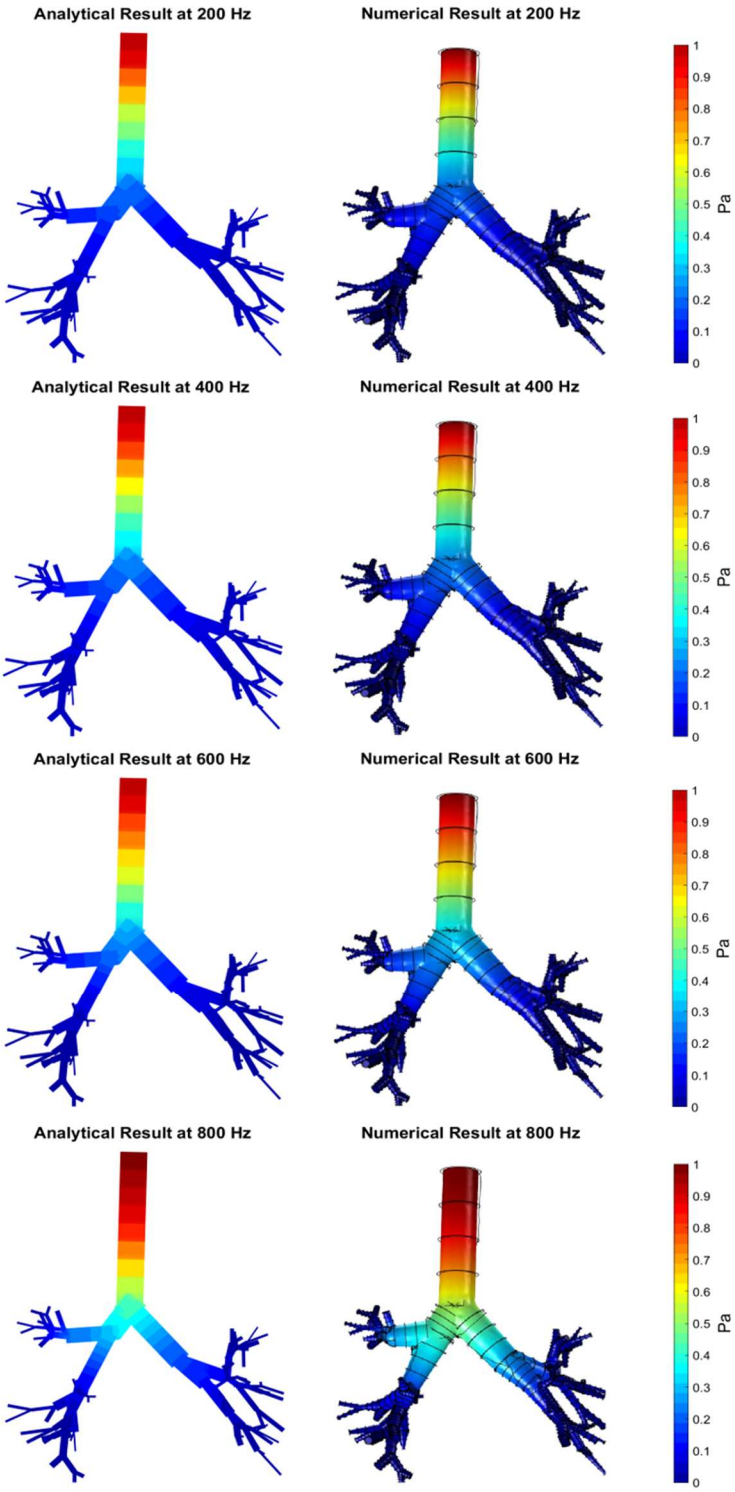

Figure 16: Real part of acoustic pressure [Pa]. Comparison between the analytical (left) and numerical (right) results at the beginning of the expiratory phase. From the top to the bottom the results at 200 Hz, 400 Hz, 600 Hz and 800 Hz are reported.

To obtain a quantitative evaluation of the precision of the analytical model an error analysis was performed in MATLAB, on the magnitude of the acoustic pressure expressed in logarithmic scale. For each branch, the numerical data were exported from COMSOL Multiphysics® in correspondence to the 9 interpolating points used in MATLAB to maximize the level of the accuracy of the analysis. Figure 17 shows the procedure of identification of the interpolating points in the COMSOL Multiphysics® interface for the inspiratory model, the very same procedure was performed on the expiratory one.

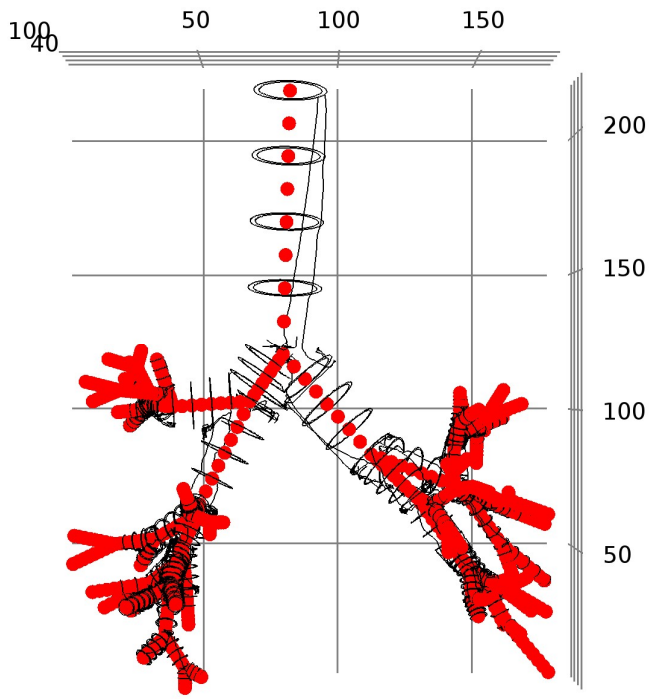

Figure 17: Identification of the interpolating points in COMSOL Multiphysics®.

Starting from the model at the beginning of inspiration the results of the error analysis in terms of visual representation and distribution are reported in Figure 18. In addition, TABLE 10 shows the median and the maximum value of the error for the four frequencies of interest.

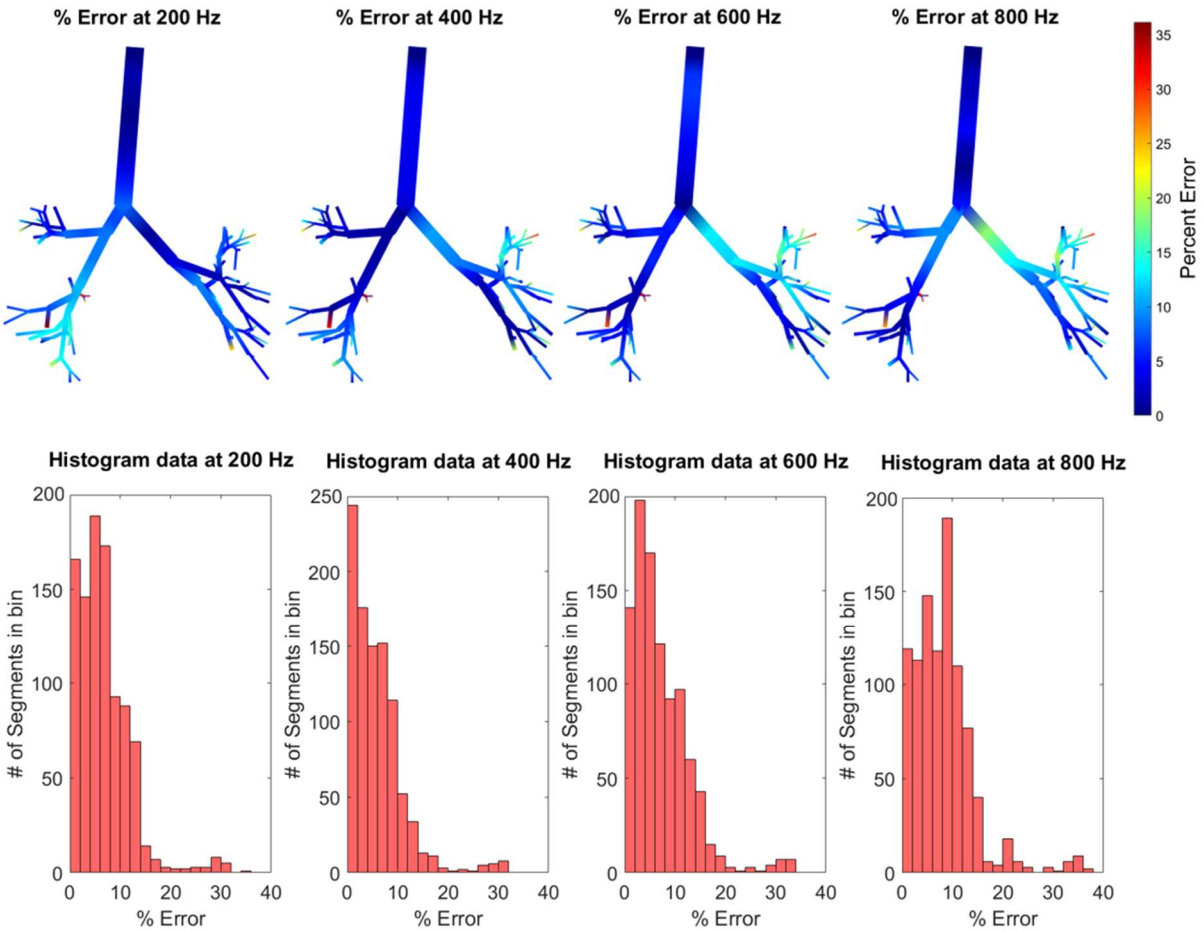

Figure 18: Error representation (top) and error distribution (bottom) for the beginning of the inspiratory phase. From the right to the left the four frequencies of interest in the following order: 200 Hz, 400 Hz, 600 Hz and 800Hz.

TABLE 10: ANALYSIS OF THE ERROR FOR THE BEGINNING OF INSPIRATORY PHASE – MEDIAN AND MAXIMUM VALUE FOR THE FOUR FREQUENCIES OF INTEREST

Frequency [Hz]	**200**	**400**	**600**	**800**
Median Error [%]	5.43	4.60	5.86	7.87
Max Error [%]	34.96	31.14	32.75	36.14

For the inspiratory phase, this analysis shows an excellent matching of the results. The error slightly increases at higher frequencies, but is still lower than 10 %. The highest errors are in the terminal branches with a peak value at 800 Hz of 36.14 %.

The results of the analysis at the beginning of expiration are shown in Figure 19.

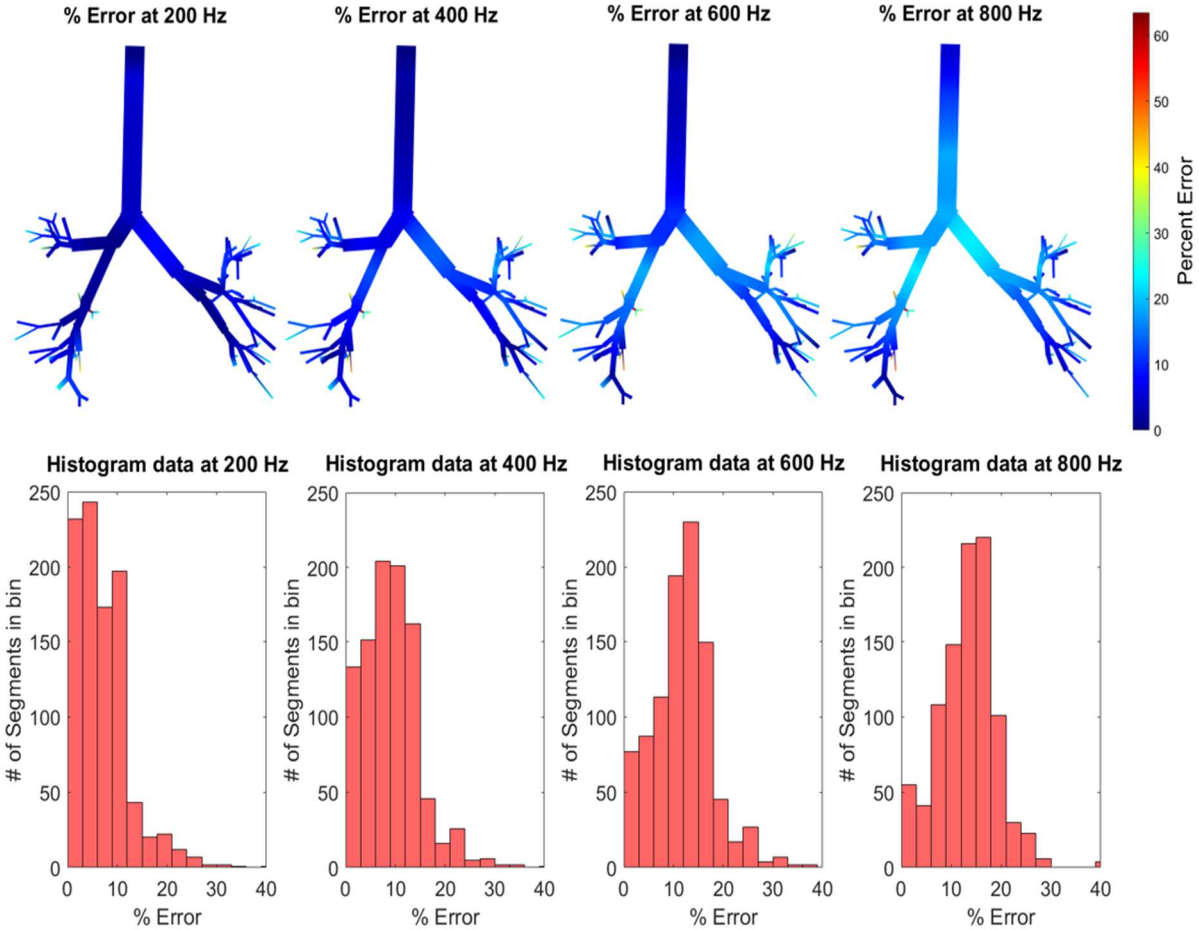

Figure 19: Error representation (top) and error distribution (bottom) for the beginning of the expiratory phase. From the right to the left the four frequencies of interest in the following order: 200 Hz, 400 Hz, 600 Hz and 800Hz.

The median and the maximum error in the case of the expiratory phase and for the frequencies of interest are reported in TABLE 11.

TABLE 11: ANALYSIS OF THE ERROR FOR THE BEGINNING OF EXPIRATORY PHASE – MEDIAN AND MAXIMUM VALUE FOR THE FOUR FREQUENCIES OF INTEREST

Frequency [Hz]	**200**	**400**	**600**	**800**
Median Error [%]	6.37	9.01	12.40	13.91
Max Error [%]	62.74	56.55	57.64	63.48

For the expiratory case the error is slightly worse, reaching relatively high values also in the left main bronchus of the tree at 800 Hz. The maximum error is 63.48 %, at 800 Hz although this value is reached for the terminal branches only.

Given the results presented in this section and the as it will be further discussed in 6.2, the model results to be validated.

5.2 Comparison Between the Beginning of Inspiratory and Expiratory Phases

The response to the inlet pressure of both the beginning of the inspiratory phase and the beginning of the expiratory phases are reported. The comparison is reported both at low frequency (LF) and at high frequency (HF). Three parameters are presented: 1) the magnitude of the acoustic pressure (in logarithmic scale), 2) the real part of the acoustic pressure and 3) the magnitude of the airways wall radial velocity (in logarithmic scale). For the pressure-related parameters, it was also analyzed the trend in the trachea and the main two bronchi. As regard the magnitude of the wall radial velocity, it was assumed the velocity to be constant over the segment and equal to the value computed at the distal interpolating point of the segment. For this parameter, only a qualitative evaluation is reported.

Figure 20 and Figure 21 report, the magnitude of the acoustic pressure in logarithmic scale at 200 Hz and the trend of the magnitude of the acoustic pressure in the trachea and the main bronchi in logarithmic scale, respectively.

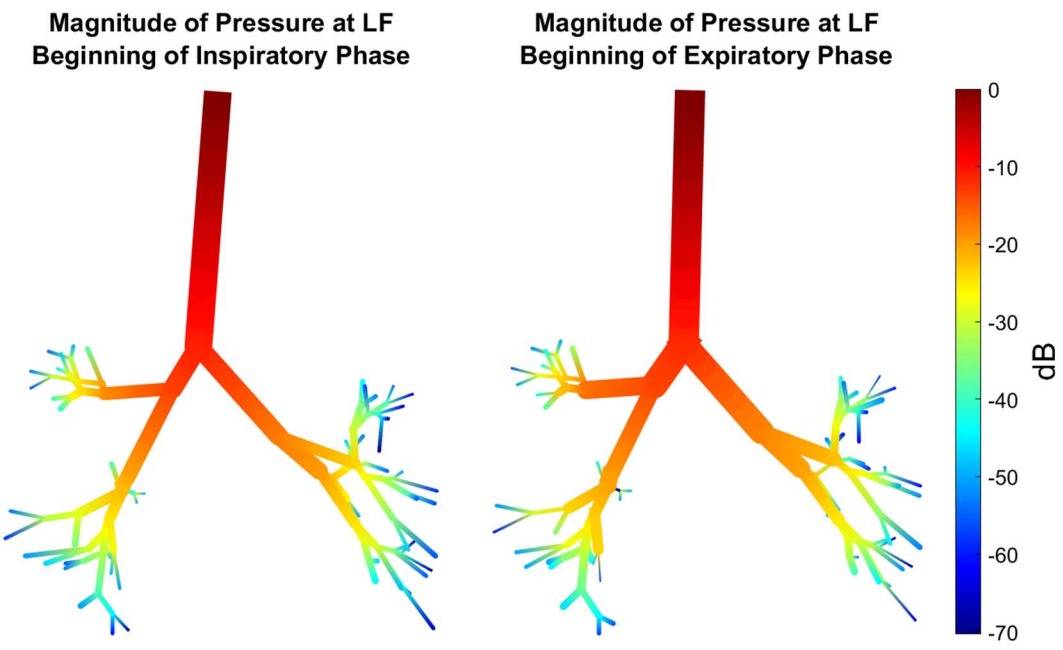

Figure 20: Magnitude of the acoustic pressure in logarithmic scale at 200 Hz. Comparison between the beginning of the inspiratory phase (left) and the beginning of expiratory phase (right)

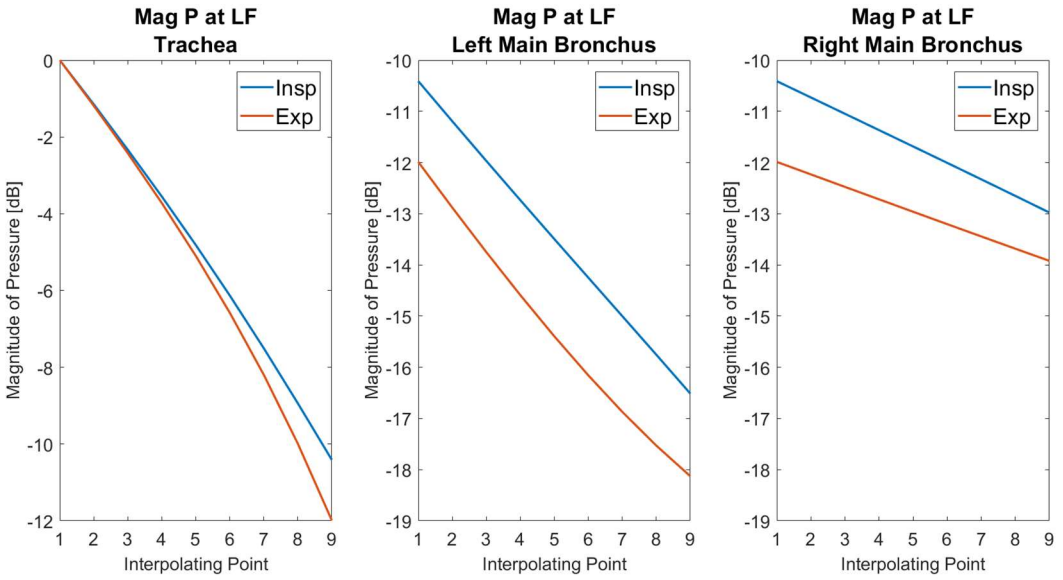

Figure 21: Trend of the magnitude of the acoustic pressure in logarithmic scale at low frequency in the trachea (left), left main Bronchus (middle) and right main bronchus (right) for the inspiratory (blue) and expiratory (orange) phases.

Figure 22 shows the magnitude of the acoustic pressure in logarithmic scale at high frequency. Figure 23 reports the corresponding trend over the trachea and the right and the left main bronchi.

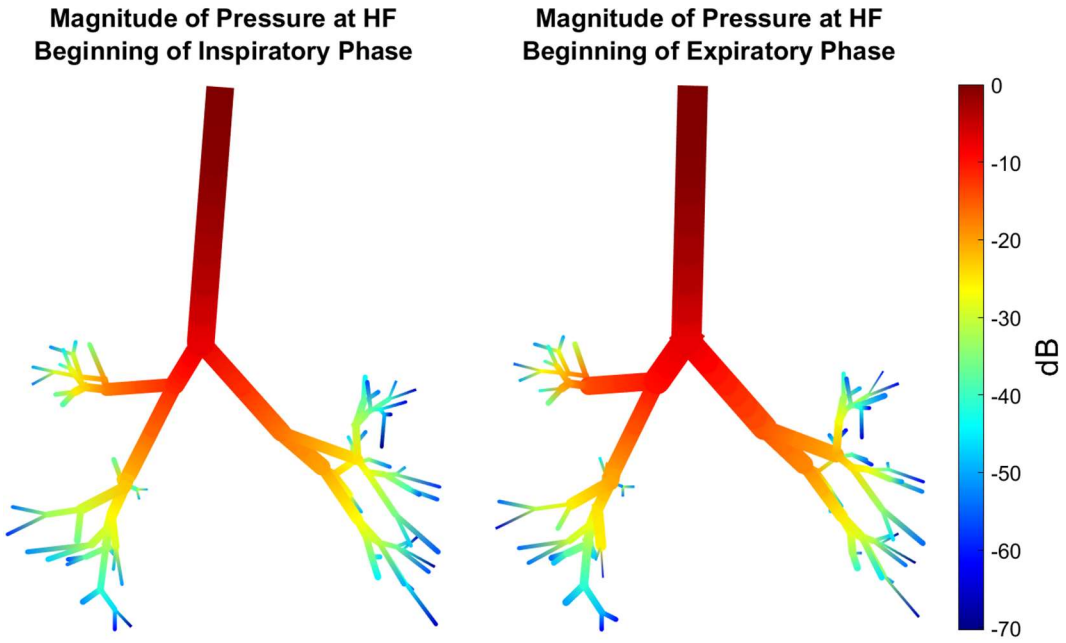

Figure 22: Magnitude of the acoustic pressure in logarithmic scale at high frequency. Comparison between the beginning of the inspiratory phase (left) and the beginning of expiratory phase (right).

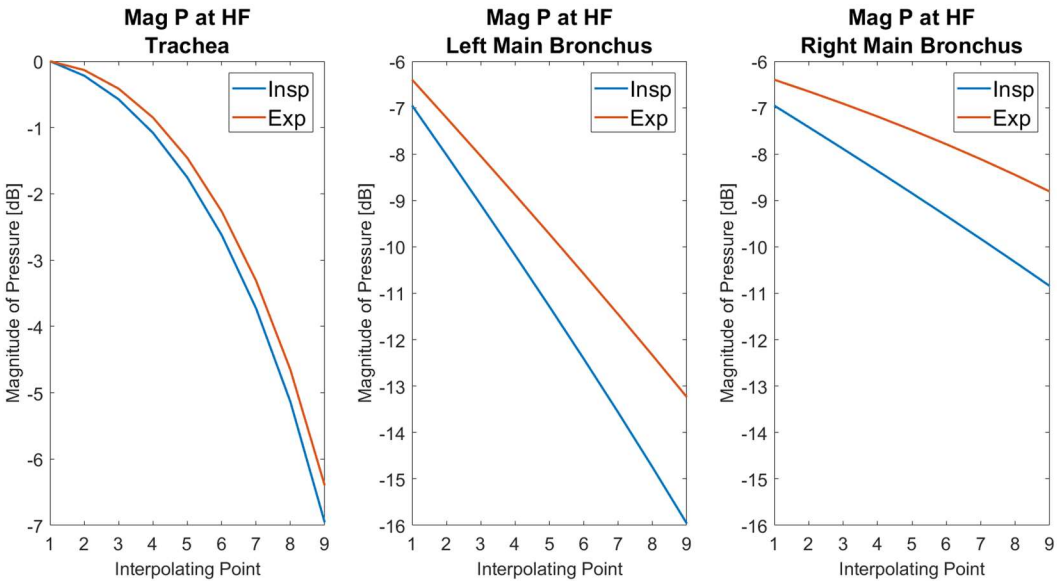

Figure 23: Trend of the magnitude of the acoustic pressure in logarithmic scale at high frequency in the trachea (left), left main Bronchus (middle) and right main bronchus (right) for the inspiratory (blue) and expiratory (orange) phases.

Figure 24 and Figure 25 report for the low-frequency case the real part of the acoustic pressure and the trend of the real part of the acoustic pressure for the segments of interest, respectively.

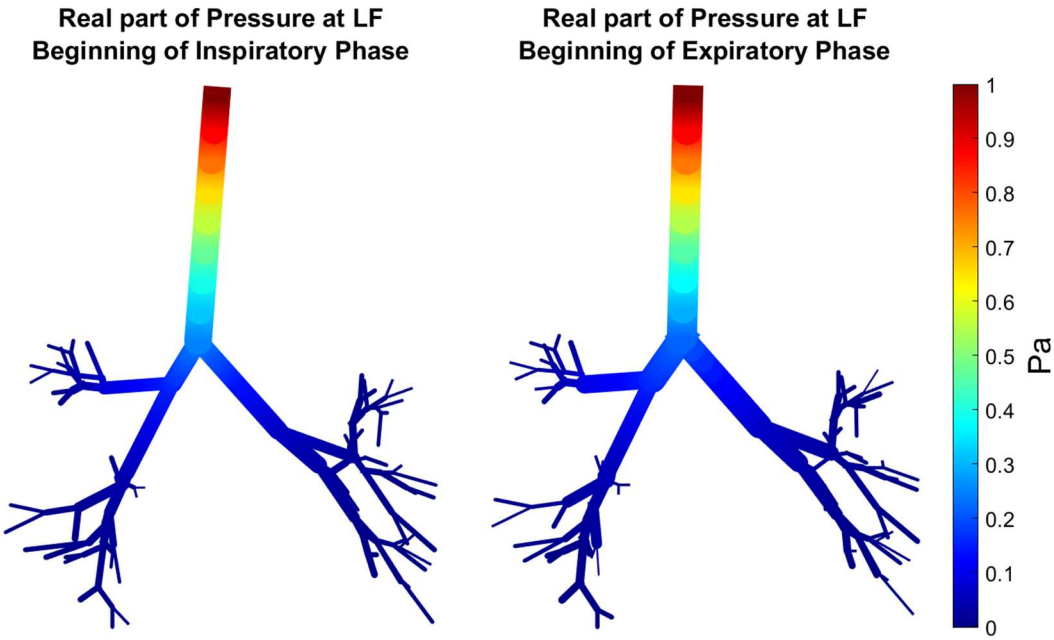

Figure 24: Real part of the acoustic pressure in logarithmic scale at low frequency. Comparison between the beginning of the inspiratory phase (left) and the beginning of expiratory phase (right).

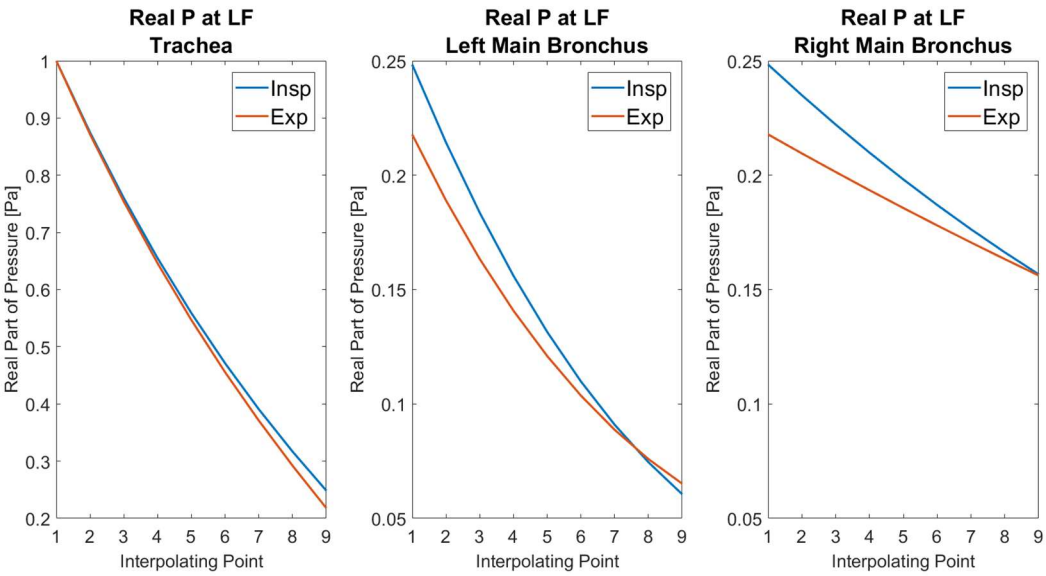

Figure 25: Trend of the real part of the acoustic pressure in logarithmic scale at 200 Hz in the trachea (left), left main Bronchus (middle) and right main bronchus (right) for the inspiratory (blue) and expiratory (orange) phases.

Figure 26 shows the distribution of the real part of the acoustic pressure at high frequency. Figure 27 reports the corresponding trend over the trachea and the right and the left main bronchi.

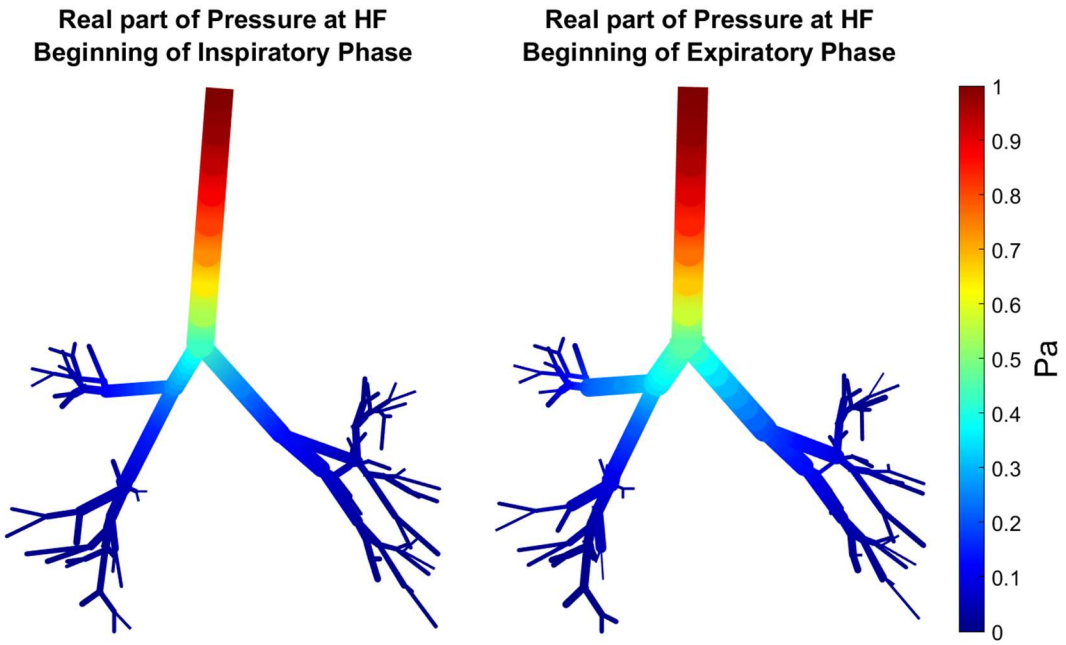

Figure 26: Real part of the acoustic pressure in logarithmic scale at high frequency. Comparison between the beginning of the inspiratory phase (left) and the beginning of expiratory phase (right).

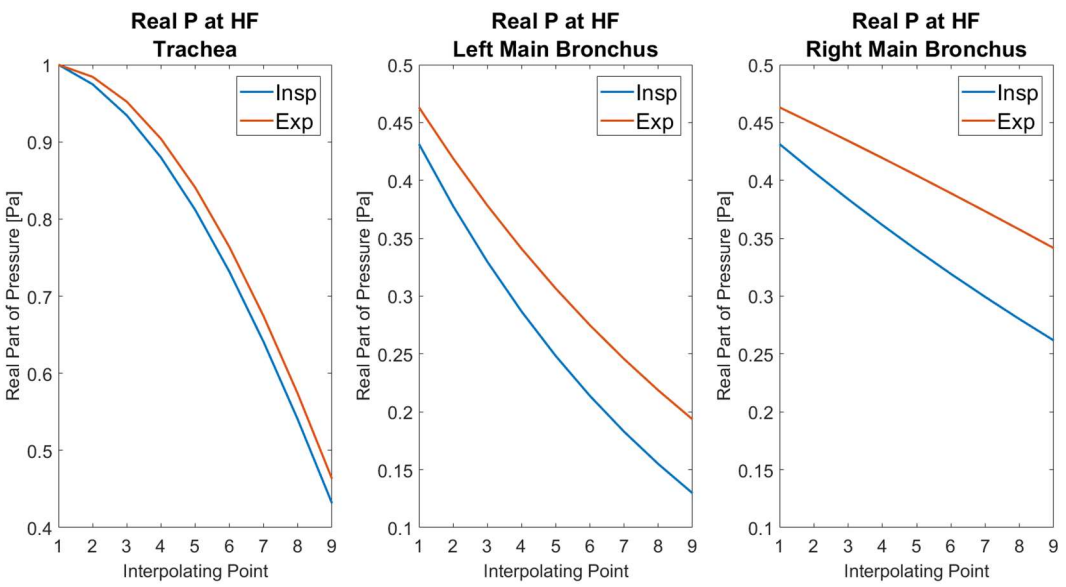

Figure 27: Trend of the real part of the acoustic pressure in logarithmic scale at high frequency in the trachea (left), left main Bronchus (middle) and right main bronchus (right) for the inspiratory (blue) and expiratory (orange) phases.

Finally, Figure 28 and Figure 29 show the magnitude of the wall radial velocity at the beginning of the inspiratory phase and at the beginning of the expiratory phase at low (Fig.28) and high (Fig. 29) frequency, respectively.

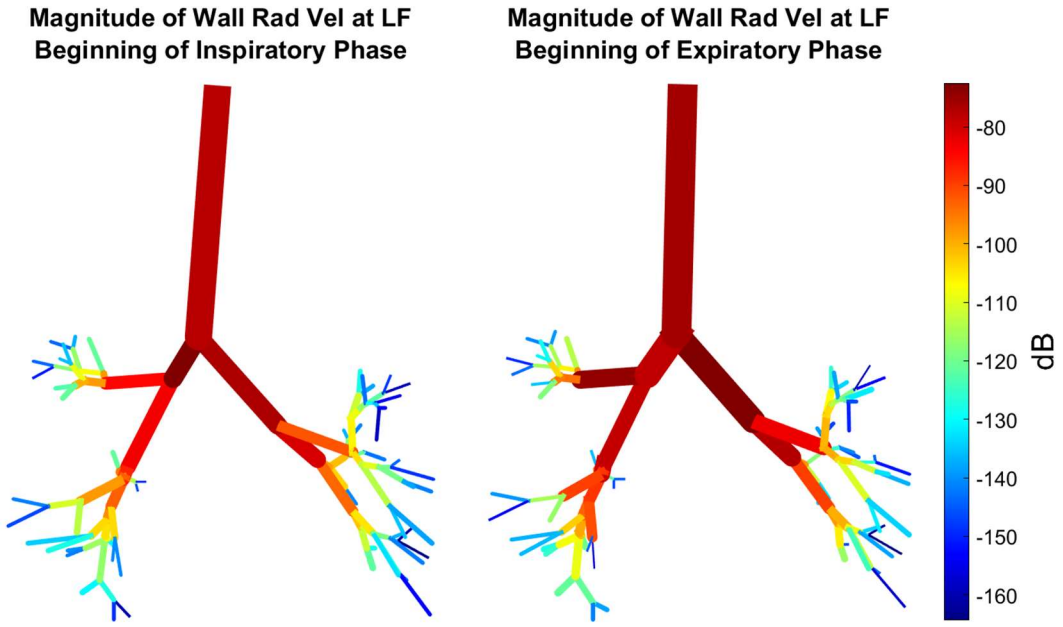

Figure 28: Magnitude of the wall radial velocity in logarithmic scale at low frequency. Comparison between the beginning of the inspiratory phase (left) and the beginning of expiratory phase (right).

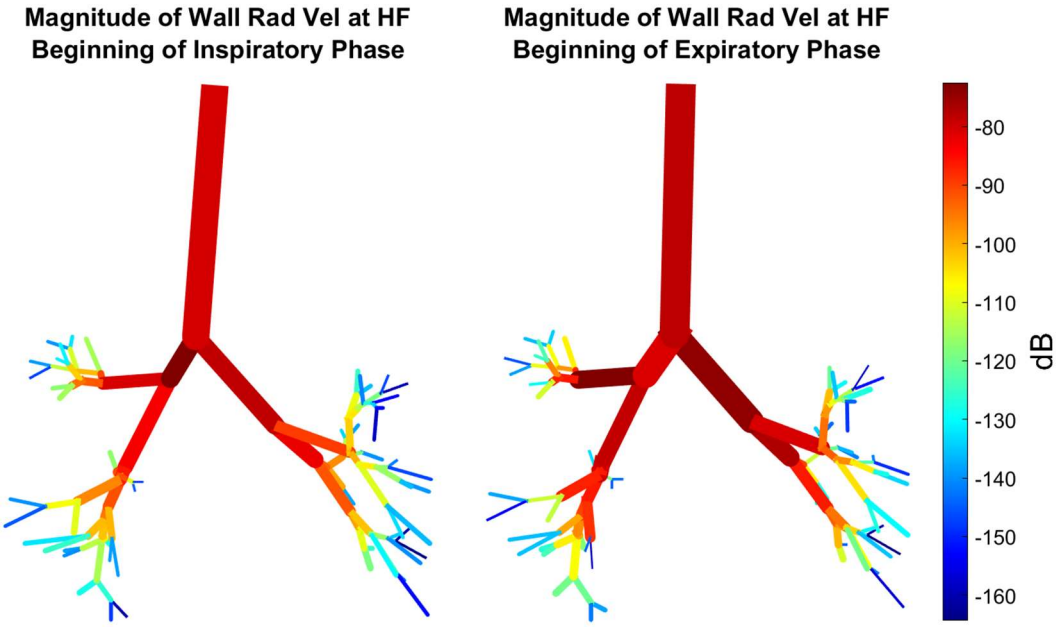

Figure 29: Magnitude of the wall radial velocity in logarithmic scale at high frequency. Comparison between the beginning of the inspiratory phase (left) and the beginning of expiratory phase (right).

The comparison of the results at low and high respiratory volumes does not show remarkable differences in terms of pressure and wall radial velocity distribution. This is especially true at the level of the trachea. Some minor differences can be noticed at the level of the right and left main bronchi. It is interesting to note that, at low frequency, both the magnitude and the real part of the acoustic pressure are higher at the beginning of the inspiratory phase. Conversely, at high frequency, they are higher at the beginning of the expiratory phase..

5.3 Simulation of Pathological Conditions

Given the results similarity between the low and the high respiratory volumes (see Section 5.2) and the associated discussion in Chapter 6, the results on the pathological conditions are reported for the inspiratory phase only. As described in section 3.2, the simulations have been obtained by properly modifying the geometry and/or the mechanical properties of the model. These alterations involved one or two parameters and are to be considered a first simplified approach toward the modelization of much more complex phenomena. The results concerning the response of the system will be presented at both low frequency (LF) and high frequency (HF). Three parameters will be evaluated: the magnitude (in logarithmic scale) and the real part of the acoustic pressure and the magnitude of the airways wall radial velocity.

5.3.1 Simulation of the Asthma Pathology

The results regarding the simulation of the asthma pathology obtained through the homogeneous alteration of thickness and radius as described in section 3.2.1 are here reported. For the magnitude and the real part of the acoustic pressure, the qualitative distribution over the entire tree and the trend in the trachea and the main bronchi are presented. In terms of wall radial velocity only the qualitative distribution is reported.

Figure 30 shows the comparison between the magnitude of the acoustic pressure in logarithmic scale in the healthy case (left) and the asthma case (right) at low frequency. Figure 31 reports

the corresponding trend over the trachea and the main bronchi for the two conditions under analysis.

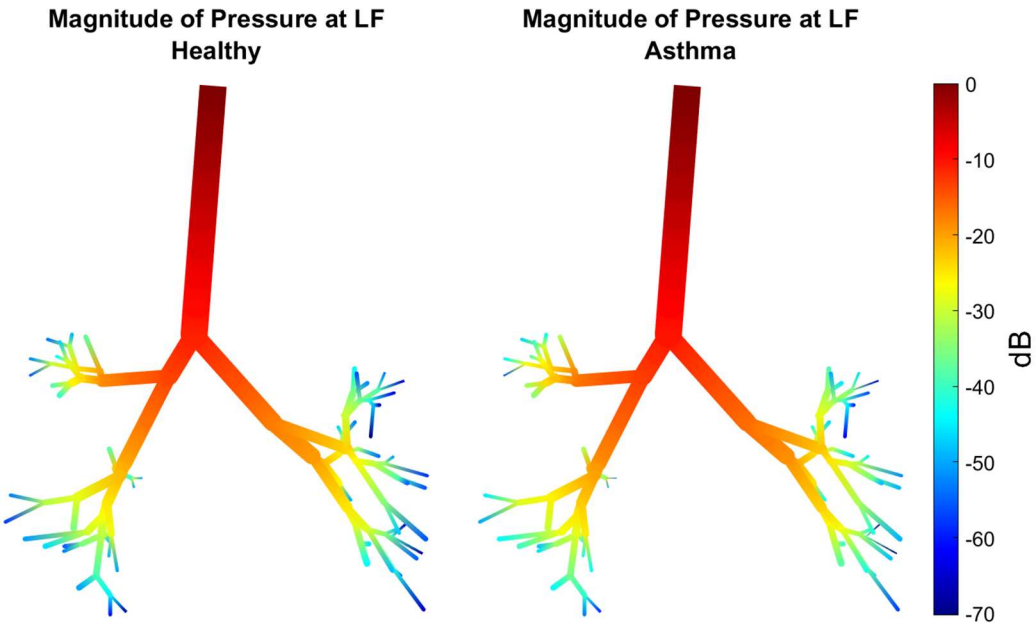

Figure 30: Magnitude of the acoustic pressure in logarithmic scale at low frequency. Comparison between healthy (left) and asthma (right).

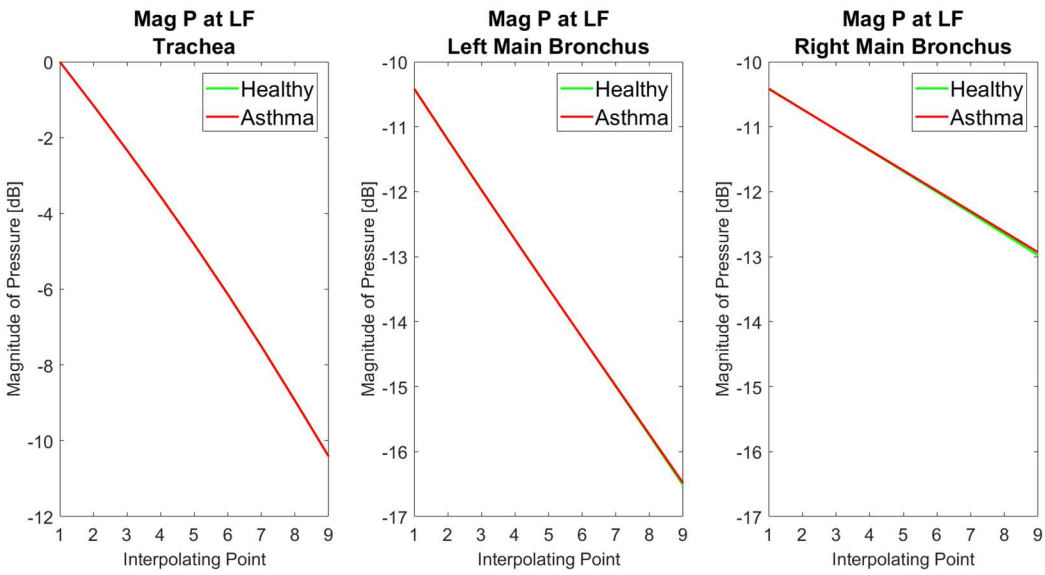

Figure 31: Trend of the magnitude of the acoustic pressure in logarithmic scale at low frequency in the trachea (left), left main Bronchus (middle) and right main bronchus (right) for the healthy case (green) and asthma case (red).

Figure 32 shows the comparison between the magnitude of the acoustic pressure in logarithmic scale in the healthy case (left) and the asthma case (right) at high frequency. Figure 33 reports the corresponding trend over the trachea and the main bronchi for the two conditions under analysis.

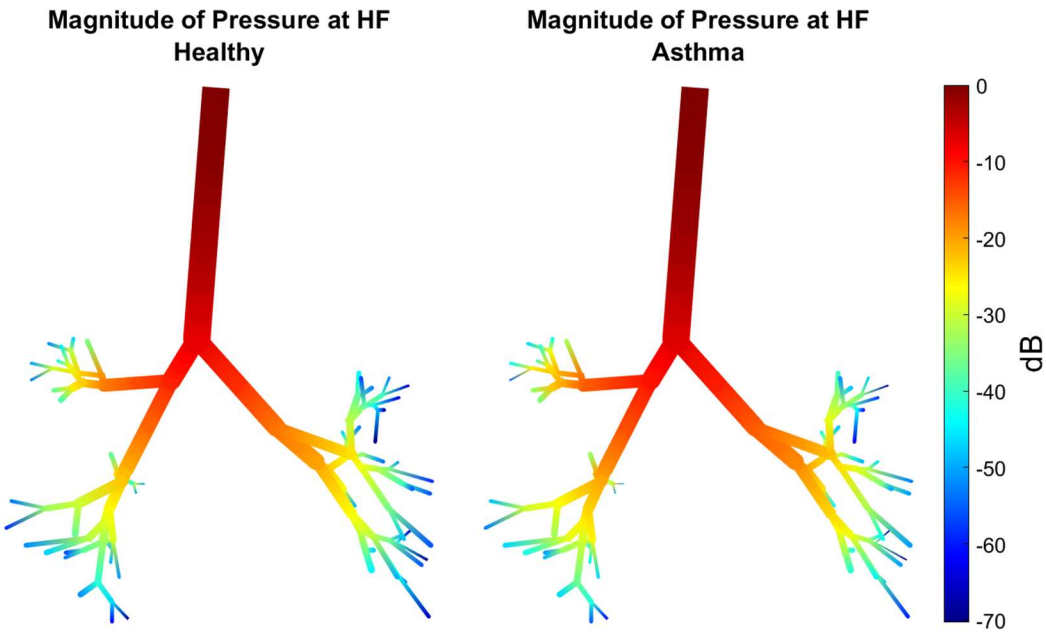

Figure 32: Magnitude of the acoustic pressure in logarithmic scale at high frequency. Comparison between healthy (left) and asthma (right).

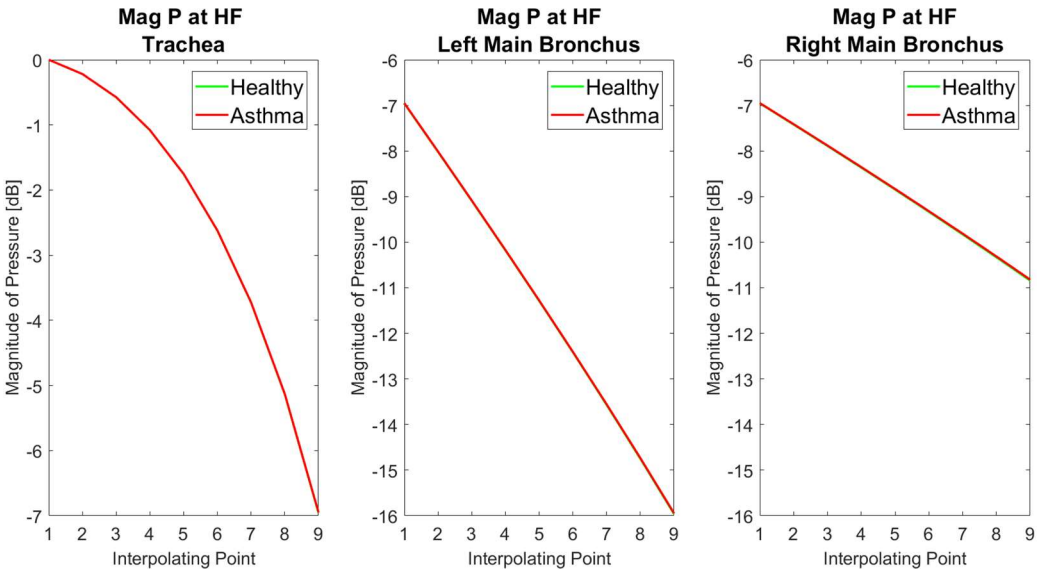

Figure 33: Trend of the magnitude of the acoustic pressure in logarithmic scale at high frequency in the trachea (left), left main Bronchus (middle) and right main bronchus (right) for the healthy case (green) and asthma case (red).

Figure 34 and 35 show the comparison between the real part of the acoustic pressure in the healthy case (left) and the asthma case (right) at low frequency and the corresponding trend over the trachea and the main bronchi under those conditions.

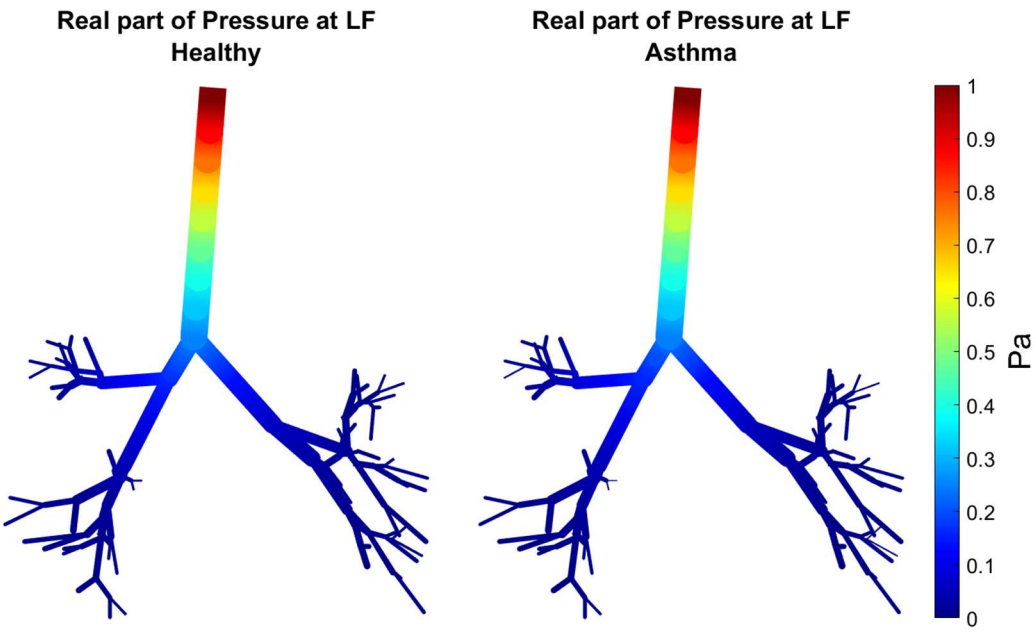

Figure 34: Real part of the acoustic pressure in logarithmic scale at low frequency. Comparison between healthy (left) and asthma (right).

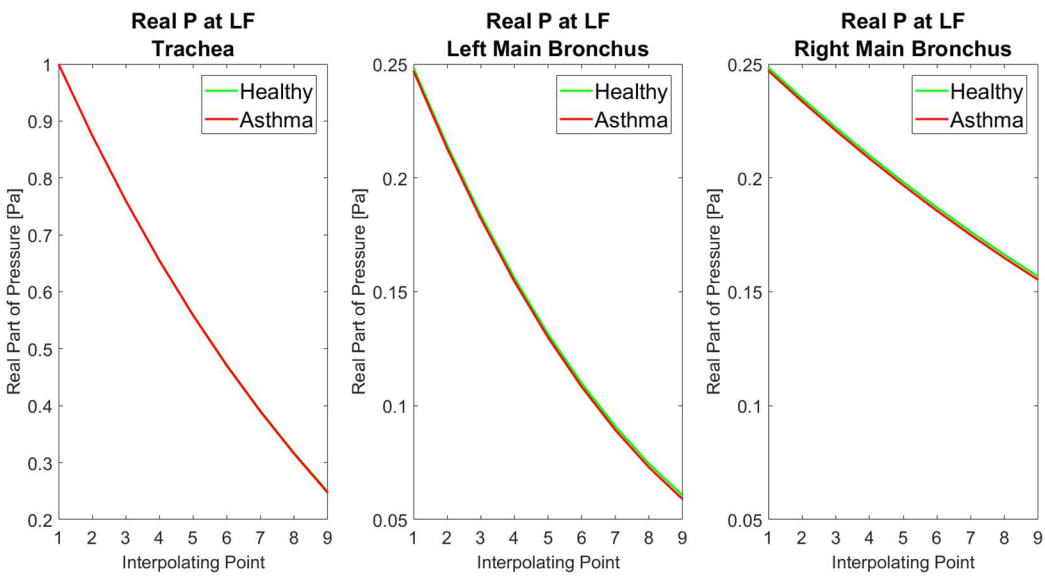

Figure 35: Trend of the real part of the acoustic pressure in logarithmic scale at low frequency in the trachea (left), left main Bronchus (middle) and right main bronchus (right) for the healthy case (green) and asthma case (red).

Figure 36 shows the comparison between the real part of the acoustic pressure in the healthy case (left) and the asthma case (right) at high frequency, while Figure 37 reports the corresponding trend over the trachea and the main bronchi for the two conditions under analysis.

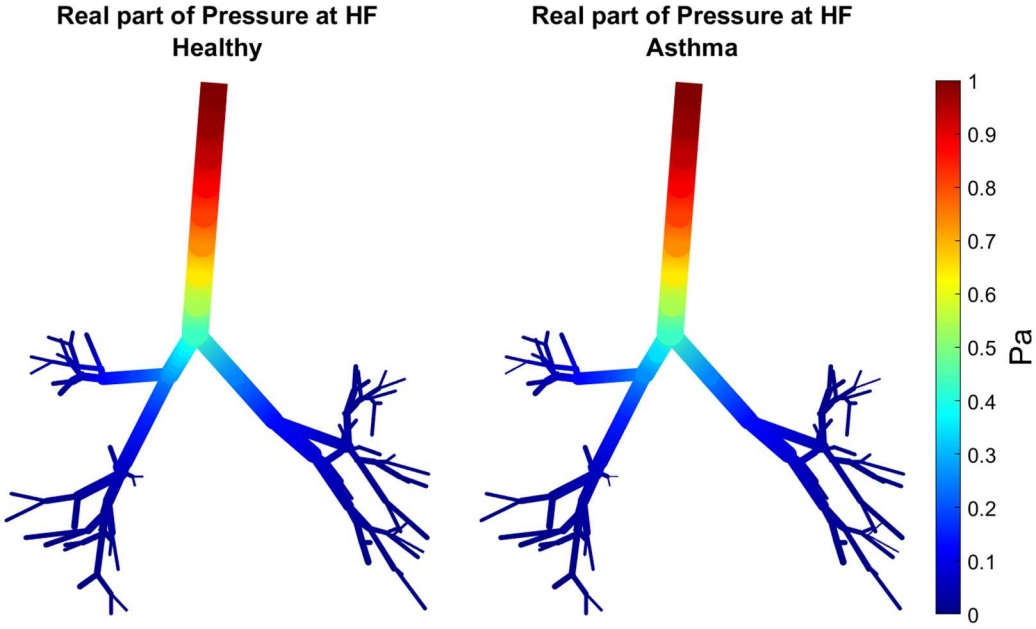

Figure 36: Real part of the acoustic pressure in logarithmic scale at high frequency. Comparison between healthy (left) and asthma (right).

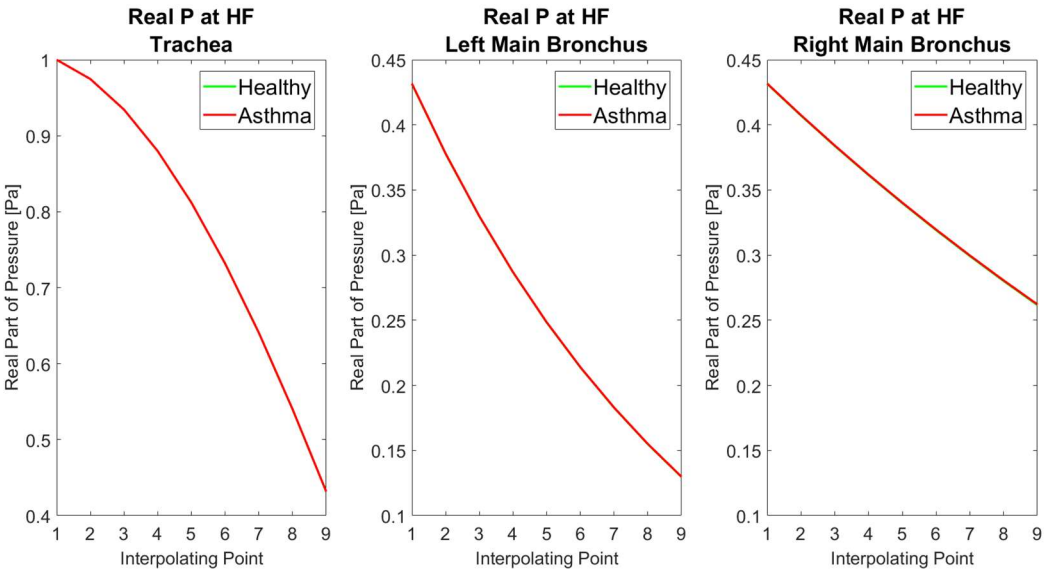

Figure 37: Trend of the real part of the acoustic pressure in logarithmic scale at high frequency in the trachea (left), left main Bronchus (middle) and right main bronchus (right) for the healthy case (green) and asthma case (red).

Finally, Figure 38 shows the comparison between the magnitude of the wall radial velocity in the healthy and asthmatic case at low frequency. Figure 39 shows the comparison between the magnitude of the wall radial velocity in the healthy and asthmatic case at high frequency.

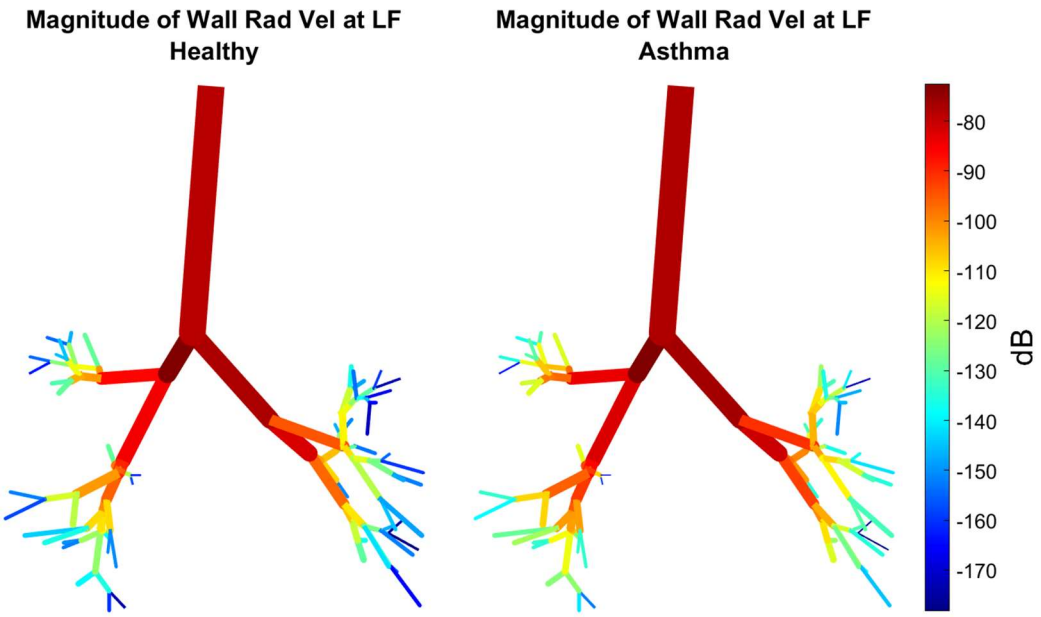

Figure 38: Magnitude of the wall radial velocity in logarithmic scale at low frequency. Comparison between healthy (left) and asthma (right).

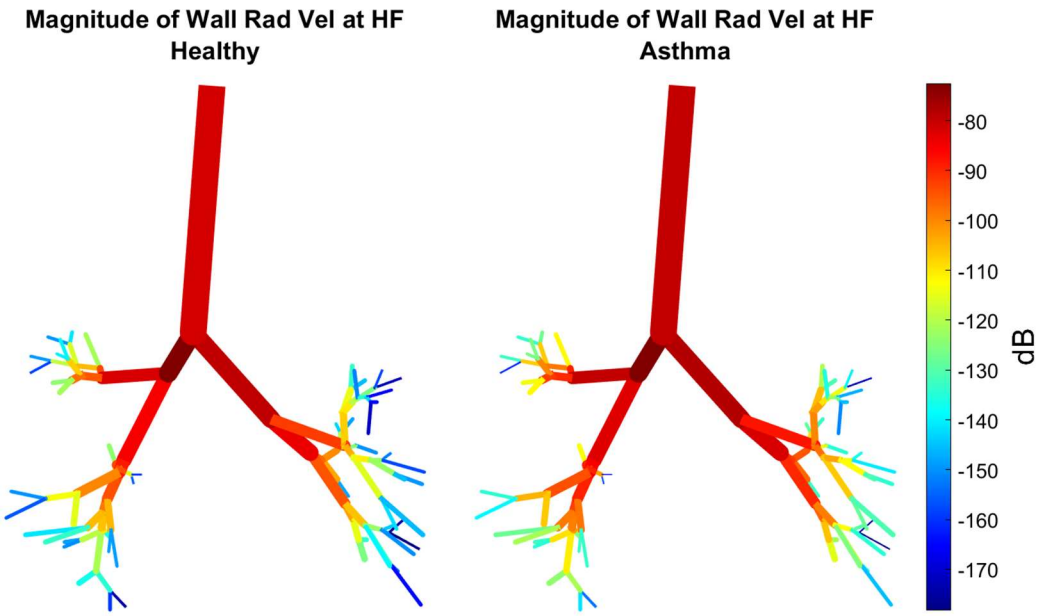

Figure 39: Magnitude of the wall radial velocity in logarithmic scale at high frequency. Comparison between healthy (left) and asthma (right).

It can be observed that, no remarkable differences can be recognized between the pathological and the healthy case for both low frequency and high frequencies. This consideration is supported not only by the qualitative analysis of both the acoustic pressure (magnitude and real part) and the wall radial velocity, but also from the respective trends for the trachea and the main bronchi which result to be almost perfectly superimposable.

5.3.2 Simulation of the Fibrosis Condition

The results regarding the simulation of the fibrosis condition are reported in the following paragraph. For the pressure-related parameters, the qualitative distribution over the entire tree and the trend in the trachea and in the main bronchi is presented. As far as the magnitude of the acoustic pressure is concerned, the analysis will be performed by the qualitative comparison of the overall distribution only.

Figure 40 shows the comparison between the magnitude of the acoustic pressure in logarithmic scale in the healthy case (left) and the fibrosis case (right) at low frequency. Figure 41 reports the corresponding trend over the trachea and the main bronchi for the two conditions under analysis.

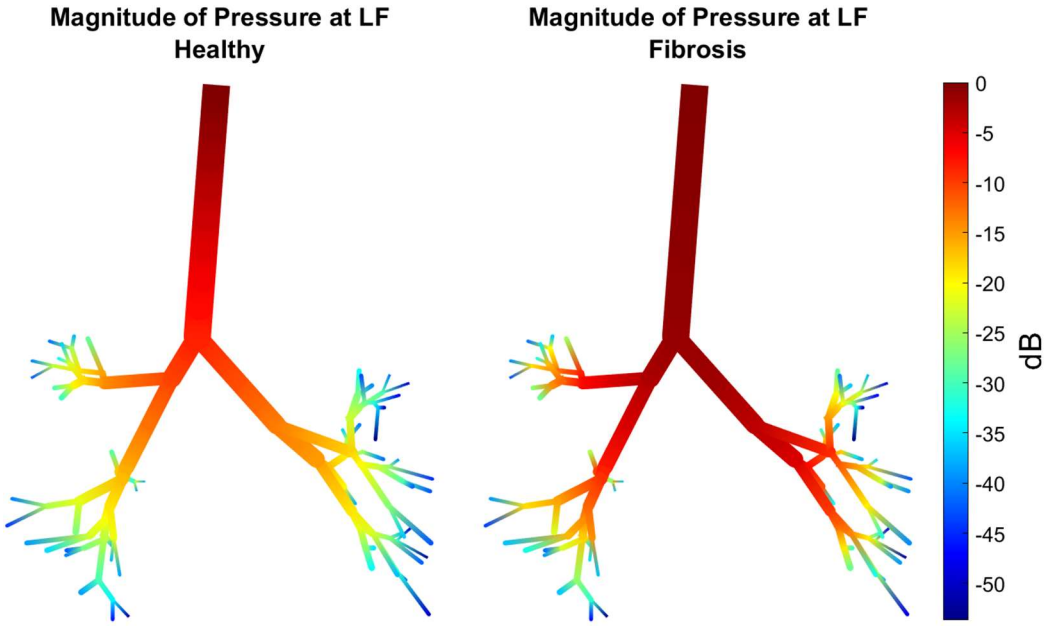

Figure 40: Magnitude of the acoustic pressure in logarithmic scale at low frequency. Comparison between healthy (left) and fibrosis (right).

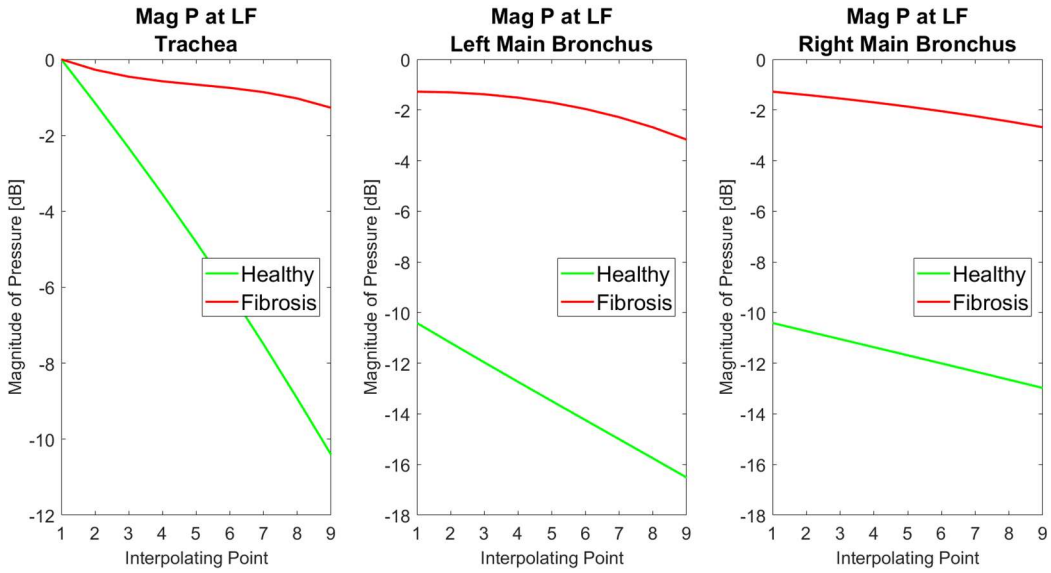

Figure 41: Trend of the magnitude of the acoustic pressure in logarithmic scale at low frequency in the trachea (left), left main Bronchus (middle) and right main bronchus (right) for the healthy case (green) and fibrosis case (red).

Figure 42 and 43 show the comparison between the real part of the acoustic pressure in the healthy case (left) and the fibrosis case (right) at high frequency the corresponding trend over the trachea and the main bronchi under those conditions.

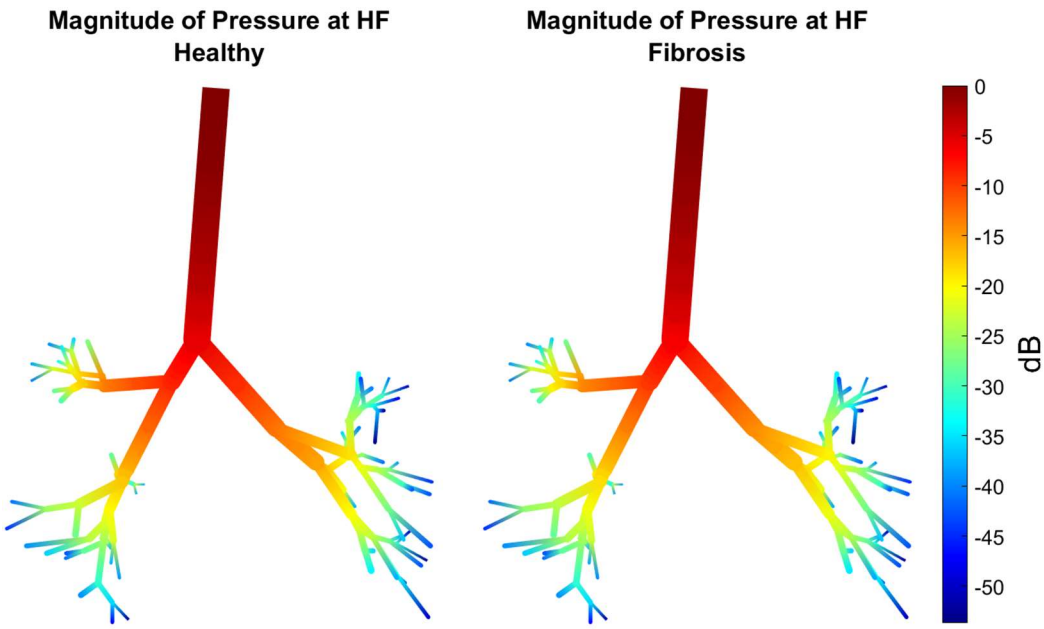

Figure 42: Magnitude of the acoustic pressure in logarithmic scale at high frequency. Comparison between healthy (left) and fibrosis (right).

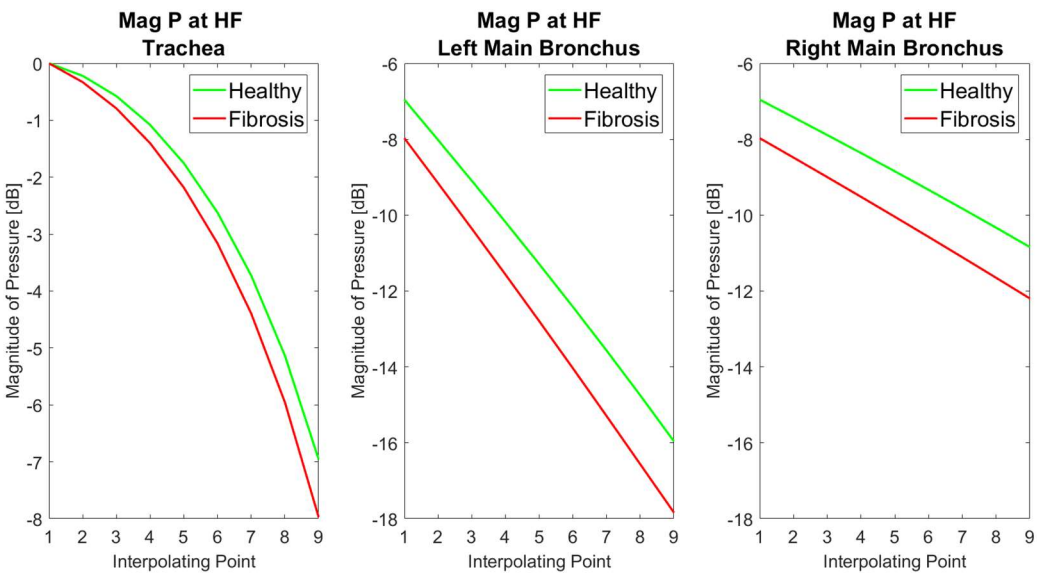

Figure 43: Trend of the magnitude of the acoustic pressure in logarithmic scale at high frequency in the trachea (left), left main Bronchus (middle) and right main bronchus (right) for the healthy case (green) and fibrosis case (red).

Figure 44 shows the comparison between the real part of the acoustic pressure in the healthy case (left) and the fibrosis case (right) at low frequency. Figure 45 reports the corresponding trend over the trachea and the main bronchi for the two conditions under analysis.

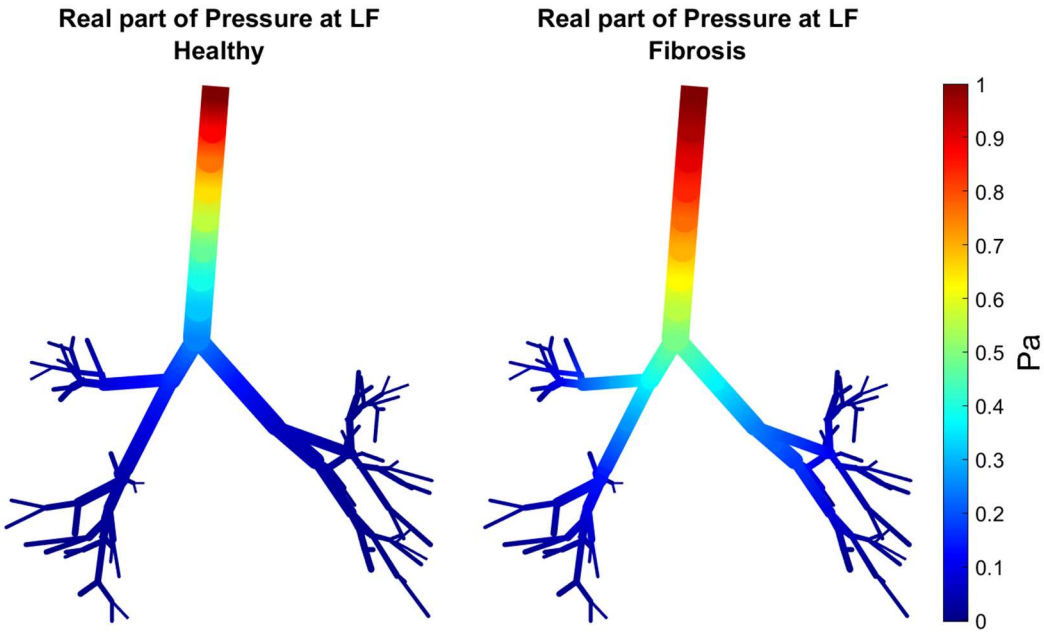

Figure 44: Real part of the acoustic pressure in logarithmic scale at low frequency. Comparison between healthy (left) and fibrosis (right).

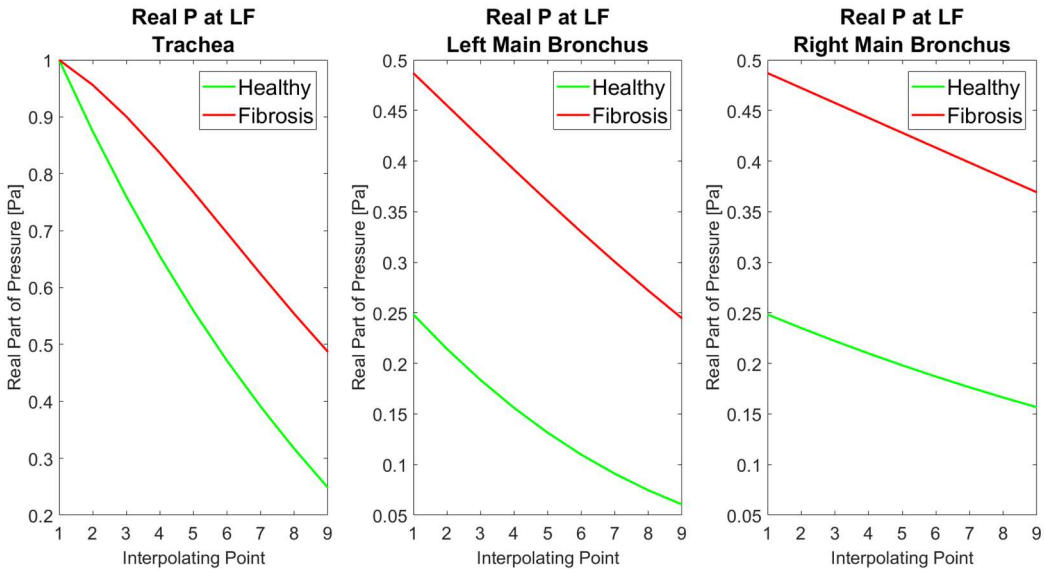

Figure 45: Trend of the magnitude of the acoustic pressure in logarithmic scale at low frequency in the trachea (left), left main Bronchus (middle) and right main bronchus (right) for the healthy case (green) and fibrosis case (red).

Figure 46 and 47 show the comparison between the real part of the acoustic pressure in the healthy case (left) and the fibrosis case (right) at high frequency the corresponding trend over the trachea and the main bronchi under those conditions.

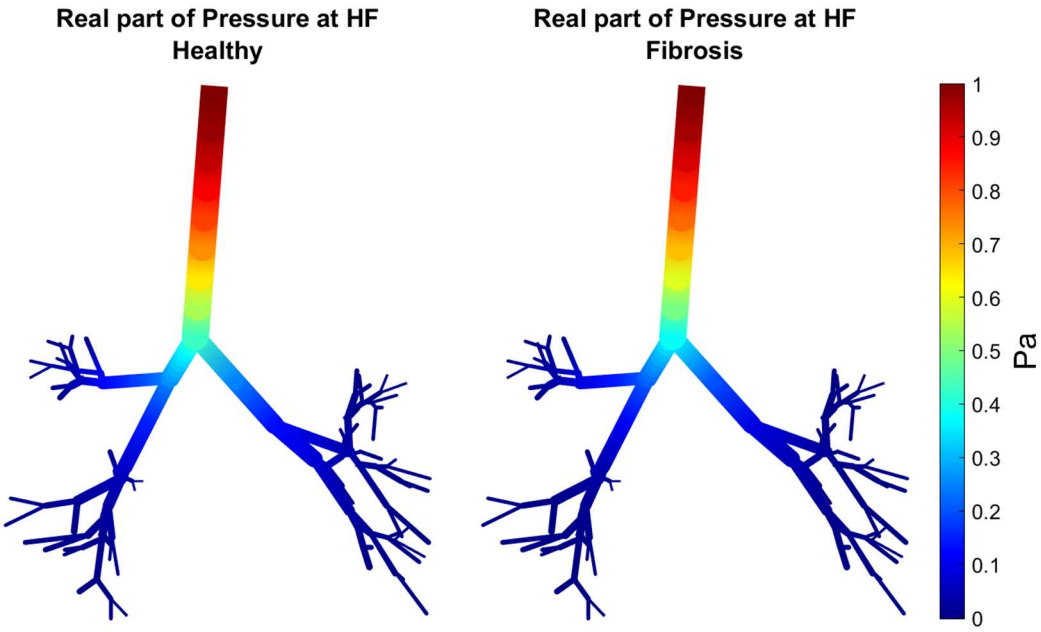

Figure 46: Real part of the acoustic pressure in logarithmic scale at high frequency. Comparison between healthy (left) and fibrosis (right).

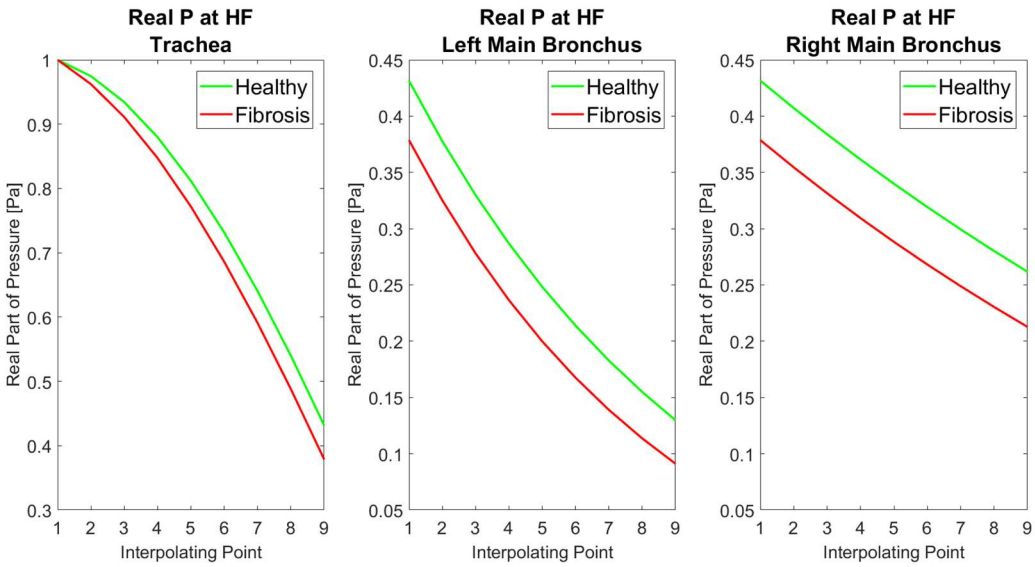

Figure 47: Trend of the magnitude of the acoustic pressure in logarithmic scale at high frequency in the trachea (left), left main Bronchus (middle) and right main bronchus (right) for the healthy case (green) and fibrosis case (red).

Finally, Figure 48 shows the comparison between the magnitude of the wall radial velocity in the healthy and asthmatic case at low frequency. Figure 49 shows the comparison between the magnitude of the wall radial velocity in the healthy and asthmatic case at high frequency.

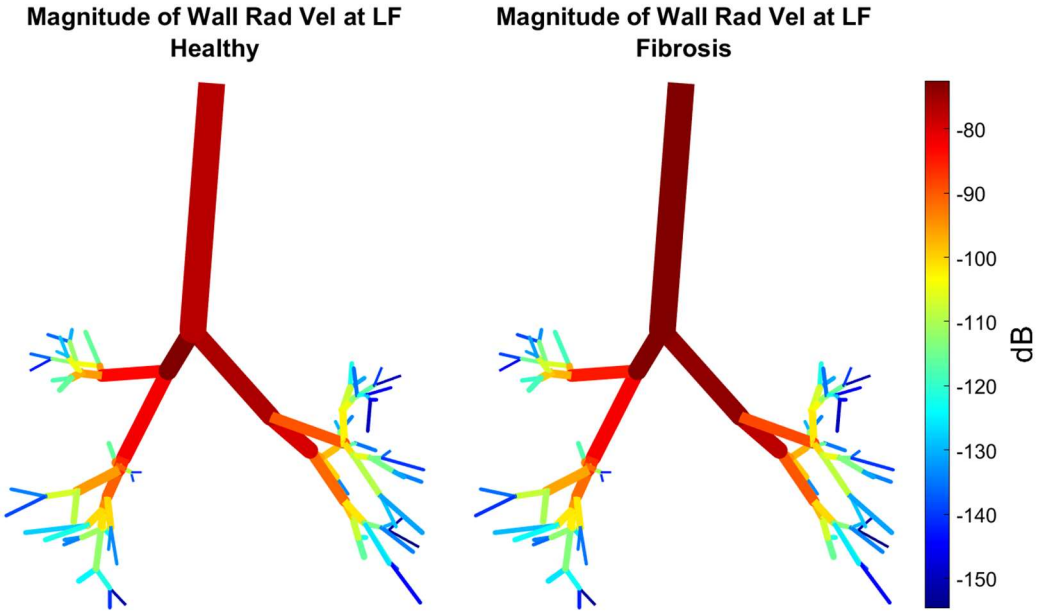

Figure 48: Magnitude of the wall radial velocity in logarithmic scale at low frequency. Comparison between healthy (left) and fibrosis (right)

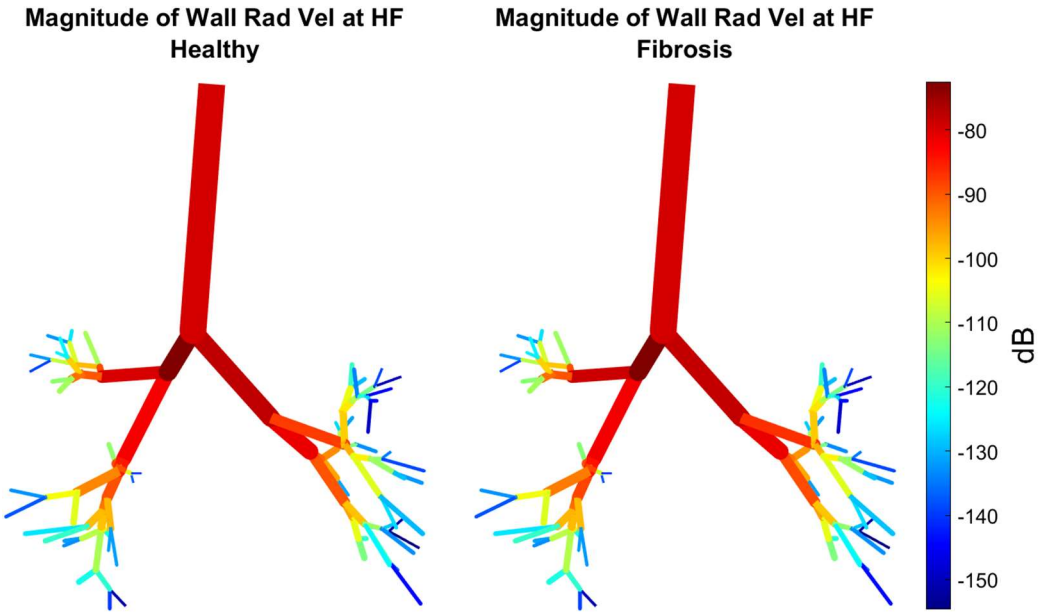

Figure 49: Magnitude of the wall radial velocity in logarithmic scale at high frequency. Comparison between healthy (left) and fibrosis (right)

At low frequency the presence of the pathology is clearly marked by a higher penetration of the acoustic wave inside the tracheo-bronchial tree. This is clearly visible from the plot of the distribution of both the magnitude and the real part of the acoustic pressure and is confirmed by the representation of the relative trends. To a lesser extent, also the qualitative analysis of the results concerning the wall radial velocity confirms the above consideration. On the contrary, at high frequency the differences are less marked as confirmed by the trend of the pressure (both magnitude and real part). In terms of wall radial velocity, no qualitative pathology-induced alteration can be recognized.

5.3.3 Simulation of the Pulmonary Infiltrate Condition

The results concerning the simulation of a pulmonary infiltrate in the lower left lobe (LLL) are here reported. For this specific pathology, it was chosen to visualize the distribution of the parameters on the tracheobronchial tree at the low and high frequencies together with the trend of the acoustic pressure in the inferior lobar bronchus, namely segment leading to the lower left lobe immediately after the bifurcation between upper and lower lobe. The segment was chosen because it is the first and largest segment moving downward the tree which is expected to face a significant variation with respect to the physiological case. The position of the segment is reported in red in Figure 50.

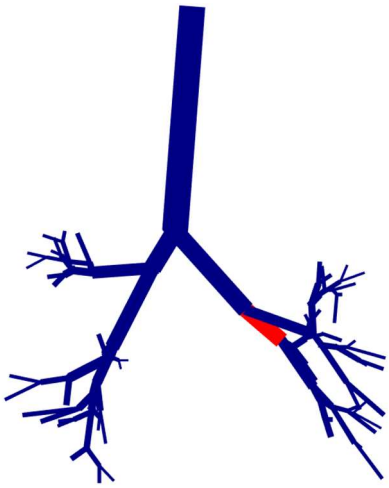

Figure 50: Position of the inferior lobar bronchus analyzed in the case of the LLL Pulmonary infiltrate

Figure 51 shows the comparison between the real part of the acoustic pressure in the healthy case (left) and the pulmonary infiltrate case (right) at low frequency. Figure 52 reports the corresponding trend over inferior lobar bronchus previously identified.

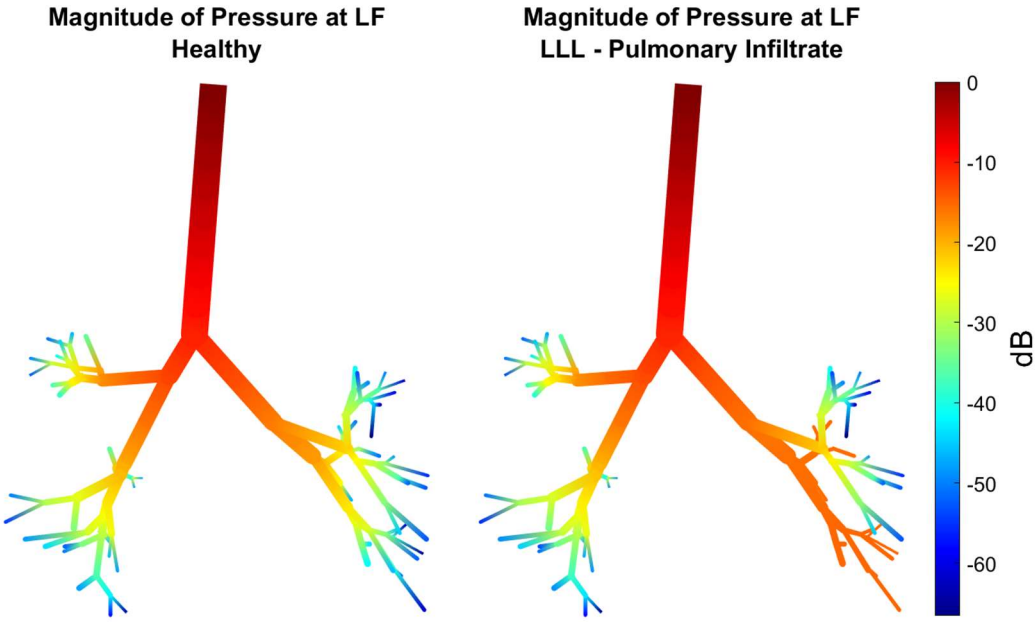

Figure 51: Magnitude of the acoustic pressure in logarithmic scale at low frequency. Comparison between healthy (left) and LLL pulmonary infiltrate (right).

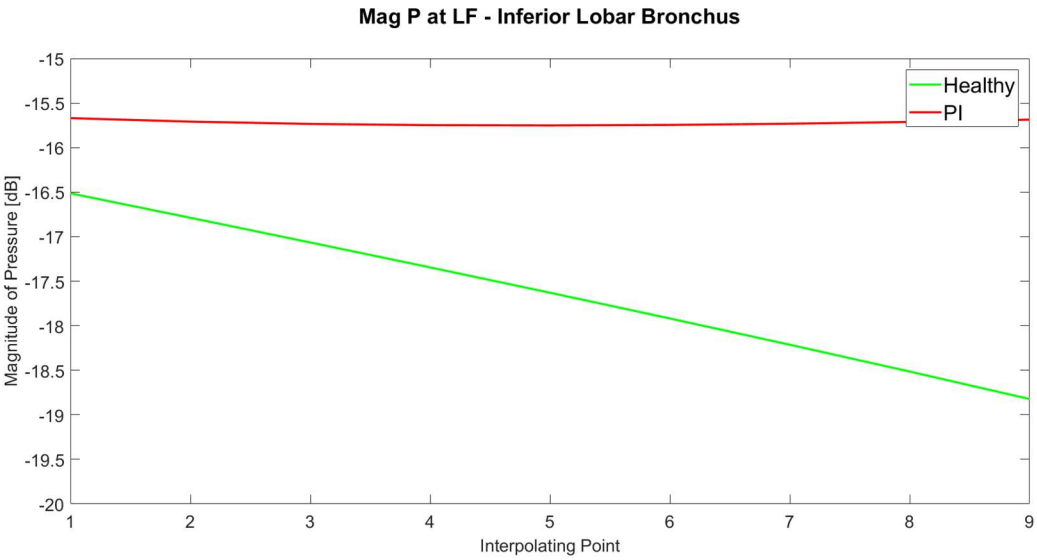

Figure 52: Trend of the magnitude of the acoustic pressure in logarithmic scale at low frequency in the inferior lobar bronchus for the healthy case (green) and pulmonary infiltration (red).

Figure 53 and 54 show the comparison between the real part of the acoustic pressure in the healthy case (left) and the pulmonary infiltrate case (right) at high frequency the corresponding trend over the above-mentioned segment.

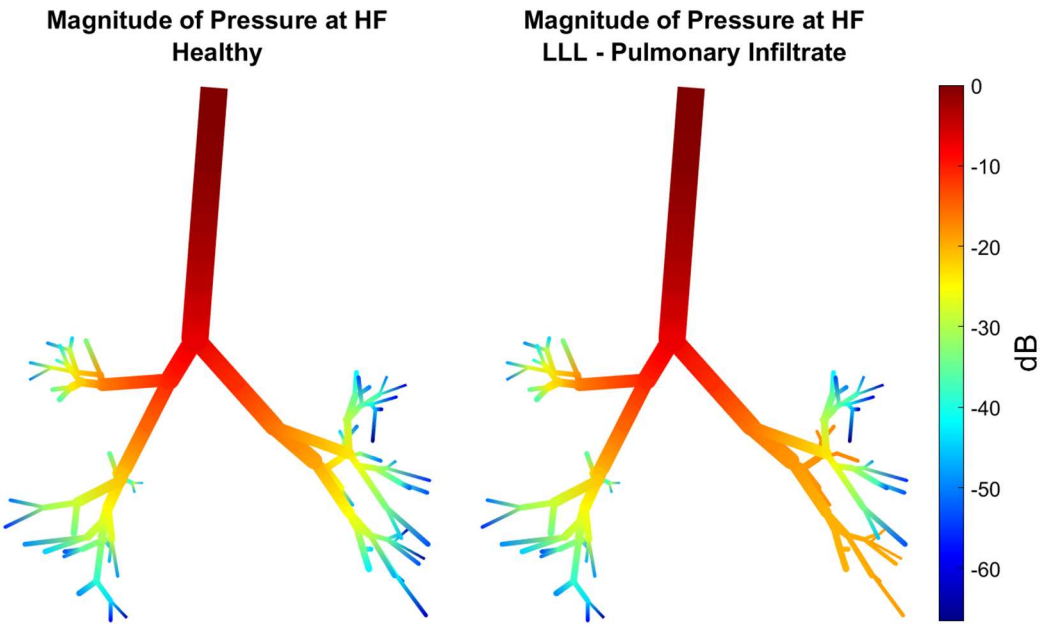

Figure 53: Magnitude of the acoustic pressure in logarithmic scale at high frequency. Comparison between healthy (left) and LLL pulmonary infiltrate (right).

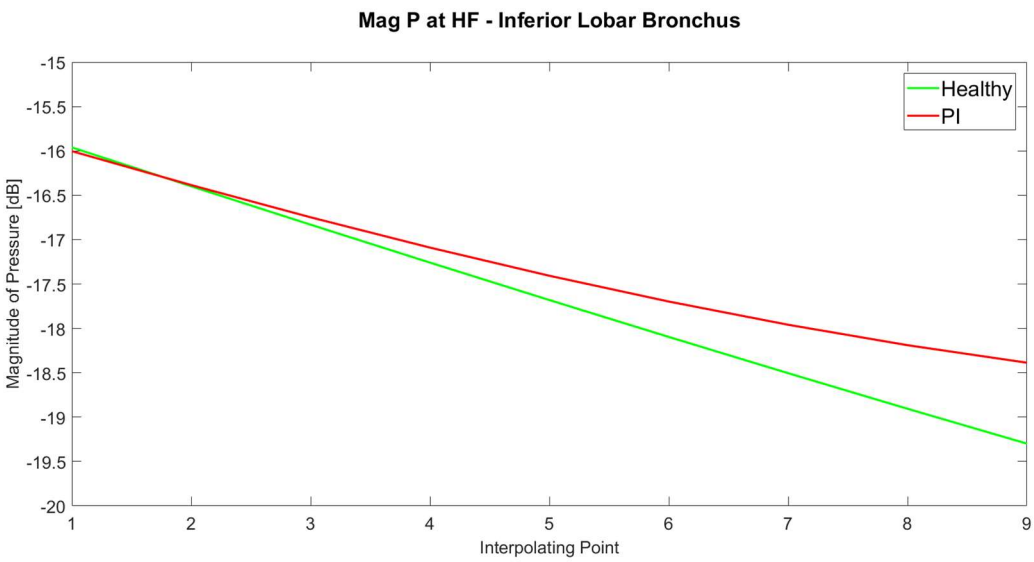

Figure 54: Trend of the magnitude of the acoustic pressure in logarithmic scale at high frequency in the inferior lobar bronchus for the healthy case (green) and pulmonary infiltration (red).

Figure 55 shows the comparison between the real part of the acoustic pressure in the healthy case (left) and the pulmonary infiltrate case (right) at low frequency. Figure 56 reports the corresponding trend over lobar inferior bronchus.

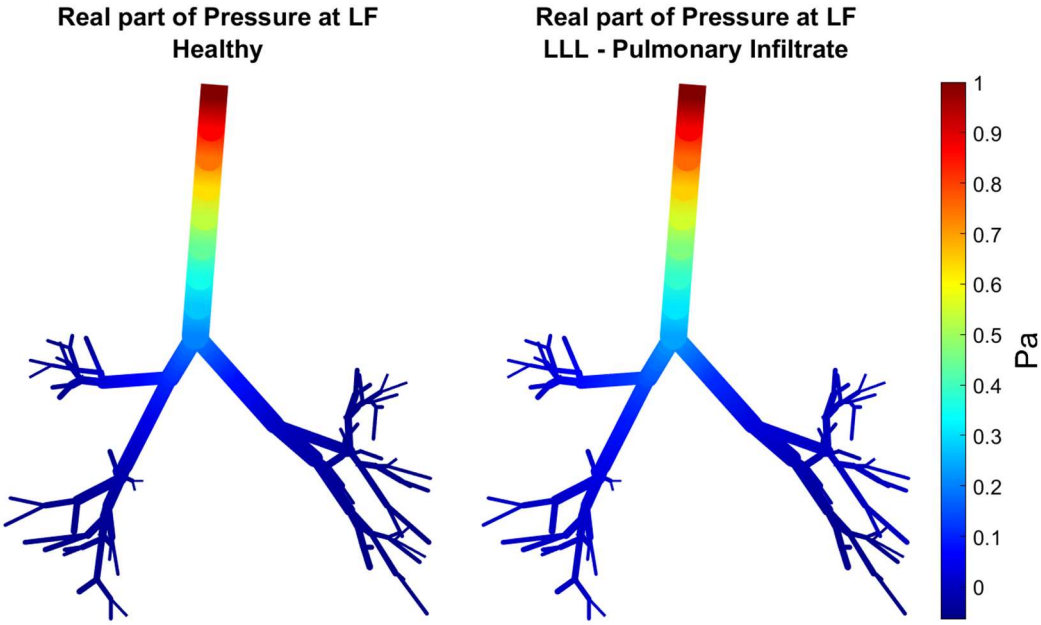

Figure 55: Real Part of the acoustic pressure in logarithmic scale at low frequency. Comparison between healthy (left) and LLL pulmonary infiltrate (right).

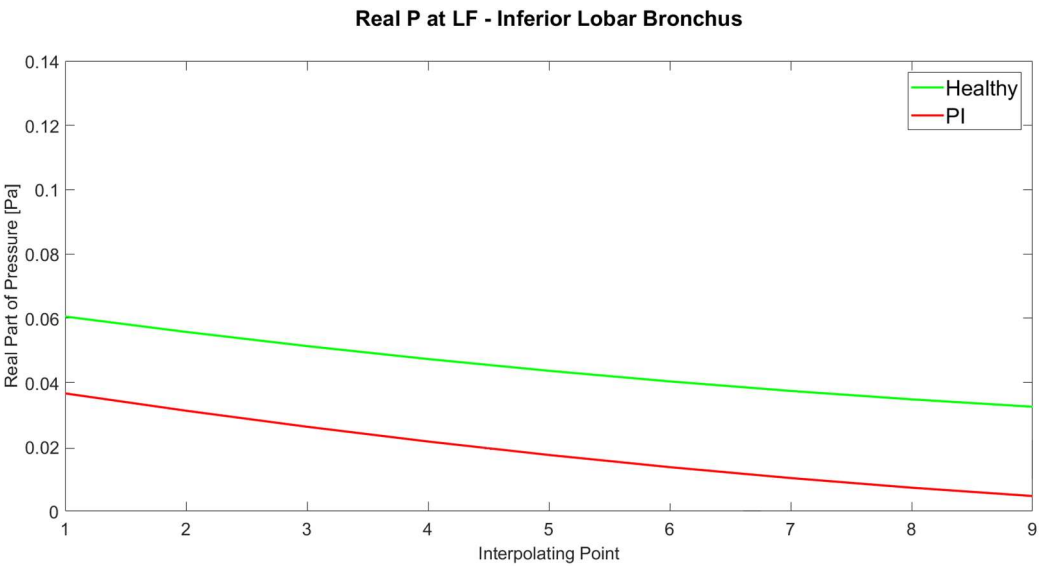

Figure 56: Trend of the real part of the acoustic pressure in logarithmic scale at low frequency in the inferior lobar bronchus for the healthy case (green) and pulmonary infiltration (red).

Figure 57 and 58 show the comparison between the real part of the acoustic pressure in the healthy case (left) and the pulmonary infiltrate case (right) at high frequency the corresponding trend over the inferior lobar bronchus.

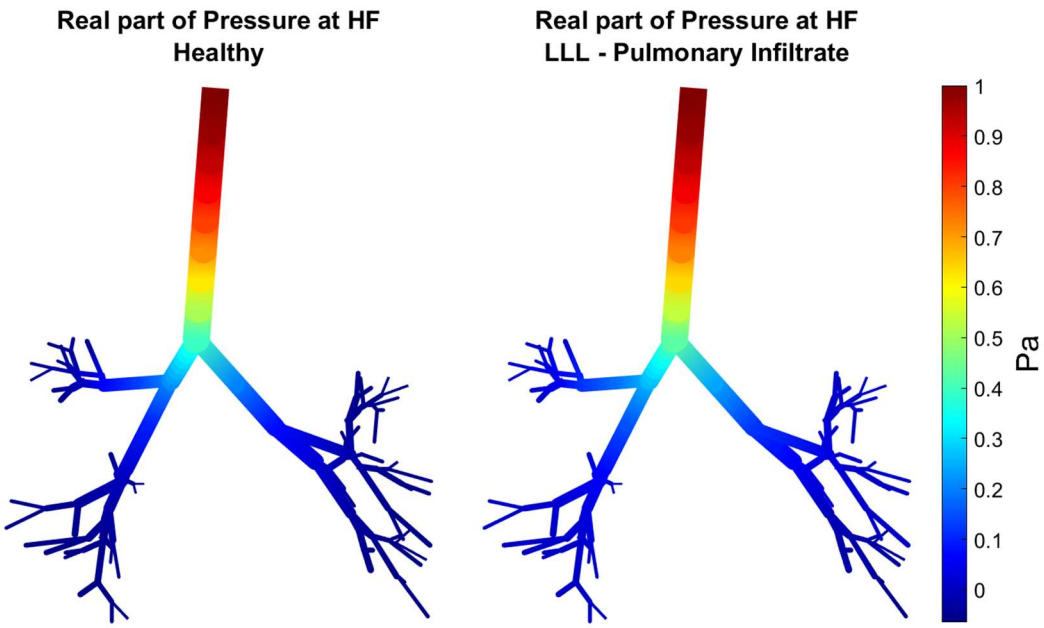

Figure 57: Real part of the acoustic pressure in logarithmic scale at high frequency. Comparison between healthy (left) and LLL pulmonary infiltrate (right).

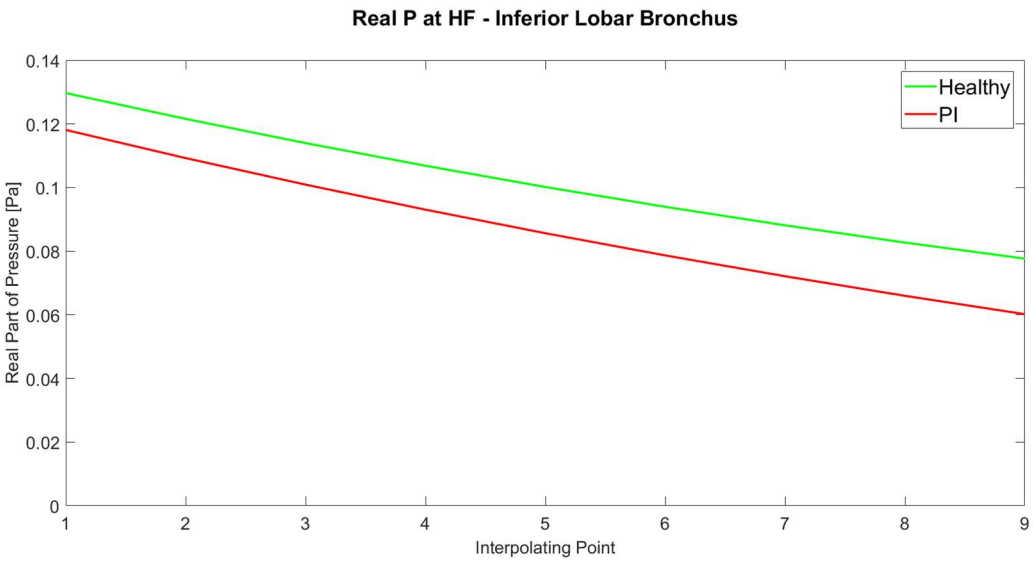

Figure 58: Trend of the real part of the acoustic pressure in logarithmic scale at high frequency in the inferior lobar bronchus for the healthy case (green) and pulmonary infiltration (red).

Finally, Figure 59 shows the comparison between the magnitude of the wall radial velocity in the healthy and pulmonary infiltrate case at low frequency. Figure 60 shows the same comparison at high frequency.

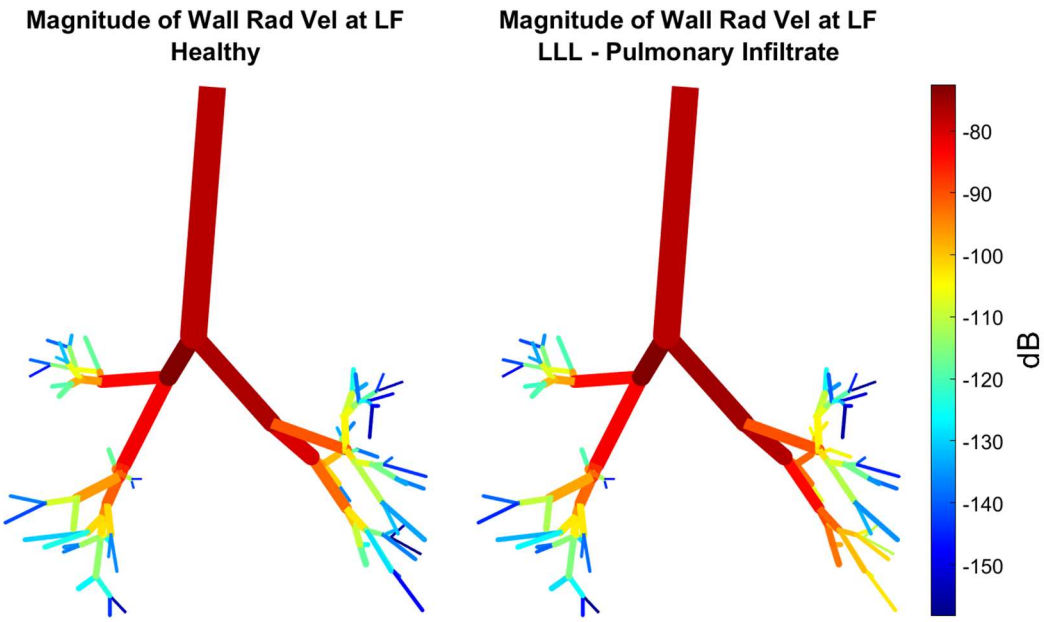

Figure 59: Magnitude of the wall radial velocity in logarithmic scale at low frequency. Comparison between healthy (left) and LLL pulmonary infiltrate (right).

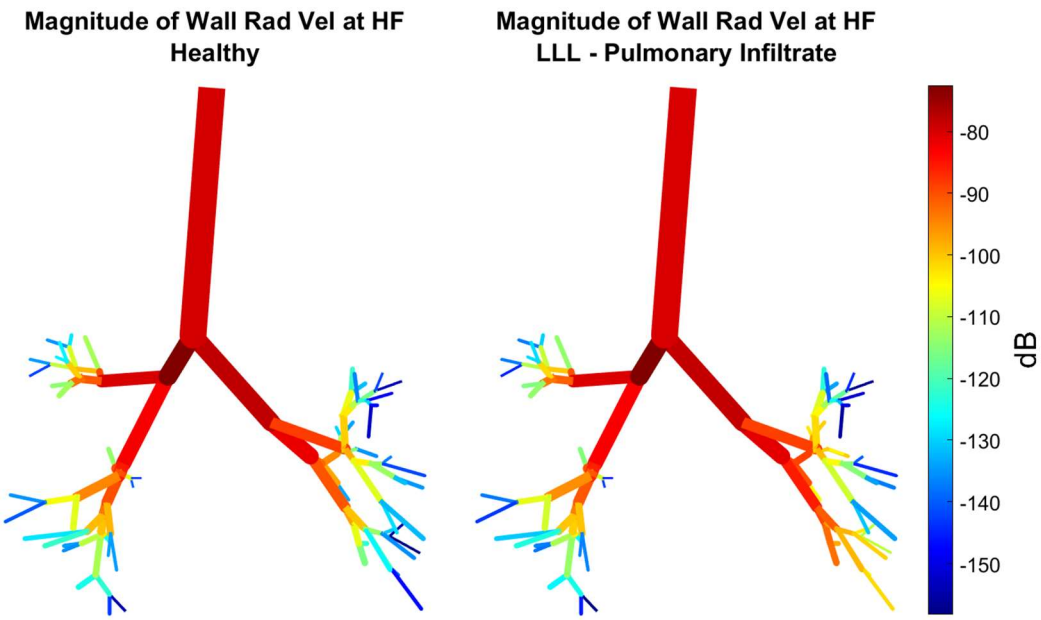

Figure 60: Magnitude of the wall radial velocity in logarithmic scale at high frequency. Comparison between healthy (left) and LLL pulmonary infiltrate (right).

For both the frequencies of interest it can be observed that the introduction of the occlusion on the lower left lobe causes the magnitude of the pressure to be significantly higher in the corresponding branches. This observation is even more evident considering the plot of the magnitude of the pressure for the healthy and the pathological cases. Not only the values but also the trends are qualitatively different. Although still evident, at high frequency this behavior seems slightly less marked. In addition, the overall distribution of pressure in the rest of the tree does not seem to be affected in a significant way.

If the real part of the acoustic pressure is considered, the trend is approximately equal in the physiological and in the pathological case. This is confirmed by the comparison between the plot of the real part of the pressure in the lower lobar bronchus for the healthy and pathological case.

In terms of magnitude of the wall radial velocity, the pulmonary infiltrate shows differences basically in the lower branches of the left lung. The alterations are strikingly evident especially at the terminal branches where the magnitude of the velocity is almost three orders higher than the healthy case.

5.4 Application of the Model to Control and Asthmatic Groups

In this section the results concerning the application of the model to the five control subjects and the five asthmatic subjects are presented. First, the outcome of the validation procedure and the data from [42] are compared to assess the reliability of the reference.

Second, the results of the acoustic impedance values and the acoustic pressure distribution are reported separately for each group, to allow the evaluation of the inter-subject variability of the acoustic parameters in relation to the different pulmonary volumes and the different frequencies. The analysis has indeed been performed at both low (RV/FRC) and high (TLC) pulmonary volumes as well as at both low (200 Hz) and high (600 Hz) frequencies.

Third, t the two groups are compared in terms of internal diameter, acoustic impedance values and acoustic pressure distribution.

In each paragraph, the results are reported for the first five generations: generation 0 denotes the trachea, generation 1 the main bronchi, generation 2 the lobar bronchi, generation 3 and 4 the segmental and sub-segmental bronchi, respectively.

In terms of acoustic impedance, the values at the input (Zin) and the terminal part (Zt) of each generation are reported, where the input denotes the end of the segments closer to the trachea and the terminal part denotes the extremity farther from the trachea, respectively.
The absolute value of the acoustic pressure is reported in each of the nine interpolating points in which it was computed by the model.

The statistical analysis is reported inter and intra groups. A normality test (Shapiro-Wilk) was preliminary performed for each data source. The statistical difference between the asthmatic and the control case is evaluated for the whole generation and not for every single interpolating point. If the hypothesis of normality of the samples is accepted, the data are compared with a t-test, whereas a Mann-Whitney test is applied in case of non-normal samples. The statistical significance is reported in the graphs as:

- *, P-value ≤ 0.05
- **, P-value ≤ 0.01
- ***, P-value ≤ 0.001

5.4.1 Validation of the Asthmatic Data

The data from [42] and their validation according to the procedure described in paragraph 5.4.1 are reported in TABLE 12. For both the reference and the measured data the mean, standard deviation (SD) and coefficient of variation (CV) are reported. In addition, the discrepancy between the literature data and the measurements obtained during the validation procedure is evaluated through the computation of the relative error with respect to the reference.

In the presentation of the results, the segments are categorized according to their position in the lungs. The following regions are identified and reported in TABLE 12: left upper lobe (LUL), left middle lobe (LML), right upper lobe (RUL), right middle lobe (RML), right lower lobe (RLL). The trachea together with the right main bronchus (RMB) and the left main bronchus (LMB) are reported separately.

TABLE 12: COMPARISON BETWEEN THE AVERAGE VALUES OF THICKNESS OF THE DATA FROM LITERATURE AND THE MEASUREMENTS OBTAINED DURING THE PROCEDURE OF VALIDATION

		Montesantos and Al.			**Validation**			**Relative Error [%]**
	Gen.	*Average [mm]*	*SD [mm]*	*CV*	*Average [mm]*	*SD [mm]*	*CV*	
Trachea	0	2.70	0.19	0.07	2.04	0.18	0.09	24.21
LMB	1	2.06	0.25	0.12	1.77	0.05	0.03	13.88
RMB	1	2.25	0.43	0.19	1.84	0.03	0.02	18.08
RUL	2	2.09	0.23	0.11	1.80	0.05	0.03	13.87
	3	1.80	0.38	0.21	1.56	0.08	0.05	13.29
	4	1.55	0.30	0.19	1.42	0.06	0.04	8.17
	5	1.56	0.41	0.26	1.47	0.03	0.02	5.83
	6	1.62	0.39	0.24	1.56	0.11	0.07	3.47
RML	2	2.12	0.63	0.30	1.71	0.13	0.08	19.34
	3	1.76	0.18	0.10	1.55	0.11	0.07	11.74
	4	1.66	0.36	0.22	1.38	0.06	0.04	16.79
	5	1.57	0.29	0.19	1.28	0.02	0.01	18.41
RLL	3	1.93	0.34	0.18	1.80	0.04	0.02	6.70
	4	1.74	0.16	0.09	1.63	0.06	0.04	5.91
	5	1.74	0.38	0.22	1.60	0.04	0.02	7.97
	6	1.63	0.31	0.19	1.43	0.19	0.13	12.00
	7	1.65	0.29	0.18	1.42	0.19	0.14	13.96
	8	1.63	0.40	0.25	1.53	0.20	0.13	6.03
LUL	2	1.89	0.19	0.10	1.82	0.06	0.03	3.55
	3	1.86	0.28	0.15	1.72	0.04	0.02	7.49
	4	1.85	0.47	0.25	1.57	0.05	0.03	15.04
	5	1.72	0.39	0.23	1.53	0.10	0.07	11.09
	6	1.56	0.01	0.01	1.55	0.07	0.05	0.60
LLL	2	2.36	0.57	0.24	1.99	0.04	0.02	15.47
	3	1.94	0.76	0.39	1.81	0.17	0.09	6.43
	4	2.00	0.49	0.25	1.71	0.08	0.05	14.32
	5	1.83	0.44	0.24	1.63	0.10	0.06	10.69
	6	1.76	0.32	0.18	1.66	0.13	0.08	5.45

The highest discrepancy is identified at the level of trachea (where the maximum relative error is located) and at the first two generations. For higher orders, the error progressively to decreases. The coefficient of variation (CV) shows that the measured data have a lower variability than the one from [42]. Nonetheless, neither the literature data nor the measured ones have a variability which can be considered statistically significant as the values of CV are far lower than 1.

5.4.2 Results for the Control Group

Figure 61 and Figure 62 report the input (Zin, black symbols) and terminal (Zt, white symbols) acoustic impedance from generation 0 to 4 at high respiratory volume (Fig. 61) and low respiratory volume (Fig. 62) in the control subjects at low (LF, circles) and high (HF, diamonds) frequencies.

The statistical analysis refers to the comparison between the overall impedance at high frequency and the corresponding value at low frequency. Each generation is analyzed separately.

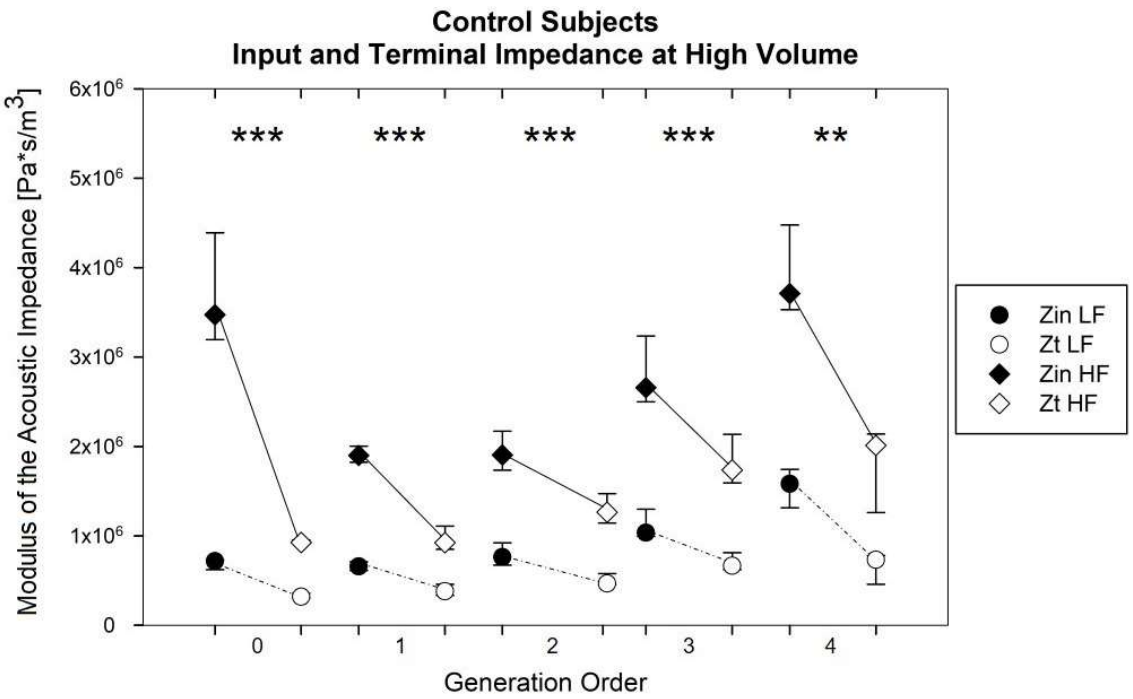

Figure 61: Input (black symbols) and terminal (white symbols) acoustic impedance from generation 0 to 4 at high respiratory volume in the control subjects. Low (circles) and high (diamonds) frequencies are reported. The symbols indicate the median values, the lower and the upper bars correspond to the 25th percentile and the 75th percentile, respectively. **, $p<0.01$; ***, $p<0.001$ between low and high frequency.

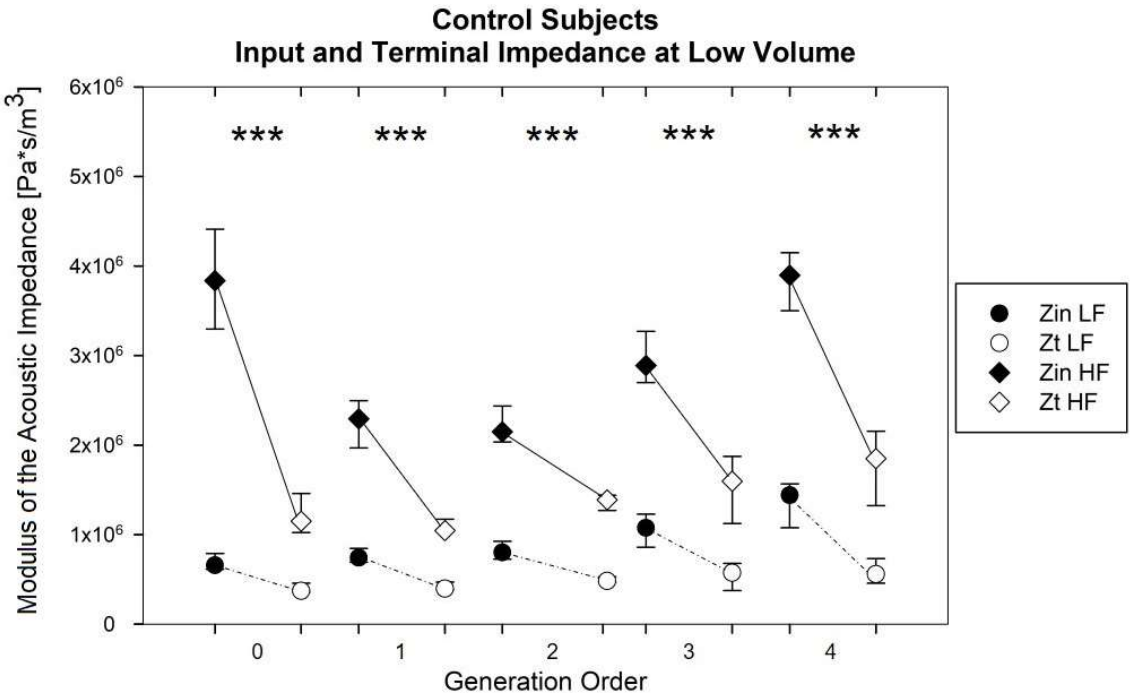

Figure 62: Input (black symbols) and terminal (white symbols) acoustic impedance from generation 0 to 4 at low respiratory volume in the control subjects. Low (circles) and high (diamonds) frequencies are reported. The symbols indicate the median values, the lower and the upper bars correspond to the 25th percentile and the 75th percentile, respectively. ***, $p<0.001$ between low and high frequency.

The impedances at different generations are quite similar at high volume and low volume for all the generations. Both the input and the terminal impedance are significantly higher at high frequency respect to low frequency $p < 0.01$, in all generations), both at low and high respiratory volumes. At low frequency, as the generation order increases, it can be observed an approximately linear increment of both the input and the terminal impedance and, within each generation, the difference between the input and terminal impedances is approximately constant. At high frequency, the trachea shows an input impedance twice the impedance of the following generation. On the contrary, the values of the terminal impedances are approximately linearly increasing with the generation order.

Figure 63 and Figure 64 show the distribution of acoustic pressure at high and low volume, respectively. In each graph, the behavior of both low (LF, black circles) and high (HF, white circles) frequencies is reported. The pressure values are reported at nine equally spaced points along each generation according to what stated in 3.2. Pressure distribution in each segment is not significantly different between the low and the high frequency.

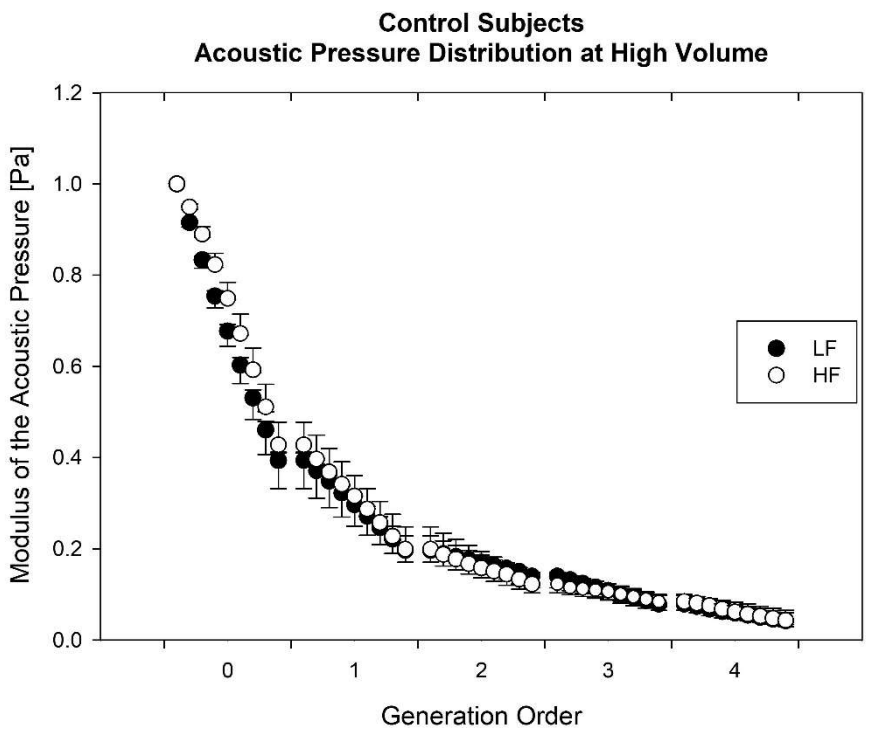

Figure 63: Acoustic pressure distribution from generation 0 to 4 at high respiratory volume in control subjects. Low frequency (black circles) and high frequencies (white circles) are reported. For each generation the values are shown along 9 equally spaced points. The symbols indicate the median value, the lower and the upper bars correspond to the 25th percentile and the 75th percentile, respectively.

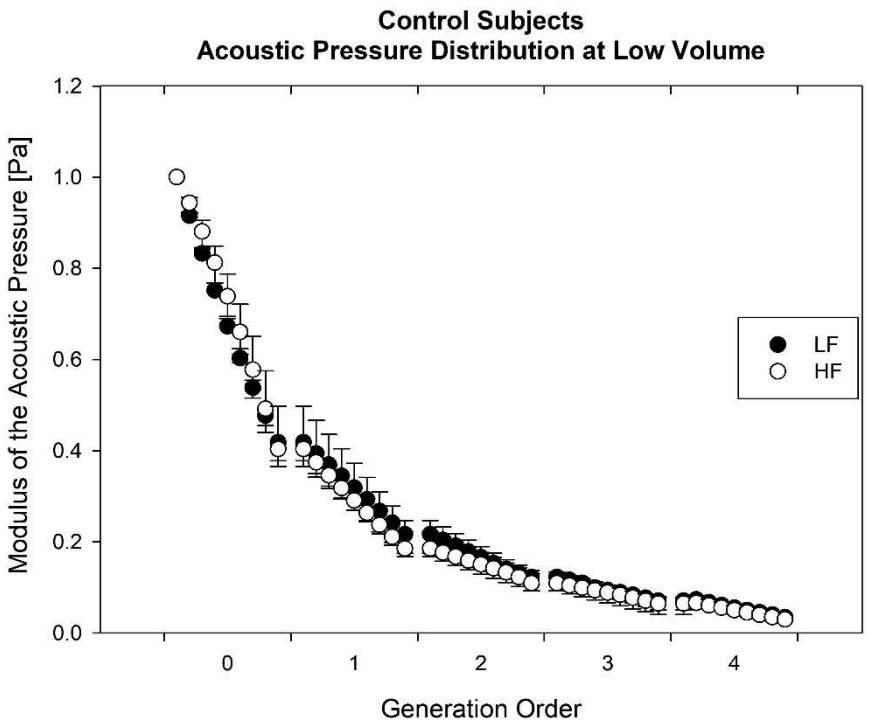

Figure 64: Acoustic pressure distribution from generation 0 to 4 at low respiratory volumes in control subjects. Low frequency (black circles) and high frequencies (white circles) are reported. For each generation the values are shown along 9 equally spaced points. The symbols indicate the median value, the lower and the upper bars correspond to the 25th percentile and the 75th percentile, respectively.

At both the respiratory volumes, the major pressure drop is at the level of the trachea where the value pressure decreases of approximately 60% of the initial value. The pressure drop continues in the following generations with a less marked trend. By the end of the 4th the pressure is almost reduced to zero. This behavior is independent from the input frequency of the acoustic wave.

5.4.3 Results for the Asthmatic Group

Figure 65 and Figure 66 show the values of the input (Zin, black) and terminal (Zt, white) acoustical impedance at high respiratory volume and low respiratory volume, respectively. Low and high frequencies are reported with circles and diamonds, respectively. The statistical analysis was performed comparing, for each generation, the overall impedance value in the segment at high frequency to the corresponding value at low frequency

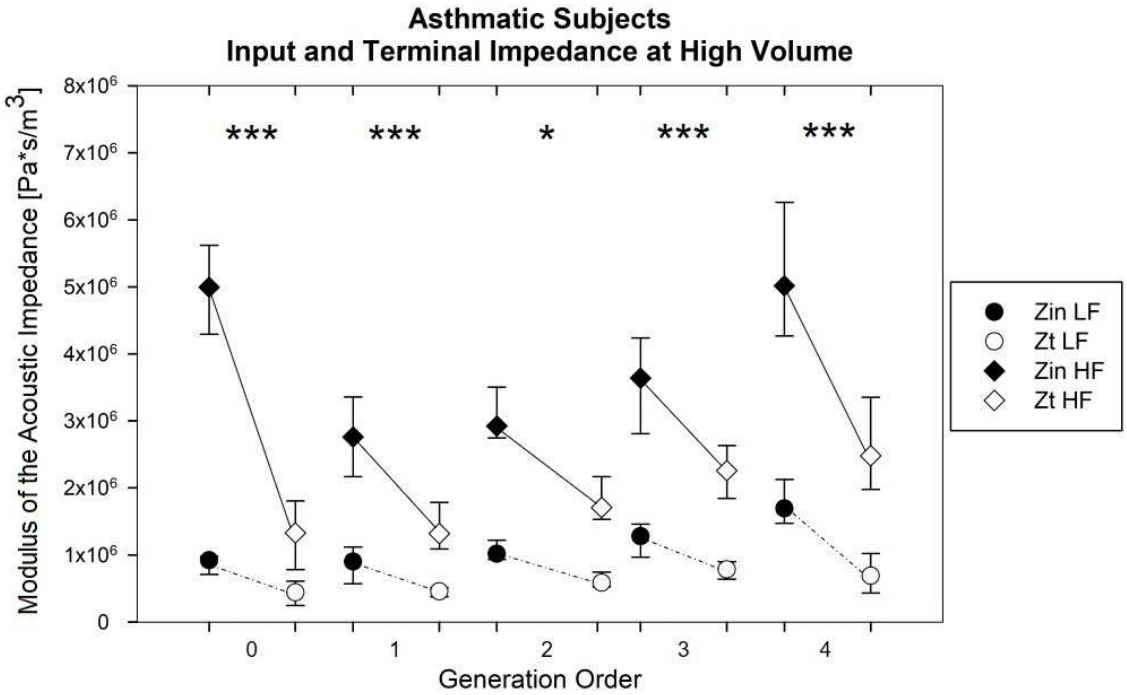

Figure 65: Input (black symbols) and terminal (white symbols) acoustic impedance from generation 0 to 4 at high respiratory volume in the asthmatic subjects. Low (circles) and high (diamonds) frequencies are reported. The symbols indicate the median values, the lower and the upper bars correspond to the 25th percentile and the 75th percentile, respectively. *, $p<0.05$; ***$p<0.001$; between low and high frequency for each generation,

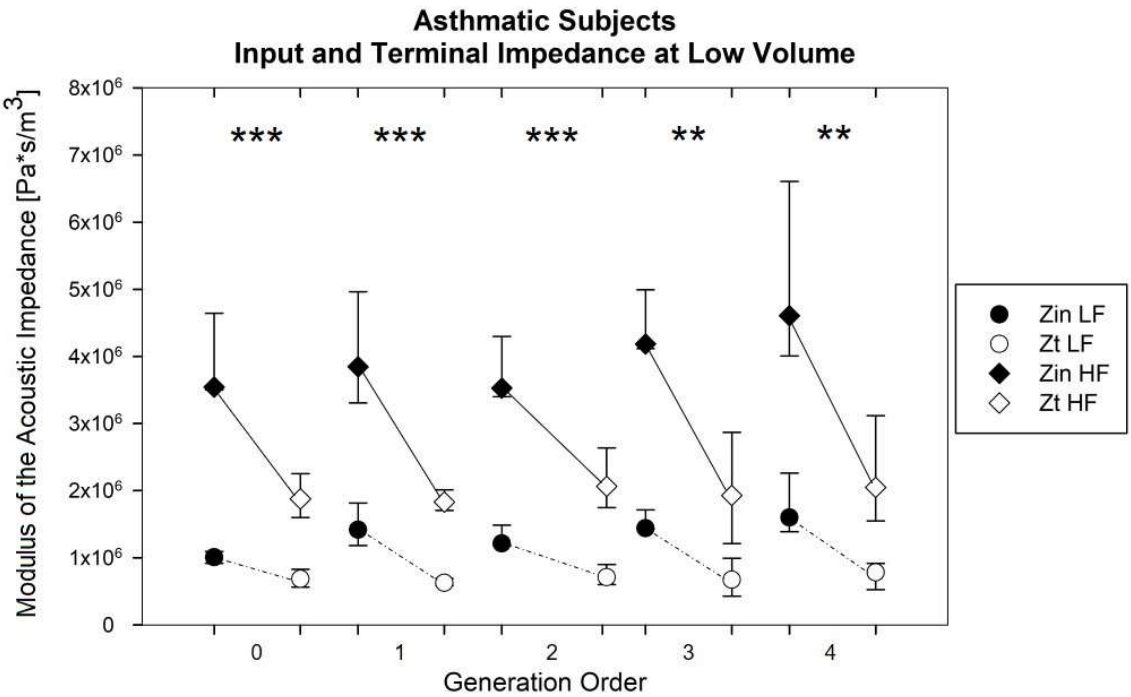

Figure 66: Input (black symbols) and terminal (white symbols) acoustic impedance from generation 0 to 4 at low respiratory volume in the asthmatic subjects. Low (circles) and high (diamonds) frequencies are reported. The symbols indicate the median values, the lower and the upper bars correspond to the 25th percentile and the 75th percentile, respectively. *, $p<0.05$; ***$p<0.001$; between low and high frequency for each generation,

Input and the terminal acoustic impedance, at both respiratory volumes, are significantly different between low and high frequency.

At high respiratory volume, both the input and the terminal impedances are higher at high frequency, with a tendency to increase with increasing generation order. At high frequency, the input impedance at the level of the trachea show the same peak as the one observed for the control group. As already mentioned, at low frequency this trend is rather linear and relatively close to the one of the healthy group.

At low respiratory volume, the trend of the impedance is more regular. The input impedance (Zin) is stably located around 3-4 million at the high frequency and around 1 million at the low frequency. The terminal impedance (Zt) is almost constant along the generations and is located around 1 and 2 million for the low and high frequencies, respectively. No peak at the level of the trachea can be observed.

Figure 67 and Figure 68 show the distribution of acoustic pressure for the low and the high respiratory volumes respectively. The absolute value of the acoustic pressure is reported for each generation. Low frequency trend is symbolized by black circles and high frequency trend is represented with white circles.

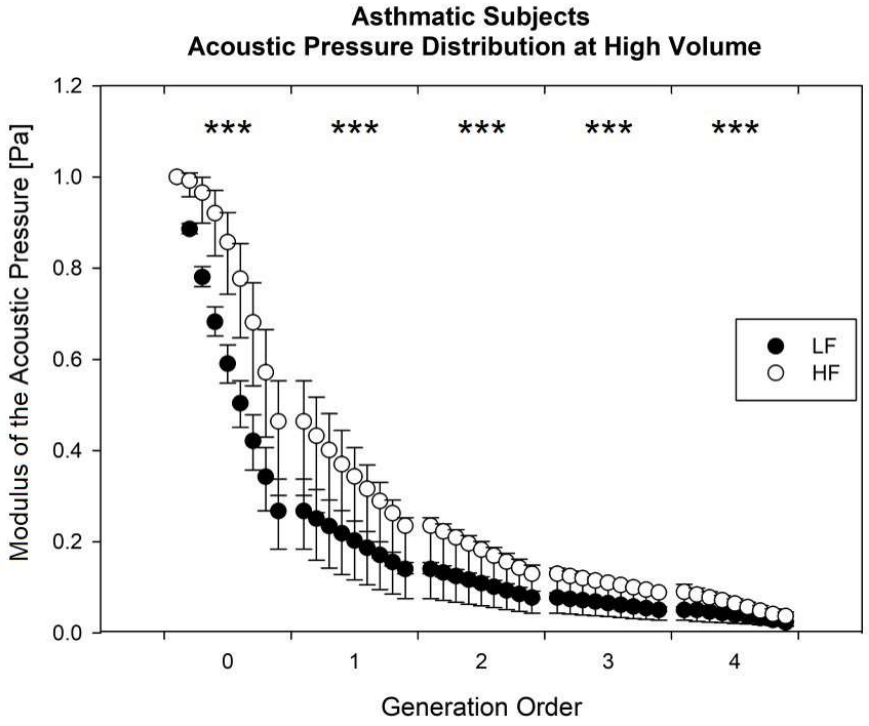

Figure 67: Acoustic pressure distribution from generation 0 to 4 at high respiratory volumes in asthmatic subjects. Low frequency (black circles) and high frequencies (white circles) are reported. For each generation the values are shown at 9 equally-spaced points. The symbols indicate the median value, the lower bar and the upper bars correspond to the 25th percentile and the 75th percentile, respectively. ***, $p<0.001$ between low and high frequency.

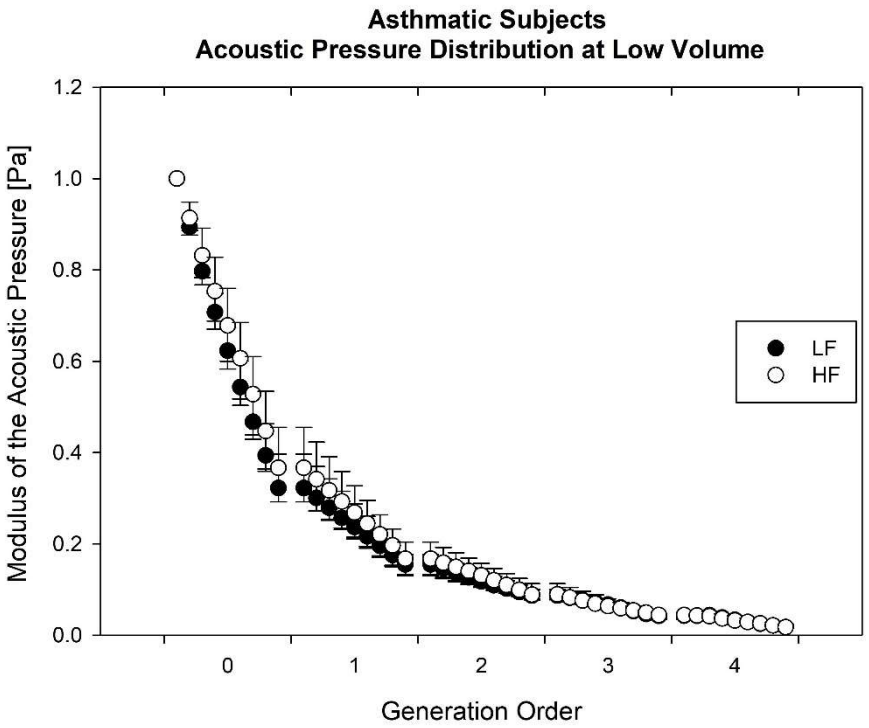

Figure 68: Acoustic pressure distribution from generation 0 to 4 at low respiratory volumes in asthmatic subjects. Low frequency (black circles) and high frequencies (white circles) are reported. For each generation the values are shown along 9 equally spaced points. The symbols indicate the median values, the lower and the upper bars correspond to the 25th percentile and the 75th percentile, respectively.

At high volume (Fig. 67), the pressure is significantly higher at high frequency, in all the generations ($p<0.001$). The pressure decrease along the trachea has a linear profile at low frequency and a parabolic profile at high frequency. At low volume (Fig. 68), no appreciable differences can be noticed between different frequencies. At both volumes and both frequencies, the major pressure drop is located at the level of the trachea. The pressure drop continues in the following generations with a less marked trend. By the end of the 4th the pressure is almost reduced to zero.

5.4.4 Comparison between the Control and the Asthmatic Group

To provide a more effective comparison the results of the control and asthmatic subjects have been averaged for each generation and analyzed together at different respiratory volumes and frequencies. All the data related to the control group are characterized by the choice of the blue color, whereas data from the asthmatic group are represented in red.

Figure 69 shows internal diameters at high respiratory volume (left) and low respiratory volume (right) in controls (blue) and asthma (red) groups. The statistical analysis is performed by comparing, for each generation, the airways' diameters in the asthmatic and the control group.

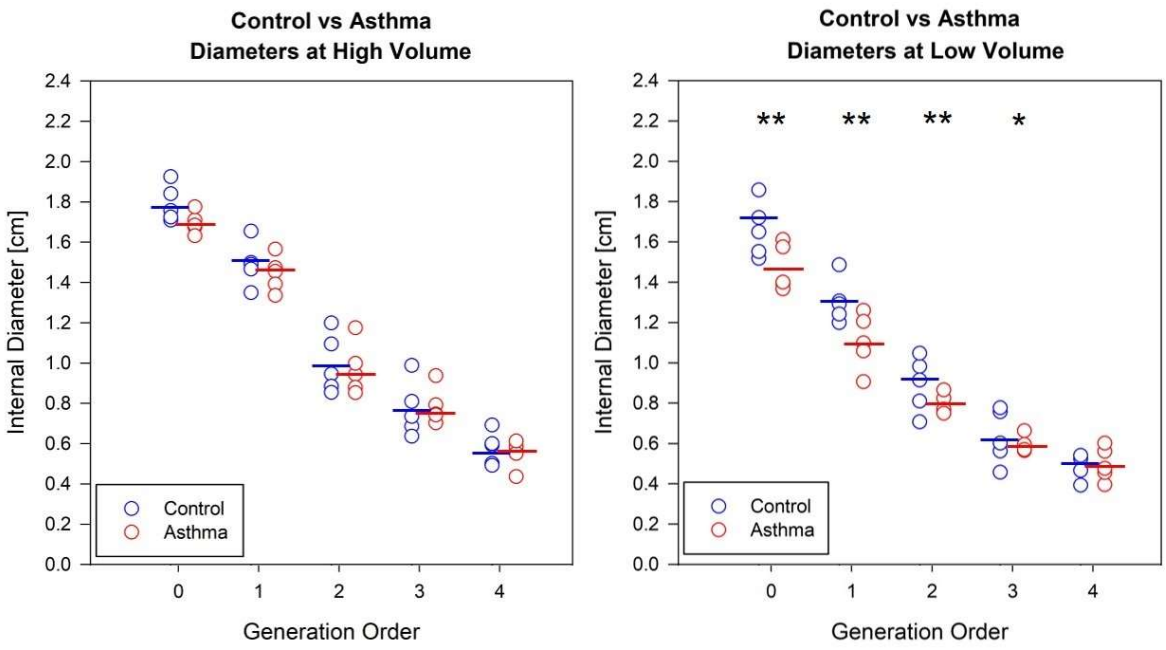

Figure 69: Internal diameter as a function of the airway generation order for control (in blue) and asthma (in red) groups. High respiratory volume case is reported on the left, whereas the low respiratory volume case is reported on the right. The mean values are reported with a blue line for the control group and with a red line for the asthmatic group. *, $p<0.05$; **, $p<0.01$ between healthy and asthma groups.

At high respiratory volume, no significant differences are found between the control and the pathological group. The extremely high intra-variability of the asthmatic group in some generations causes the diameter of the pathological case to be relatively close to the one of the control case.

At low respiratory volume, the diameters are significantly lower in asthma than in controls with p-values equal to 0.008, 0.001, 0.009 and 0.026 for the generation 0, 1, 2 and 3, respectively.

Figure 70 shows the values of the acoustic impedance of the two groups for both high volume and low volume at low frequency (LF), whereas Figure 71 provides the same comparison at high frequency (HF). In both cases the absolute value is reported as a function of the airway generation order. Input impedances are represented with filled symbols and terminal impedances with empty ones. The statistical analysis compare the overall impedance value in the asthmatic and the healthy group. Each generation is analyzed separately.

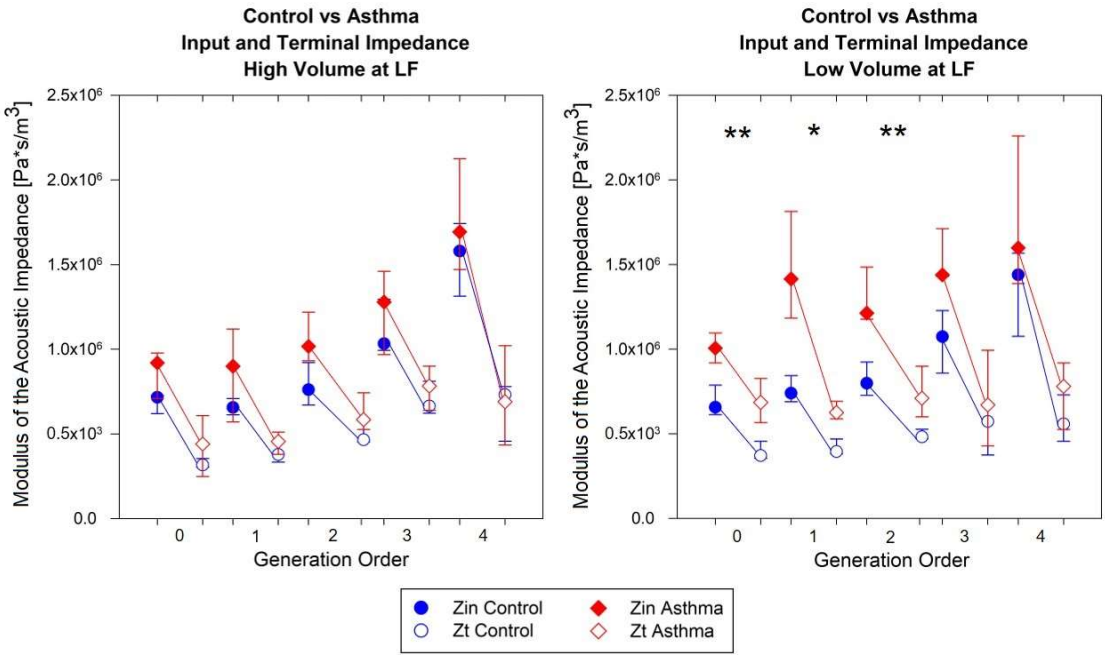

Figure 70: Acoustic impedance as a function of the airway generation order for control (in blue) and asthma (in red) groups at low frequency. High respiratory volume case is reported on the left, whereas the low respiratory volume case is reported on the right. Filled symbols indicate the median input impedance, whereas empty symbols represent the median terminal impedance, the lower and the upper bars correspond to the 25th percentile and the 75th percentile, respectively. *, $p<0.05$; **, $p<0.01$ between healthy and asthma group

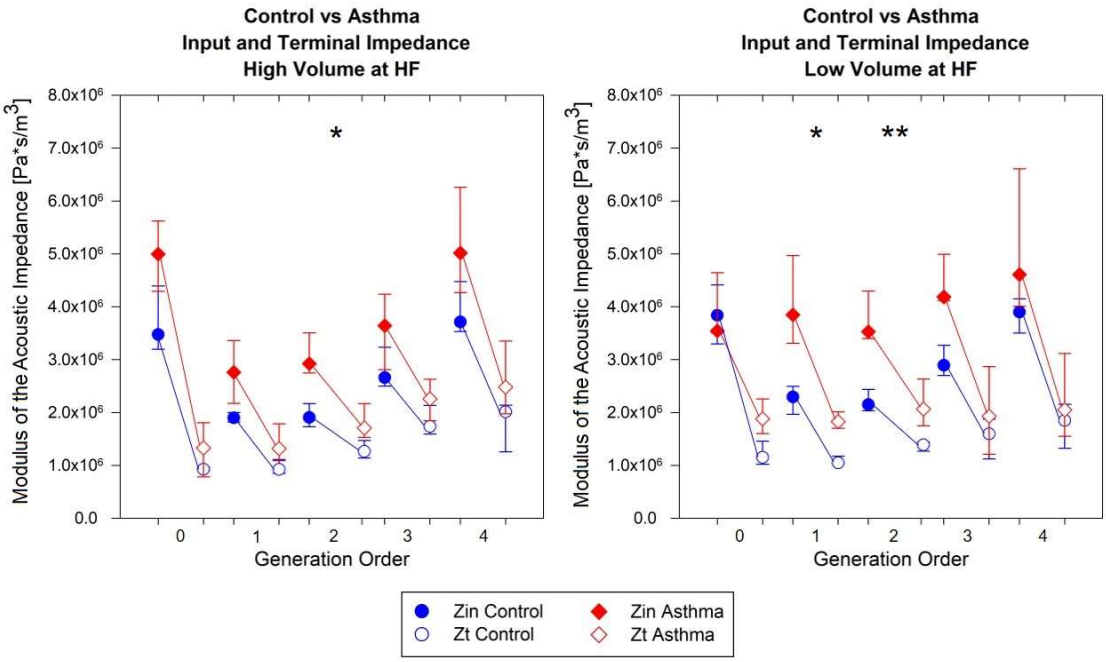

Figure 71: Acoustic impedance as a function of the airway generation order for control (in blue) and asthma (in red) groups at high frequency. High respiratory volume case is reported on the left, whereas the low respiratory volume case is reported on the right. Filled symbols indicate the median input impedance, whereas empty symbols represent the median terminal impedance, the lower and the upper bars correspond to the 25th percentile and the 75th percentile, respectively. *, $p<0.05$; **, $p<0.01$ between healthy and asthma group

At low frequency (Figure 70), although the acoustic impedance (both input and terminal) is constantly higher in the asthmatic case with respect to the healthy one, the results are significant only for the low volume case, with significant differences in the first three generations, with p-values equal to 0.002 in generation 0, 0.045 in generation 2 and to 0.008 in generation 3.

At high frequency (Figure 71), the values are similar for both lung volumes with significant differences at high-volume in generation 2 (p=0.017) and at low volume, in generation 1 (p=0.031) and generation 2 (p=0.007). It can be observed also that the range of variation of both the input and the terminal impedance is higher in the asthmatic population with respect to the healthy one.

The distribution of the acoustic pressure in health and asthma is reported in Figure 72 at high volume (left) and low volume (right) at low frequency (LF). Figure 73 shows the acoustic pressure in health and asthma at high volume (left) and low volume (right) at high frequency (HF). The trend for the control group is symbolized by blue circles while the trend of the asthmatic group is represented with red circles. The statistical analysis is performed comparing, for each generation, the overall pressure distribution in the segment in the healthy and pathological case.

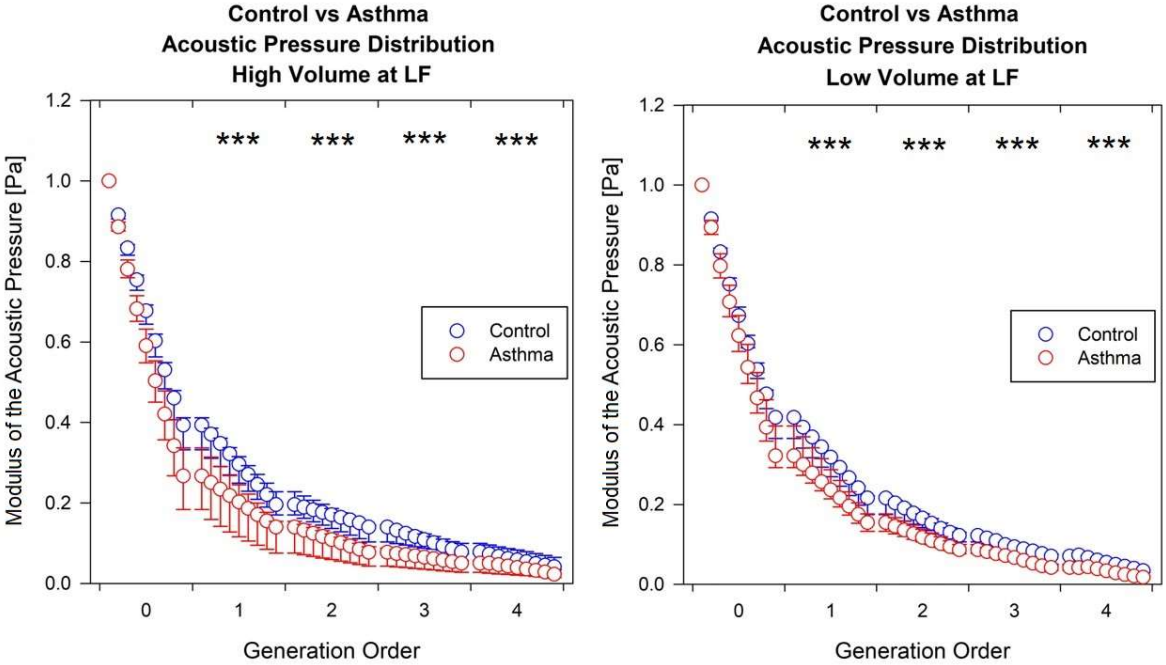

Figure 72: Acoustic pressure distribution as a function of the airway generation order for control (in blue) and asthma (in red) groups at low frequency. High respiratory volume case is reported on the left, whereas the low respiratory volume case is reported on the right. The symbols indicate the median value, the lower and the upper bars correspond to the 25th percentile and the 75th percentile, respectively. For each generation the values are shown along 9 equally spaced points. ***, $p<0.001$ between health and asthma

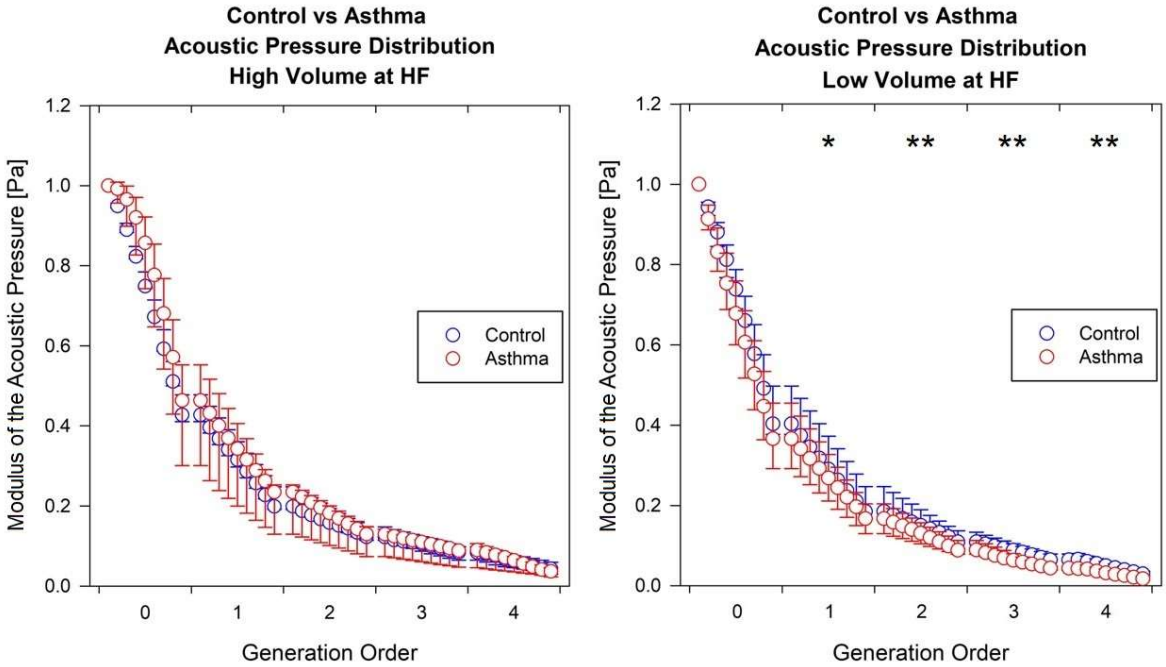

Figure 73: Acoustic pressure distribution as a function of the airway generation order for control (in blue) and asthma (in red) groups at high frequency. High respiratory volume case is reported on the left, whereas the low respiratory volume case is reported on the right. The symbols indicate the median value, the lower and the upper bars correspond to the 25th percentile and the 75th percentile, respectively. For each generation the values are shown along 9 equally spaced points. *, $p<0.05$; **, $p<0.01$ between health and asthma

At low frequency (Figure 72), asthma has a significant lower acoustic pressure distribution respect to healthy (p-value < 0.001) at all the generations with the only exception of the trachea (generation 0). This is verified for both high and low respiratory volumes.

On the contrary, at high frequency (Figure 73), asthma has a significant lower acoustic pressure distribution respect to healthy only at low volume. The significance of the results is, however, far lower than the low frequency one described above, with p-values for generation 1, 2, 3 and 4 respectively equal to 0.018, 0.004, 0.003 and 0.001.

It is interesting to notice, once again, that the inter-variability in the group population, is, in general, qualitatively higher in the asthmatic case with respect to the healthy. This fact can be clearly appreciated at low frequency, high volume (Figure 72, right) and at high frequency, high volume (Figure 73, right).

CHAPTER 6

DISCUSSION

In this dissertation, the frequency-domain response of a human tracheobronchial tree to an input acoustic wave of constant amplitude (1 Pa) and frequency ranging between 200 and 800 Hz was analyzed. In the first part of this project, the model was validated and applied to evaluate the response of the tracheobronchial tree during two phases of the respiratory cycle: the beginning of the inspiratory phase and the beginning of the expiratory phase. The system was modeled with a one-dimensional waveguide considering a fluid (air) embedded in compliant viscoelastic airways wall made of soft tissue only. A Voigt model was used to simulate the frequency dependent response of the wall tissue of the airways. The analytical code developed in MATLAB was validated via COMSOL Multiphysics® numerical finite element analysis and successively used for the simulation of some specific pathological conditions such as asthma, fibrosis and pulmonary infiltrate. These simulations were performed starting from the simplified assumption of being able to model a pathology by properly modifying one or at most two parameters related either to the geometry itself or to the mechanical properties of the constituent materials. In the analysis of the effect of such pathological induced alterations both high and low frequencies were considered.

The second part of the project focused on the asthma pathology. The model was applied to real pathological data and geometries obtained from CT. The population of the study involved five control (healthy) subjects and five asthmatic subjects. From each two geometries were obtained: one at high respiratory volume and one at low respiratory volume. Once again both low and high frequencies were analyzed. The results were at first presented separately for

the control and the asthmatic group. Successively the two groups were compared with the ambitious goal of identifying some specific markers of the pathology. This kind of approach tried to account for the complexity of the structural and morphometrical alteration induced by a pathology and has to be considered a more rigorous extension to what has been done in the first part of the project.

6.1 General Consideration on the Acoustic Behavior of the System

The overall response of the system is highly dependent on the mutual interactions between the fluid and the airway walls especially in terms of energy transfer occurring at their interface. As a general statement, it can be inferred that a wave propagating in a medium is characterized by a certain energy. This energy can either dissipated because of the properties of the medium or transferred to the airways wall. The predominance of one phenomenon over the other is conditioned by the impedance mismatch between the fluid and the wall of the airways. The transmission of energy is maximum when the two impedances have equal values and decreases in a monotonic way when the mismatch increases. In other words, a higher impedance mismatch causes the energy to be less likely transferred to the wall (and therefore to be stored in the fluid longer) whereas a lower impedance mismatch determines a facilitated and more rapid energy transfer from the fluid to the wall.

After the energy is transferred to the wall, it starts being dissipated. The dynamics of the dissipation process, at this point, is dependent on the material properties of the wall. As already mentioned the wall viscoelastic behavior was approximated by a Voigt model, consequently the elastic modulus can be expressed by equation 3.2. According to this relation, it can be observed that as the frequency increases there is an increase in the viscous term and consequently an increase in the damping effect. Given a certain amount of energy transferred to the wall, a higher energy dissipation is associated with higher frequencies. However, the

kinetics of dissipation of energy in the airways walls cannot be directly observed in our simulations.

As it can be easily observed from the analysis of the results the model shows a marked frequency-dependent behavior and this is the reason why several frequencies were analyzed in this project. To understand this behavior, it should be recalled the impedance type analogy used in modelling the response of the system. This analogy is implicit in the expression of formula (2.41) and, at first approximation, allows to model each acoustic element (in other term each segment) as reported in Figure 74.

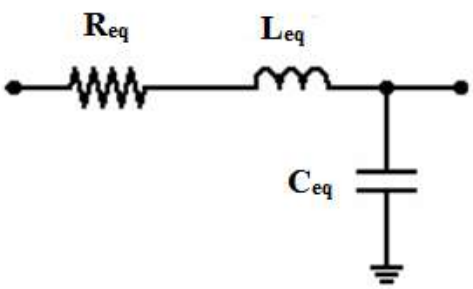

Figure 74: Transmission Line Analogy. Resulting circuit for each element

In such model, the voltage drop over the electrical element and the electrical current through that component represents the acoustic pressure drop over the acoustical component and the flux generated because of the pressure. The symbols L_{eq}, R_{eq}, C_{eq} correspond to the acoustic inertance, resistance and compliance respectively and consider both the properties of the walls and of the medium. The inertance represents the mass of the medium and of the walls, the compliance models the ability of these two components to expand and compress and finally the resistance is associated with the dissipation phenomena from the fluid to the walls. The appropriateness and the assumptions underlying this model are widely reported in literature [2], [45], [47] and will not be analyzed in this dissertation. What is of interest is the behavior

of the response of such a system in the frequency domain. It is known that the value of impedance relative to the inertance is directly proportional to the frequency, whereas the value of the compliance relative to impedance shows an inverse proportionality with respect to the frequency. Consequently, at low frequencies and with a certain degree of approximation the inertance can be considered a short circuit and the compliance and open circuit. On the contrary, at high frequencies the inertance behaves like an open circuit and the compliance as a short circuit. In terms of pressure (voltage), a short circuit is always negligible as (for definition) it does not induce any modification. For this reason, it is possible to infer that at lower frequencies the effect of the compliance is predominant over the effect of the inertia whereas for high frequencies inertia plays a much more relevant role with respect to the compliance. This result will deeply affect the successive considerations in the comparisons between the pathological and the physiological cases (see paragraphs 6.4.2, 6.4.3).

In the specific case of the tracheobronchial tree, the fluid to deal with is air. As reported in TABLE 5 and TABLE 6 the air properties are remarkably different than the one of the soft tissue composing the wall structure. Consequently, the impedance mismatch is in general high even for relatively low frequencies. When the frequency is increased, because of relation (2.38) the impedance of the airways wall is increased, whereas the properties of the fluid are not modified. This causes the impedance mismatch to become furthermore evident as the frequency increases. Recalling what has been stated above, a higher impedance mismatch determines a lower energy transfer rate between the fluid and the wall. As more energy remains stored in fluid, the pressure tends to penetrate more deeply in the tree. This trend can be easily observed considering the trend of the real part of the acoustic pressure for different frequencies of both the analytical and numerical results reported in section 5.1.

6.2 Validation of the Model

The qualitative comparison of the results of the two parameters considered for the validation of the analytical model, namely the magnitude (in logarithmic scale) and the real part of the acoustic pressure clearly show a good agreement between the results obtained in MATLAB and the numerical simulations in COMSOL. The results are consistent all over the four frequencies of interest. The validity of the model was proved also via the analysis of the relative error between the analytical and numerical results.

Given the excellent results for the inspiratory phase and the acceptable matching in the case of the expiratory phase analyzed in 5.1, the analytical model is considered to be validated. The increased discrepancies between the analytical and numerical results at higher frequencies could be attributed to the choice of the nominal element size in the meshes used for the numerical simulations. This nominal dimension ought to be at least an order of magnitude smaller than the lowest wavelength and it is known that as frequency increases, wavelength gets shorter. Although it was verified that the meshes used in this dissertation meet the above-mentioned requirement in term of nominal element size, it is also true that, especially at 800 Hz, the margin of error increases.

6.3 Comparison Between the Beginning of Inspiratory and Expiratory Phases

The diameter of the airways varies according to the respiratory cycle. This is confirmed by the plot of the diameters reported in Figure 6 and Figure 7. In general, during the inspiratory phase the airways exhibit an increment of the diameter and a reduction of the thickness, whereas in the expiratory phase the diameter is reduced and the thickness increased. In this dissertation, the very beginning of both phases was evaluated, consequently the morphometry of the airways at the beginning of each phase is still similar to the end of the previous one. In other words, it is possible to observe that at the beginning of the inspiratory phase the diameter of airways is

relatively lower than the diameter at the beginning of the expiratory phase. Nonetheless, the variations of the geometry seem to have a negligible effect on the acoustic of the tracheobronchial tree in the two phases. This is confirmed both by the visual representation of the three parameters presented in the result section and by the respective trend plots (see paragraph 5.2). On one hand, the similar response of the two phases can be ascribed to the fact the variations of the geometry themselves are relatively small and therefore hardly resolvable in term of acoustic analysis. This result is in line with the theoretical previsions as the two geometries were acquired at tidal volume and therefore in normal condition of inhalation and expiration. On the other hand, it should be considered that the creation of the geometry from the CT images introduced a certain degree of approximation causing a mitigation of the differences between the two phases. Finally, the fact that we are dealing with a simplified geometry both in terms of number of segments (only the first 7 generations were recognizable) and in terms of modelization of each branch (segments do not exhibit any tempering and curvature) can be an additional reason for the relative similarity between the respiratory phases considered.

Given the results obtained in paragraph 5.2 and the relative resemblance of the parameters of interest in the two respiratory phases considered it was decided to simulate the pathologic conditions only for the inspiratory case.

6.4 Simulation of Pathological Conditions

Although a very simplified approach to simulate the pathologies was used in this first part of the project, the hypothesis that the pathology induced alterations of the airways in terms of mechanical and geometrical properties significantly affect the sound propagation throughout the tracheobronchial tree is supported by most of the results in section 5.3. This is reflected on the distribution and the value of the acoustic parameters mentioned in this dissertation, namely

the acoustic pressure and the wall radial velocity. It can be stated that in particular for the fibrosis and the pulmonary infiltrate it is possible to identify specific markers that differentiate the pathological case from the physiological one. This is *per se* significant from a clinical perspective even though it necessary to remember that, in order to obtain data that really could be applied to a clinical context, the model should be extended to account for the coupling with the lung parenchyma and the chest surface. This extended model would allow to compare the analytical results of the simulations (especially in terms of wall radial velocity) with *in-vivo* measurements performed with Scanning Laser Doppler Vibrometry and, possibly, with MRE.

6.4.1 Simulation of the Asthma Pathology

The pathology of asthma was analytically simulated by increasing the thickness (h) of small airway segments (diameter lower than 2 mm) of 1.5 times. For those segments the radius of the cross-section was reduced proportionally to the new thickness values accordingly to equation (3.3). As already mentioned in 5.3.1, the modelling approach used in the simulations does not show any significant difference between the healthy and pathological condition. Two possible explanations can be found. Firstly, the approach used to simulate the pathology is extremely simplified. The assumption of a homogeneous bronchoconstriction throughout the small airways is at least arguable as asthma is indeed well-known for being and heterogeneous disease. As it will be analyzed later 6.4.1, having an inhomogeneous increment of thickness with an associate reduction of the diameter along the tree, have a significant impact on acoustic pressure propagation. The effects of such an alteration are clearly visible even at the level of the first generations.

Secondarily, it must be pointed out that the geometries used for the validation of the model, consisted of a reduced number of segments as only the very first five or six generations were clearly recognizable during the construction of the geometry. As a consequence, there are very

few segments that can be reasonably considered to be small airways and which have been altered by the choice of the parameters of the simulation. The model should be therefore tested on a fully grown (even algorithmically) tree to assess whether in presence of a larger number of airways with a diameter smaller than 2 mm, there will be alteration in terms of acoustic pressure distribution to which the geometry proposed in this thesis was not sensitive.

At the state of art, what can be inferred from the simulations performed in this work is that a simplified (mono-parametric, if it is considered that the alteration of diameter is someway proportional to the alteration of thickness) alteration of the geometry is not sufficient to represent the complexity of the asthma phenomenon.

6.4.2 Simulation of the Airways Fibrosis Condition

The stiffening of the airways characteristic of pathological fibrosis was modeled by increasing the elastic modulus of the airways wall of a factor 5. This multiplicative factor causes the compliance of the wall to drastically reduce, which determines the wall impedance to increase significantly as outlined by equation (2.40). The mismatch between the wall impedance and the fluid impedance becomes higher causing the pressure to penetrate the tree much more deeply in the pathological case then in the healthy one. This trend is clearly observable at low frequency. However, the results at high frequency do not seem to be affected as both the color plot and the trend in the trachea and main bronchi are negligibly modified. This behavior can be ascribed to the frequency dependency of the acoustical elements (compliance and inertance) used in of the model for the computation of the impedance. As it was previously stated, the compliance is predominant at lower frequencies, whereas at higher frequencies the role of the inertance is more relevant. By multiplying the elastic modulus by a factor 5, the compliance is deeply affected (namely reduced), whereas the inertance is left unaltered. At low frequency, the modification in compliance are clearly represented by the different response of the system.

At high frequency, the compliance still is higher that the physiological condition, but its effect in term of pressure alteration is minimal as it behaves like a short circuit: at this high frequency, the effect of the inertance is of first importance and, as already mentioned, the inertance itself was not altered. This determines the results at high frequency to be relatively similar in the comparison between the physiological and the pathological fibrotic case. In addition to that, several studies have confirmed that in low frequency range tissue properties primarily influence the response of the system whereas at higher frequency range, tissue properties become less important and airway caliber become more influential. This is confirmed by the results of the simulations. In terms of wall radial velocity: at low frequency, it is possible to observe that the magnitude of the velocity is significantly higher in the fibrotic case than in the healthy case. This difference is substantial at the level of the trachea and the main bronchi whereas it tends to become less evident moving down the tracheobronchial tree. Given that the magnitude of the velocity is a parameter directly proportional to the pressure, it is not surprising that at high frequency where there is not a significant variation of the distribution of the pressure (see above), also the magnitude wall radial velocity seems basically unaffected by the introduction of the pathology.

6.4.3 Simulation of the Pulmonary Infiltrate Condition

Pulmonary infiltrate localized in the lower lobe of the left lung was simulated. The increased resistance of the tree was modelled by multiplying the impedance of the left lower lobe terminal branches by a factor 10^5. The remarkably different trends of the magnitude of pressure between the healthy and the pathological cases can be ascribed to the increased terminal impedance in the lobe affected by the pathology. The creation of a hard-sound boundary determines the waves to be completely reflected with no further propagation on the tree. According to the

combination of phase between the incident and reflected way it is possible to hypothesize that a constructive impedance occurs causing an increase of pressure in that section of the tree.

The consideration according to which the distribution of pressure in the rest of the tree does not seem to be affected in a significant way gives a possible hint on the fact that an extremely localized pathology might not be reflected throughout the tracheo-bronchial tree.

The fact that the trend of the real part of the pressure is approximately equal in the physiological and in the pathological case, whereas the magnitude is different, implies that the main changes in terms of pressure distribution are related to the imaginary component of the pressure itself.

The trend of wall radial velocity can be possibly explained considering that the occlusion is acoustically correspondent to a hard-sound boundary. When a propagating wave reaches a hard boundary, it doesn't further propagate downstream but is instead reflected upstream. In this way, air is forced to interact with the walls determining an increment of pressure which in turn causes a higher wall radial velocity. Pulmonary infiltrate creates an airway blockage, causing the downstream gas exchange segments to be inaccessible. This blockage causes an increased acoustic impedance, and thus increased acoustic load on the surrounding airway walls leading to increased wall radial velocity in those segments.

6.5 Application of the Model to Control and Asthmatic Group

In the previous part of the work it was verified that the model is sensitive to mono-parametric modifications (either geometrical or structural) resembling pathology induced changes in the tracheobronchial tree. In addition to that, it was demonstrated that for the fibrosis and pulmonary infiltrate cases those alterations of the parameters resulted in measurable changes in the acoustic impedance values and the acoustic pressure propagation inside the system. On the contrary, the mono-parametric simulation of asthma did not show any substantial difference with respect to the physiological case. This result raises the interrogative on whether an

extremely simplified simulation of a pathology is sufficient to model the extreme complexity of a real disease. Besides, up to now, no prove of the effective reliability of the model on real pathological data was provided. Given the consideration mentioned above, in the second part of the project model was tested on a population consisting of five asthmatic subjects and the results compared to a control group composed of an equal number of subjects. This operation was done to achieve two main goals: firstly, to evaluate the sensitivity of the model to real pathological data and assess the discrepancy between a simplified simulation and a more complete simulation able to model the heterogeneity and the complexity of the pathology. Secondarily, it was of interest to identify one or more specific parameters to be used as markers of the pathological condition providing a further step towards a possible clinical application of the model.

The discussion presented on the following paragraphs is focused on those two objectives. The interpretation of the results themselves lacks the rigorousness that would be given by a proper background in literature as the study of acoustic pressure propagation in the tracheobronchial tree is still an open field of research, especially in the case of pathological conditions. Nonetheless, the comparison of the two groups over the different respiratory volumes and the different frequencies provides a valuable first insight towards the identification of those markers and conditions that, in a future perspective, will possibly allow the application of the model in a clinical context which was the main objective of this project.

6.5.1 Validation of the Asthmatic Data

The comparison between the reference data from [42] and the measurement obtained with the Full Width Half Maximum (FWHM) method on the asthmatic CT images show that the FWHM tends to underestimate values with respect to literature data, in each segment at each generation. The underestimation of thickness using this method is known from literature, even so the

FWHM method has been subject to several validation procedures and is nowadays broadly accepted. Given those considerations, the trend of the error and the very high standard deviation of the data in literature, the results obtained during the validation procedure show a good agreement with the reference and have indeed been used to assign the values of thickness to the correspondent airway segments for the pathological case.

6.5.2 Analysis of the Results for the Control Group

In terms of geometry, the control group shows internal diameters at high volumes larger than the ones measured at low volume. In general, the alteration of the so called "large airways" at different respiratory volumes can be reasonably considered negligible if compared to modifications at the level of smaller segments. In addition to that, the limitations and simplification in the approach used for the generation of the geometry, together with a certain inter-variability in the study group could possibly affect the overall analysis causing the differences between the high and the low volumes to be less marked.

In terms of acoustic impedance, the frequency dependency of the impedance is known by literature and is implicit in the definition of the model. The fact that the values of the impedance are higher at high frequency can be possibly explained considering that the higher the frequency the more the system tends to behave as a rigid series of tubes causing the acoustic impedance to increase.

As mentioned in 5.4.2, especially at low frequencies, the impedance variation across the segment remains approximately constant at all the generation and could possibly mean that to an increase of the terminal impedance corresponds a proportional increase of the input one.

The peak in terms of input impedance at the trachea observed only for the high-frequency case for both high and low volumes is a peculiar feature. Provided that the acoustic impedance can be considered a measure of the amount by which the motion induced by a pressure applied to

a surface is impeded, the high value registered at high frequency at the level of the trachea means that the motion of the segment is drastically reduced with respect to others. Therefore, the passive properties of the trachea at high frequency are predominant with respect to the other generations and it is reasonable to ascribe those differences to the geometrical properties of the trachea itself and to the fact that it is the longest and the thickest segment under analysis.

The acoustic pressure distribution at the two respiratory volumes does not show any significant difference between the high and low frequencies. Also, the values at low and high volumes are relatively similar. This result is in accordance to what observed in 6.3 and the relative discussion can be extended to this case.

Finally, the relation with the acoustic impedance is of difficult interpretation. The significant difference in the distribution of the acoustic impedance between high and low frequencies is not actually reflected in the distribution of the pressure. Only at the level of the trachea it can be noticed, at both volumes, that the median values of the pressures at high frequency are generally higher than the one at low frequency. This variation, however, is not such to create a statistically relevant significance. It is known that the two parameters are related through a third variable which is the acoustic flow across the segment. A future direction of this project to allow a better understanding of the result could be the evaluation of this third parameter.

6.5.3 Analysis of the Results for the Asthmatic Group

The internal diameter for the asthmatic subjects shows remarkable differences between low respiratory volume and high respiratory volume. High volume diameters are shown to be larger than the low volume ones and this behavior agrees to what observed before for the control group, but it is interesting to notice that the differences are in this case significant. The presence of the pathology seems to increase the discrepancies in the geometries between the low and the high volumes. In the asthmatic group it is reasonable to expect an increased variability between

the two volumes due to the heterogeneity of the pathology. It is known that at low respiratory volume the airways affected by asthma tend to collapse and reduce their diameter is a more marked way with respect to the physiological case. Nonetheless, it is still to be evaluated how far the observed behavior can be ascribed to the pathology and not to possible imprecisions in the generation of the geometry and the limited number of subjects in the study.

In terms of acoustic impedance, the results in the pathological case confirms that at high frequency the system tends to behave more rigidly causing the acoustic impedance to increase. The analysis at high frequency reveals that the input impedance at the level of the trachea shows the same peak as the one observed for the control group.

In terms of acoustic pressure, it has been observed at high volume, that the pressure reduction along the trachea is linear for low frequency and assumes a parabolic profile for high frequency, meaning that at high frequency the pressure drop is mainly located at the distal part of the segment. At high volume the pathology seems to have determined a more marked frequency dependency response of the model at least for the trachea. This behavior is not strictly dependent on the alterations occurring at the specific generations analyzed, but must be considered the reflection of the overall alteration of pressure propagation all over the three.

6.5.4 Comparison between the Control and the Asthmatic Group

The control and the asthmatic group has been performed considering the following three parameters: the internal diameters, the acoustic impedance and the distribution of the acoustic pressure. For those parameters, which are known to be frequency dependent, the analysis was performed comparing the two different respiratory volumes at both high and low frequencies.

In term of diameters, it is reasonable not to expect remarkable differences between the two groups especially at the level of the generation orders under analysis. It is, indeed, broadly accepted that the characteristic diameter reduction in asthmatic subjects generally involves high

order airways. This should be verified also at low volume. The differences that can be observed from the values of diameters at low volume can, consequently, be ascribed either to the inter-variability of the subjects composing the two study groups or, more likely, to the procedure of generation of the geometry that by itself, introduces some errors and simplifications (in particular considering the diameter constant and equal to the mean value of the diameter at the inlet of the segment and the one at the outlet) which may be reflected in the final result.

The analysis of the acoustic impedance at low and high frequencies reported in Figure 70 and Figure 71, is controversial. On one hand, it is undeniable that this parameter is affected by the pathology, as the statistical analysis reveals especially in the low frequency-low volume case and in the high frequency-low volume case. This would lead to the consideration that the acoustic impedance is higher in the asthmatic case, which is in line to what expected. On the other hand, it cannot be identified any specific trend as the statistical significance of the results is limited to specific generations (1st and 2nd) and it never extends to the successive generations, which theoretically are more likely to be affected by the pathology. To identify a specific marker of the pathology considering as a reference parameter the acoustic impedance further studies are required.

In terms of acoustic pressure distribution, the analysis at low frequency at both the respiratory volumes (Figure 72) shows that the differences between the pathological and the control groups are extremely significant for all the generations with the only exception of the trachea (generation 0). The most evident consideration is that the pressure in the asthmatic case results to be always lower than in the control one. As shown in Figure 73 high frequencies are proved to be less effective in identifying the differences between the two groups, although it is still possible to recognize significant differences. The consideration according to which the inter-variability in the group population, is, in general, extremely higher in the asthmatic case with respect to the healthy one supports the evidence that asthma is a heterogenous disease and

airways of the same order in different subjects can be affected with different modalities and severity.

As the main goal of this part of the project was identifying a possible marker of pathology which clearly differentiate the asthmatic group with respect to the healthy one some considerations can be made.

Firstly, the analysis of the diameters is not sufficient to provide valuable information aimed at the evaluation and identification of the pathological case in the airway generations considered. Asthma is not expected to impact significantly, in terms of bronchoconstriction, on large segments. At high volumes the differences are indeed negligible, whereas at low frequency the differences cannot be considered fully reliable because of the possible errors during the manual procedure of generation of the geometries.

Secondly, the analysis of the acoustic impedance shows remarkable differences at low volumes and low frequency where in the pathological case is significantly higher than the healthy case for the first three generations. At high frequency there are some differences, but it cannot be clearly identified any specific trend.

Finally, acoustic pressure distribution is the parameter which appears to be more sensitive to pathological induced alterations of the tracheobronchial tree. At low frequency and for both high and low volumes this is strikingly evident with statistical significances characterized by $p < 0.001$. At high frequency, the only statistically significant differences can be identified for the high volume case. The results suggest the evidence that in the asthmatic population the acoustic pressure is lower than the physiological one.

In conclusion, to identify and assess the presence of the asthma pathology the use of low frequency is proved to be most effective. This is especially true considering the acoustic pressure distribution, but is verified also by the analysis of the acoustic impedance. As this last parameter is more sensitive to alterations at low respiratory volume, the choice of an analysis

at low respiratory volume and low frequency (around 200 Hz) seems to maximize the possibility of finding evidence of pathology.

Another interesting consideration is that the pressure drop is located mainly at the trachea and the main bronchi where 80% of the pressure is dissipated. At the level of inlet of the 4th generation the values of pressure are equal to 10% of the original one and progressively decrease reaching almost 0 by the end of the generation. Nonetheless even those few generations (a fully grown tracheobronchial tree is generally devolved up to the 24th generation) are enough to reflect the pathology induced alterations along the tree. The development of a more complex and complete geometry will therefore allow a better characterization of the phenomena, both in physiological and pathological conditions, but it is arguable to think to extend analysis in terms of acoustic pressure distribution to further generations: at most one or two more generations could indeed suffice.

As a final remark, the overall application of the model to real pathological data clearly shows that, in case of complex pathologies (like asthma or for example COPD), a mono-parametric simplification of the effect of the pathology may not be suitable. Comparing what presented above to what observed for in 6.4.1, it is evident that relying on a more rigorous approach allows not only to collect more information, but in the case of asthma, influences the possibility of the model to be even sensitive to the pathological condition.

6.6 Limitations of the Model

Although the work presented in this thesis tried to be as comprehensive and precise as possible, the nature itself of the process of modeling implies the introduction of some assumptions and simplifications. A model is generally a trade-off between the possibility to accurately describe the phenomena of interest and the necessity to obtain results in a reasonable computational time.

Two main categories of limitations can be recognized in the adopted model: one related to the generation of the geometry and one related to the acoustic simulations themselves. In terms of geometry, the tracheobronchial trees analyzed were not fully grown. The number of segments constituting each tree was limited by the resolution of the CT and the effective capability to recognize them during the procedure of extrapolation of the geometry. In general, the trees at high respiratory volume analyzed in this project did not developed further than the seventh/eight generation, for a maximum number of segments equal to 155. For the geometries at lower respiratory volumes, this number was even lower. This is obviously a relevant simplification as far as the complexity of the geometry is concerned.

In MATLAB, every segment was approximated with a perfectly cylindrical tube of constant radius. No physiological tempering of the airways was considered. In COMSOL, to generate the cross-section of the branches, a gradual and constant reduction from the maximum proximal value to the minimum distal one was assumed. Both these approaches only partially resemble the physiological changes in cross-section of the human airways. Furthermore, in both the 1D geometry used in MATLAB and the 3D geometry in COMSOL, the segments modelling the airways were assumed to be completely straight. In addition to that, for the validation procedure, the minimum value of the thickness was imposed to be relatively high (500 micrometers) to be able to generate a mesh for the numerical simulation composed of reasonable number of elements. The limitation on the minimum value of the thickness allowed also to avoid having elements in the numerical simulations which were too small, further reducing the time necessary for the simulations. The generation of more consistent geometries between MATLAB and COMSOL Multiphysics® would have probably further reduced the error in the validation of the model. At the same time, a more physiological based geometry would enhance the possibility to properly model the effect of the pathologies.

As far as the analytic acoustic simulations are concerned, a main limitation is the assumption regarding soft tissue and cartilage having the same material properties and consequently considering the wall of the airways to be composed of soft tissue only. The introduction of the cartilage is expected to have a significant impact on the magnitude of the wall radial velocity, whereas the effect on the acoustic pressure itself could possibly be less pronounced. Even with the above-noted extension, the presented modeling approach still does not account for all potential acoustic wave propagation modes within the subglottal pulmonary system. It neglects other wave types, such as shear or other transverse waves that may arise at structural interfaces of the segments.

Another remark should be done on the simulation of the pathologies. It is understood that in this dissertation only some aspects of the mentioned diseases or pathological conditions were considered during the preliminary simulations. This can barely simulate the complexity of the morphometrical, biological and mechanical alterations generally associated with the clinical picture of a respiratory disease. The analysis of the result in these preliminary simulations of pathology lack of the rigorousness of a proper statistical analysis and is to be considered as first qualitative assessment to be further investigated. The application of the model to the two study groups for the asthma pathology clearly shows the limits of a mono-parametric alteration. Even so, to achieve a better understanding of the actual alterations in terms of acoustic parameter (especially for the acoustic impedance) the model should be applied to a larger number of subjects.

In addition to that, the quantification in terms of mechanical and structural chances induced by the pathology is extremely poorly analyzed in literature and subjected to a remarkable inter-studies variability.

As a final consideration, it is important to acknowledge the fact that the study of the acoustics in the tracheobronchial tree and its proper modeling are still open field of research.

Few effective models can be found in literature and only a limited part of them deals with acoustic pressure. Although, this proves the innovative approach developed in this approach, it also causes a significant lack of information to validate and interpret the results obtained. Further studies will be certainly necessary.

6.7 Conclusions

The model validated and used in this thesis has been proven to effectively and accurately describe the acoustic response of the human tracheobronchial tree to a known input acoustic pressure over a defined frequency range (from 200 Hz to 800 Hz). Despite the limitations described in the previous section, this model provides a first significant insight to the acoustic properties of the airways and to the alterations induced by some pathological conditions. In addition to that, it should be considered that the computational time of the analytical code in MATLAB is around 7.16 seconds, visualization included, for a multifrequency analysis. This value assumes even more significance if compared to the finite element method simulations where, to obtain result for frequencies ranged from 200 Hz to 800 Hz, more than one hour is required.

The application of the model to real asthmatic data in the second part of the project proved the applicability of the model to a more complex scenario, confirming its versatility.

The potential application of such a model are countless from both a clinical and a research point of view. In a long-term perspective, this model might eventually support clinicians in their everyday practice of diagnosis providing a useful and immediate comparison with the auscultation technique. As a more short-term goal, this model could be compared and used in association with elastography imaging techniques based on, for example, laser vibrometry and magnetic resonance elastography to provide quantitative information regarding both the physiological and pathological conditions of the respiratory system.

6.8 Future Directions

The analysis of the acoustics of the respiratory tract and the study of the pathology-induced alterations is still an open research field. In the first place, there is an impelling necessity of collecting data regarding the mechanical properties of the constituent materials of the airways wall tissue especially in terms of their modification in response to the pathology. Several experiments can be conducted with the goal of collecting this information such as Scanning Laser Doppler Vibrometry (SLDV) and *ex-vivo* mechanical characterization via tension/compression tests as well as creep/recovery simulations. In addition to that, the new emerging field of Magnetic Resonance Elastography (MRE) could be useful this first objective. Once the data regarding the tissue mechanics have been collected, they can be easily introduced in the analytical model to enhance the precision of its predictions. This data must be coupled with the introduction of a more physiological based structure of the airways wall where also the cartilage content is considered: this should be done at least for the first 16 generations of the tracheobronchial tree where the cartilage fraction cannot be neglected. The generation procedure will need a further review to implement the possibility to create more complex tracheobronchial tree from the CT data. It would be extremely useful the possibility to consider the natural tempering of the airways together with a modelization which accounts for the physiological sinuosity of the airways. In terms of pathological simulations, the same study performed for the asthma case should be extended to the fibrosis and the pulmonary infiltrate to evaluate the appropriateness of simulating those pathologies with a simplified approach.

The model should be also revalidated experimentally via SLDV and MRE, to obtain a further confirmation of its validity.

The following step toward a possible and ambitious clinical application would be a radical change of perspective in terms of input of the model: the input is to be modified from a chosen pressure at the inlet of the trachea to the physiological (or pathological) breath sounds which

generation occurs inside the tracheobronchial tree. Finally, to be comparable with the auscultation technique the model should extended to account for the surrounding lung structure and the coupling with the chest surface.

APPENDIX

<u>Comparison between the results of Royston et Al. [6] and Jackson et Al. [3]</u>.

The inversion and rearrangement of equation (2.45) leads to

$$Z_T^{(n)}[\omega]\frac{P_{in}^{(n)}[\omega]}{P_T^{(n)}[\omega]} = \frac{Z_{in}^{(n)}[\omega]\left(Z_T^{(n)}[\omega]sinh\left(\gamma_0^{(n)}[\omega]l^{(n)}\right) + Z_0^{(n)}[\omega]\,cosh\left(\gamma_0^{(n)}[\omega]l^{(n)}\right)\right)}{Z_0^{(n)}[\omega]}$$

By introducing the definition of $Z_{in}^{(n)}[\omega]$ according to
(2.30) in the equation above the following system is obtained.

$$\begin{cases} Z_T^{(n)}[\omega]\dfrac{P_{in}^{(n)}[\omega]}{P_T^{(n)}[\omega]} = \dfrac{Z_{in}^{(n)}[\omega]\left(Z_T^{(n)}[\omega]sinh\left(\gamma_0^{(n)}[\omega]l^{(n)}\right) + Z_0^{(n)}[\omega]\,cosh\left(\gamma_0^{(n)}[\omega]l^{(n)}\right)\right)}{Z_0^{(n)}[\omega]} \\ Z_{in}^{(n)}[\omega] = \dfrac{Z_T^{(n)}[\omega]cosh(\gamma_0^{(n)}[\omega]l^{(n)}) + Z_0^{(n)}[\omega]sinh(\gamma_0^{(n)}[\omega]l^{(n)})}{cosh(\gamma_0^{(n)}[\omega]l^{(n)}) + \left(Z_T^{(n)}[\omega]/Z_0^{(n)}[\omega]\right)sinh(\gamma_0^{(n)}[\omega]l^{(n)})} \end{cases}$$

By solving

$$Z_T^{(n)}[\omega]\frac{P_{in}^{(n)}[\omega]}{P_T^{(n)}[\omega]} = \frac{\left(\frac{Z_T^{(n)}[\omega]\cosh\left(\gamma_0^{(n)}[\omega]l^{(n)}\right)+Z_0^{(n)}[\omega]\sinh\left(\gamma_0^{(n)}[\omega]l^{(n)}\right)}{\cosh\left(\gamma_0^{(n)}[\omega]l^{(n)}\right)+\left(Z_T^{(n)}[\omega]/Z_0^{(n)}[\omega]\right)\sinh\left(\gamma_0^{(n)}[\omega]l^{(n)}\right)}\right)\left(Z_T^{(n)}[\omega]sinh\left(\gamma_0^{(n)}[\omega]l^{(n)}\right)+Z_0^{(n)}[\omega]\,cosh\left(\gamma_0^{(n)}[\omega]l^{(n)}\right)\right)}{Z_0^{(n)}[\omega]} =$$

$$\frac{Z_T^{2(n)}[\omega]\,cosh\left(\gamma_0^{(n)}[\omega]l^{(n)}\right)sin\left(\gamma_0^{(n)}[\omega]l^{(n)}\right)+Z_T^{(n)}[\omega]\,Z_0^{(n)}[\omega]cosh^2\left(\gamma_0^{(n)}[\omega]l^{(n)}\right)+Z_T^{(n)}[\omega]Z_0^{(n)}[\omega]sinh^2\left(\gamma_0^{(n)}[\omega]l^{(n)}\right)+Z_0^{2(n)}[\omega]\,cosh\left(\gamma_0^{(n)}[\omega]l^{(n)}\right)sinh\left(\gamma_0^{(n)}[\omega]l^{(n)}\right)}{Z_0^{(n)}[\omega]\,cosh\left(\gamma_0^{(n)}[\omega]l^{(n)}\right)+Z_T^{(n)}[\omega]sinh\left(\gamma_0^{(n)}[\omega]l^{(n)}\right)} =$$

$$\frac{Z_T^{(n)}[\omega]\,cosh\left(\gamma_0^{(n)}[\omega]l^{(n)}\right)\left(Z_0^{(n)}[\omega]\,cosh\left(\gamma_0^{(n)}[\omega]l^{(n)}\right)+Z_T^{(n)}[\omega]sinh\left(\gamma_0^{(n)}[\omega]l^{(n)}\right)\right)+Z_0^{(n)}[\omega]sinh\left(\gamma_0^{(n)}[\omega]l^{(n)}\right)\left(Z_0^{(n)}[\omega]\,cosh\left(\gamma_0^{(n)}[\omega]l^{(n)}\right)+Z_T^{(n)}[\omega]sinh\left(\gamma_0^{(n)}[\omega]l^{(n)}\right)\right)}{\left(Z_0^{(n)}[\omega]\,cosh\left(\gamma_0^{(n)}[\omega]l^{(n)}\right)+Z_T^{(n)}[\omega]sinh\left(\gamma_0^{(n)}[\omega]l^{(n)}\right)\right)} =$$

$$Z_T^{(n)}[\omega]cosh(\gamma_0^{(n)}[\omega]l^{(n)}) + sinh(\gamma_0^{(n)}[\omega]l^{(n)})\;Z_0^{(n)}[\omega]$$

The result is indeed the same of the rearranged equation for $P_{rat}^{(n)}[\omega]$ by Jackson and Al.

Analogous computation can be performed starting from equation (2.44) leading to the same solution.

CITED LITERATURE

[1] K. Horsfield, "Morphometry of airways," *Handb. Physiol.*, no. 78, pp. 75–88.

[2] G. R. Wodicka, K. N. Stevens, H. L. Golup, E. G. Cravalho, and D. C. Shannon, "A Model of Acoustic Transmission in the Respiratory System," vol. 36, no. 9, 1989.

[3] A. C. Jackson, B. Suki, M. Ucar, and Hab, "Branching airway network models for analyzing high-frequency lung input impedance," *Am. Physiol. Soc.*, 1993.

[4] A. C. Jackson, R. H. Habib, B. Suki, S. A. Wood, and W. Mitzner, "Serial distribution of airway diameters from input impedance and computed tomography," *Ann. Biomed. Eng.*, vol. 23, no. 6, pp. 740–749, 1995.

[5] R. H. Habib, R. B. Chalker, B. Suki, and A. C. Jackson, "Airway Geometry and Wall Mechanical Properties Estimated from Subglottal Input Impedance in Humans," *J. Appl. Physiol.*, vol. 77, pp. 441–451, 1994.

[6] T. J. Royston, S. Acikgoz, M. B. Ozer, H. a. Mansy, and R. H. Sandler, "Advances in Computational Modeling of Sound Propagation in the Lungs and Torso with Diagnostic Applications," *Biomed. Appl. Vib. Acoust. Ther. Bioeffect Model.*, p. 32, 2008.

[7] Z. Dai, "The Audible Human Project: Modeling Sound Transmission in the Lungs and Torso," 2013.

[8] Z. Dai, Y. Peng, H. A. Mansy, R. H. Sandler, and T. J. Royston, "Experimental and computational studies of sound transmission in a branching airway network embedded in a compliant viscoelastic medium," *J. Sound Vib.*, vol. 339, pp. 215–229, 2015.

[9] B. Henry and T. J. Royston, "A multiscale analytical model of bronchial airway acoustics," *J. Acoust. Soc. Am.*, vol. 142, no. 4, pp. 1774–1783, 2017.

[10] D. U. Silverthorn, *Human Physiology - An integrated approach*. 2010.

[11] M. Thiriet, *Anatomy and Physiology of the Circulatory and Ventilatory Systems*. 2013.

[12] S. Standring, *Gray's Anatomy - 41st Edition*. 2015.

[13] M. S. Kavuru, A. C. Mehta, and J. F. T. Jr, "Applied Anatomy of the Neck," no. February, pp. 1–4, 2012.

[14] P. M. Boiselle and D. A. Lynch, *CT of the Airways*.

[15] B. T. Finucane, B. C. H. Tsui, and A. H. Santora, *Principles of Airway Management, 4th Ed*, vol. 82, no. 6. 1996.

[16] J.A Verschakelen, *Computed Tomography of the Lung*. 2010.

CITED LITERATURE

[17] E. A. Gabriel and T. Salerno, *Principles of Pulmonary Protection in Heart Surgery*.

[18] J. H. Bates, *Lungs Mechanics*. 2009.

[19] S. Yim Yeh and R. Schwartzstein, "Asthma: Pathophysiology and Diagnosis," in *Asthma, Health and Society A Public Health Perspective*, 2010.

[20] T. R. Bai and D. A. Knight, "Structural changes in the airways in asthma: observations and consequences.," *Clin. Sci. (Lond).*, vol. 108, no. 6, pp. 463–77, 2005.

[21] T. R. Bai, J. Cooper, T. I. M. Koelmeyer, P. D. Paré, and T. D. Weir, "The Effect of Age and Duration of Disease on Airway Structure in Fatal Asthma," vol. 162, pp. 663–669, 2000.

[22] S. Godfrey, "Asthma and COPD," *Asthma COPD*, pp. 699–711, 2002.

[23] A. Cancellieri, G. Dalpiaz, M. Maffessanti, A. Pesci, R. Polverosi, and M. Zompatori, *Diffuse Lung Disease: Clinical Features, Pathology, HRCT*. 2006.

[24] G. Maloney, E. Anderson, and D. M. Yealy, "Pneumonia and Pulmonary Infiltrates," in *Tintinalli's Emergency Medicine: A Comprehensive Study Guide, 8e*, J. E. Tintinalli, J. S. Stapczynski, O. J. Ma, D. M. Yealy, G. D. Meckler, and D. M. Cline, Eds. New York, NY: McGraw-Hill Education, 2016.

[25] J. Ribeiro and B. Fisher, "Eosinophilic Lung Desease," *Pediatr. Respir. Rev.*, vol. 3, pp. 278–284, 2002.

[26] a Siddiqui and S. Ahmed, "Pulmonary manifestations of sickle cell disease," *Postgrad. Med. J.*, vol. 79, no. 933, pp. 384–390, 2003.

[27] M. Bahoura, "Pattern recognition methods applied to respiratory sounds classification into normal and wheeze classes," *Comput. Biol. Med.*, vol. 39, no. 9, pp. 824–843, 2009.

[28] S. Reichert, R. Gass, C. Brandt, and E. Andrès, "Analysis of respiratory sounds: state of the art.," *Clin. Med. Circ. Respirat. Pulm. Med.*, vol. 2, pp. 45–58, 2008.

[29] P. Piirila and A. R. A. Sovijarvi, "Crackles: Recording, analysis and clinical significance," *Eur. Respir. J.*, vol. 8, no. 12, pp. 2139–2148, 1995.

[30] J. Fredberg and S. Holford, "Discrete lung sounds: crackles (rales) as stress-relaxation quadrupoles.," *J. Acoust. Soc. Am.*, vol. 73, pp. 1036–1046, 1983.

[31] B. A. Reyes, S. Charleston-Villalobos, R. Gonzalez-Camarena, and T. Aljama-Corrales, "Analysis of discontinuous adventitious lung sounds by Hilbert-Huang spectrum.," *Annu. Int. Conf. IEEE Eng. Med. Biol. Soc.*, vol. 2008, pp. 3620–3, 2008.

CITED LITERATURE

[32] A. Bohadana, G. Izbicki, and S. S. Kraman, "Fundamentals of lung auscultation.," *N. Engl. J. Med.*, vol. 370, no. 8, pp. 744–51, 2014.

[33] Z. Wang, S. Jean, and T. Bartter, "Lung sound analysis in the diagnosis of obstructive airway disease," *Respiration*, vol. 77, no. 2, pp. 134–138, 2009.

[34] H. Pasterkamp, S. S. Kraman, and G. R. Wodicka, "State of the Art Advances Beyond the Stethoscope," *Am. J. Respir. Crit. Care Med.*, vol. 156, no. 3, pp. 974–987, 1997.

[35] S. A. Taplidou and L. J. Hadjileontiadis, "Wheeze detection based on time-frequency analysis of breath sounds," *Comput. Biol. Med.*, vol. 37, no. 8, pp. 1073–1083, 2007.

[36] P. Forgacs, *Lung Sounds*. 1978.

[37] A. H. Benade, "On the propagation of sound waves in a cylindrical conduit," *J. Acoust. Soc. Am.*, vol. 44, no. 2, pp. 616–623, 1968.

[38] R. H. Habib, B. Suki, J. H. Bates, and A. C. Jackson, "Serial Distribution of Airway Mechanical Properties in Dogs: Effects of Histamine," *J. Appl. Physiol.*, vol. 77, pp. 554–566, 1994.

[39] A. B. Dubois, A. W. Brody, D. H. Lewis, and B. F. J. Burgess, "Oscillation mechanics of lungs and chest in man," *J. Appl. Physiol.*, vol. 8, pp. 587–594, 1956.

[40] J. J. Fredberg and J. A. Moore, "Distributed Response of Complex Branching Networks," *J. Acoust. Soc. Am.*, vol. 63, pp. 954–961, 1978.

[41] S. Miyawaki, M. H. Tawhai, E. A. Hoffman, S. E. Wenzel, and C.-L. Lin, "Automatic construction of subject-specific human airway geometry including trifurcations based on a CT-segmented airway skeleton and surface," *Biomech. Model. Mechanobiol.*, 2016.

[42] S. Montesantos *et al.*, "Airway Morphology From High Resolution Computed Tomography in Healthy Subjects and Patients With Moderate Persistent Asthma," *Anat. Rec.*, vol. 296, no. 6, pp. 852–866, 2013.

[43] C. A. Schneider, W. S. Rasband, and K. W. Eliceiri, "NIH Image to ImageJ: 25 years of image analysis," *Nat Meth*, vol. 9, no. 7, pp. 671–675, Jul. 2012.

[44] H. O. Coxson, "Quantitative Computed Tomography Assessment of Airway Wall Dimensions: Current Status and Potential Applications for Phenotyping Chronic Obstructive Pulmonary Disease," *Proc. Am. Thorac. Soc.*, vol. 5, no. 9, pp. 940–945, 2008.

[45] P. Harper, S. S. Kraman, H. Pasterkamp, and G. R. Wodicka, "An acoustic model of the respiratory tract.," *IEEE Trans. Biomed. Eng.*, vol. 48, no. 5, pp. 543–550, 2001.

CITED LITERATURE

[46] C. M. Ionescu, P. Segers, and R. De Keyser, "Mechanical properties of the respiratory system derived from morphologic insight," *IEEE Trans. Biomed. Eng.*, vol. 56, no. 4, pp. 949–959, 2009.

[47] R. W. Guelke and A. E. Bunn, "Trasmission Line Theory applied to Sound Wave Propagation in Tubes with Compliant Walls," *Acustica*, vol. 48, pp. 101–107, 1981.

VITA

NAME	Lorenzo Aliboni
EDUCATION	M.S. in Bioengineering, University of Illinois at Chicago, Chicago, United States of America, 2017 B.S. in Biomedical Engineering, Politecnico di Milano, Milan, Italy, 2015 Secondary School Degree, Liceo Scientifico Leonardo da Vinci, Milan, Italy, 2012
RESEARCH EXPERIENCE	01/2017-06/2017 Research Assistant in the Acoustics and Vibrations Laboratory at University of Illinois at Chicago 01/2015-09/2015 Activity in the Laboratory of Biomechanics and Biomaterials at Politecnico di Milano 01/2014-09/2014 Activity in the Novel, Emerging Computing System Technologies Laboratory (NECST) at Politecnico di Milano